R 433

Technical Report

MECHANICS OF RAISING AND LOWERING HEAVY LOADS IN THE DEEP OCEAN: CABLE AND PAYLOAD DYNAMICS

April 1966

BUREAU OF YARDS AND DOCKS

U. S. NAVAL CIVIL ENGINEERING LABORATORY

Port Hueneme, California

MECHANICS OF RAISING AND LOWERING HEAVY LOADS IN THE DEEP OCEAN: CABLE AND PAYLOAD DYNAMICS

Technical Report R-433

Y-F015-01-01-001(b)

by

P. Holmes, Ph D

ABSTRACT

Based on a theoretical analysis of the cable and payload dynamics during lowering or raising heavy loads in the deep ocean given in Project Trident Technical Report No. 1370863, further calculations of the maximum dynamic stresses expected in the lowering cable are presented covering a wide range of cable and payload parameters. The theoretical analysis is adapted to a proposed design procedure, and two typical design examples are given, the results of which are discussed in terms of the safety of the lowering or raising operations.

In order to make the design procedure applicable with a greater degree of confidence, it is considered necessary to make measurements of cable tensions and load and ship motions during a full-scale operation to fill in deficiencies of data and provide a basis for verification of theory and calculations. In particular, data are needed on the coefficients of drag and mass, which at this stage must of necessity be estimates.

CONTENTS

INTRODUCTION

The work described herein was carried out as part of BuDocks Task No. Y-F015-01-01-001, "Structures in Deep Ocean," which originated from the requirement of the Bureau to attain a deep ocean engineering capability in keeping with the increased emphasis on the deep ocean as an operating environment for naval forces. This report is the result of work performed under Task No. Y-F015-01-01-001(b), "Mechanics of Raising and Lowering Heavy Loads in the Deep Ocean."

The objectives of this work were to analyze and report on the results of predictions of the forces in lines and the acceleration and displacements of loads of various shapes during raising and lowering operations in the deep ocean. The study is based on, and an extension of, a theoretical analysis by Arthur D. Little, Inc., given in Project Trident Technical Report No. 1370863 of the Bureau of Ships, entitled "Stress Analysis of Ship-Suspended Heavily Loaded Cables for Deep Underwater Emplacements."[1]

THEORY

The problem considered in this report is that of a load suspended from a ship or moored platform by means of a single cable, as shown in Figure 1.* The maximum depth for such a lowering or raising operation is assumed to be on the order of 20,000 feet.

The requirements are (1) to analyze this problem so as to predict the cable and the load dynamics, in particular the maximum dynamic stress induced in the cable as a result of the motions of the suspension point, and (2) to provide a design procedure for evaluating such stresses for a given load under specified conditions of sea-surface oscillations.

Solution of this problem is recognized to be difficult in view of the nonlinearities introduced in the damping due to drag forces of vertical oscillations of the load. A simplified solution has been obtained by Arthur D. Little, Inc., as given in the Project Trident report. A brief résumé of the analysis presented in that report is given here, details of which may be found in Appendix A.

The equation of motion of an element of the cable initially located at a distance x from the support point is given by

$$\frac{\partial^2 u}{(\partial t')^2} + \beta_c \frac{\partial u}{\partial t'} = \frac{\partial^2 u}{(\partial x')^2} \qquad (1)$$

* Figures 1 through 35 are presented immediately after the main body of text.

The boundary condition at the load is given in the form

$$\frac{\partial^2 u}{(\partial t')^2} + \mu \frac{\partial u}{\partial x'} + B \left| \frac{\partial u}{\partial t'} \right| \frac{\partial u}{\partial t'} = 0 \tag{2}$$

A secondary boundary condition is that the displacement of the suspension point is known for all time.

In the above equations, $u(x, t)$ is the displacement at time t of a point on the cable originally located at a distance x from the suspension point. Hence the second boundary condition is that

$$u(o, t) \text{ is known for } t > 0. \tag{3}$$

The following nomenclature applies:

$$\beta_c = \frac{K L}{\rho_c c S} \tag{4a}$$

$$\mu = \frac{\rho_c S L}{M_a} \tag{4b}$$

$$c^2 = \frac{E}{\rho_c} \tag{4c}$$

$$x' = \frac{x}{L} \qquad t' = \frac{t c}{L} \tag{4d, e}$$

and

$$B = \frac{C_D \rho A}{2 M_a} \tag{4f}$$

where* ρ_c = density of the cable

S = material cross-sectional area of the cable

E = modulus of elasticity of the cable

K = constant of friction on the cable due to the surrounding water

* Notations are defined where they first appear and are summarized for convenience on a foldout page at the back of the report.

c = velocity of sound in the cable

M_a = virtual mass of the load

C_D = drag coefficient appropriate to the load

A = projected area of the load in the direction of motion

L = length of cable

ρ = density of sea water

The difficulty in obtaining an exact solution to Equation 1 subject to the boundary conditions, Equations 2 and 3, arises from the nonlinear term $|\partial u/\partial t'|(\partial u/\partial t')$ in Equation 2. This difficulty is avoided in the A. D. Little report[1] by an approximation which is described in Appendix A.

Defining a normalized displacement amplitude U' equal to U divided by $|U_o|$ and noting that U_1' is the value of U' at the load, a solution for U' as a function of x' is given by

$$U' = U_1' \cos \omega' y' + C \sin \omega' y' \tag{5}$$

where C is a complex constant and

$$y' = 1 - x' \tag{6a}$$

$$\omega' = \frac{\omega L}{c} \tag{6b}$$

Hence the maximum value of the dynamic stress in the cable is given by

$$(\Sigma'_{max})^2 = (\omega')^2 (U_1')^2 [1 + \tan\varphi (\tan\Psi + \sec\Psi)] \tag{7}$$

where $$(U_1')^2 = \frac{\cos^2(\omega' + \varphi)}{2\beta^2 \sin^2\varphi \sin^2\omega'} \left\{ \left[1 + \frac{\beta^2 \sin^2\omega' \sin^2 2\varphi}{\cos^4(\omega' + \varphi)} \right]^{1/2} - 1 \right\} \tag{8}$$

$$\varphi = \arctan \frac{\omega'}{\mu}, \qquad 0 \le \varphi \le \frac{\pi}{2} \tag{9}$$

$$\Psi = \arctan \left[\frac{1}{2} \beta^2 (U_1')^2 \tan\varphi - \cot 2\varphi \right], \qquad -\frac{\pi}{2} \le \Psi \le \frac{\pi}{2} \tag{10}$$

$$\beta = \frac{4 C_D \rho A |U_o|}{3 \pi M_a} \tag{11}$$

and

$$\left| \Sigma'_{max} \right| = \frac{L \Sigma_d}{|U_o| E} \tag{12}$$

In the A. D. Little report, Equation 7 together with Equations 8, 9, and 10 was solved by use of a digital computer to give the maximum dynamic stress as a function of the nondimensional frequency ω' for various values of β and μ. A similar procedure was adopted in this report for two reasons, firstly to investigate the variation of stress over a wide range of ω', β, and μ, and secondly as a means of providing the basis of a design procedure for cables used for lowering or raising heavy loads to or from the deep ocean floor.

The cable and load system considered herein is a part of the overall lowering system consisting of the vessel from which the operation is performed, its response to the wave action present during the lowering or raising process, and the resulting oscillations of the cable and load. Within existing theoretical limitations of knowledge about waves and ship motions, and under the restrictions of a linear theory, the problem of the response of a ship or platform to a particular sea state has been solved in terms of certain probabilistic models by Kaplan and Putz.[2] Pierson and Holmes[3] in a note on the engineering applications of the Kaplan and Putz report outlined a procedure for the determination of the response of a drilling barge to sea states 3, 4, and 5. The results are obtained in terms of the probability of occurrence of various amplitudes of motion in heave, surge, sway, yaw, pitch, and roll. The Cuss-I ocean-bottom drilling barge was used as an example, but the calculations as carried out by Kaplan and Putz may be applied to other ships or moored platforms, given the use of a digital computer.

Details of the program, which was written for an IBM 1620 computer, are given in Appendix C. For the purposes of this analysis, the calculations were divided into sections based on the relative values of ω' required for prototype computations.

Equation 6b relates the required range of ω' to the length of and velocity of sound in the cable. It is assumed that ω, the frequency of oscillation of the cable-suspension point, has a maximum value on the order of 2.00 radians per second and that the maximum length of the cable is 20,000 feet. Then the required range of ω' is determined by the velocity of sound, c, in the cable. For steel and polypropylene cables, c is approximately 12,000 and 2,000 feet per second respectively, resulting in maximum nondimensional frequencies of 3.33 and 20.00.

Initially the range of β was chosen as 0.10 to 7.00, and values of μ equal to 0.10, 0.50, 1.00, 2.00, 5.00, and 10.00 were used. Preliminary computations for a typical design problem indicated that lower values of μ would also be required, and corresponding additional computations were carried out as shown in the results which follow.

Pierson and Holmes indicate the methods whereby the root-mean-square (RMS) values of motion in each mode for each sea state may be determined. For the purposes of this report, the oscillation of most concern is that in heave, and knowing the RMS value of heave motions in sea state 4, for example, estimates can be made of the extreme value of heave to be expected in a given time. This procedure thus provides a basis for specifying the range of $|U_o|$ to be used in determining values for use in the design computations. The correlation between sea, ship, and cable stresses is discussed further later on in the text in the application of the results obtained herein to two hypothetical prototype cases.

RESULTS

As illustrated above in the theoretical analysis, the parameters influencing the dynamic stresses can be tabulated as follows:

Cable Parameters

L_{max} = maximum length of cable

S = material cross-sectional area of cable

w = weight of cable per unit length

E = modulus of elasticity of cable

Σ_d = allowable maximum dynamic stress in the cable

Load Parameters

M = mass of the load

A = cross-sectional area of the load

C_m = coefficient of mass

C_D = coefficient of drag

ρ = density of sea water

Ship or floating Platform Motions in Heave

$|U_o|$ = amplitude of heave

ω = frequency of heave (rad/sec)

These specific variables are combined as follows:

$$\beta = \frac{4 C_D \rho A}{3 \pi C_m M} |U_o| \tag{11}$$

$$\mu = \frac{w L}{M_a} \tag{4b}$$

$$\omega' = \frac{\omega L}{c} \tag{6b}$$

and

$$\left|\Sigma'_{max}\right| = \frac{L \Sigma_d}{|U_o| E} \tag{12}$$

Values of the normalized amplitude of the maximum dynamic stress, $|\Sigma'_{max}|$, were calculated for four ranges of nondimensional frequency, ω'. The ranges were as follows:

$\pi/5 \leq \omega' \leq 7.0\pi$ in increments of $\pi/5$

$\pi/10 \leq \omega' \leq 1.4\pi$ in increments of $\pi/10$

$0 \leq \omega' \leq \pi/2$ in increments of $\pi/10$

$0 \leq \omega' \leq 0.10$ in increments of 0.01

The specific values of μ used in the computations were 0.005, 0.01, 0.03, 0.05, 0.10, 0.50, 1.00, 2.00, and 5.00. For low ranges of ω', additional values of μ were used as shown on the appropriate graphs. At each value of μ, calculations were performed for β = 0.10, 0.30, 0.50, 0.70, 1.00, 3.00, 5.00, and 7.00 over the two higher ranges of ω', and values of β = 0.25, 0.50, 1.00, 3.00, 5.00, and 7.00 over the two lower ranges of ω'. The results of these computations are presented in Figures 2 through 7 for the lowest range of ω' and in Figures 8 through 13 for the second lowest range. For the range $\pi/10 \leq \omega' \leq 1.4\pi$, it was found that the stress calculated at values of ω' near π were zero. Figure 14 illustrates this discontinuity. In order to investigate this behavior, Equations 7, 8, 9, and 10 were combined and evaluated as ω' approached $n\pi$, where n = 1, 2, 3,... Details of this evaluation are given in Appendix B, the result being given in the form

$$\lim_{\omega' \to n\pi} (\Sigma'_{max})^2 = (n\pi)^2 \left[1 + K \left\{ \frac{1}{2}\beta^2 K - \frac{1}{2K} - \frac{K}{2} + \left[1 + \left(\frac{1}{2}\beta^2 K + \frac{1}{2K} - \frac{K}{2} \right)^2 \right]^{1/2} \right\} \right] \tag{13}$$

where β is the parameter defined previously, Equation 11, and $K = n\pi/\mu$. The solid dot in Figure 14 is the stress calculated from Equation 13 at that particular value of β and μ. The values of $|\Sigma'_{max}|$ as determined from Equation 13 were used in plotting Figures 15 through 22 as and when necessary. The apparent discrepancies in the computer calculations are considered to be due to rounding-off errors inherent in the computational procedures.

Figure 23 is included to indicate the variation of $|\Sigma'_{max}|$ with β for a particular value of μ. Figure 24 shows the variation of maximum dynamic stress for the highest frequency range $\pi/5 \leq \omega' \leq 7.0\pi$ for particular values of β and μ. As can be seen, the maximum dynamic stress is highly dependent upon the nondimensional frequency. Since in any application of these curves the peak values of $|\Sigma'_{max}|$ must be considered, the results for this range of frequencies are presented in a simplified form in Figures 25 through 32, where each curve is drawn through the maximum values of $|\Sigma'_{max}|$ in the same manner as the dashed line in Figure 24. Each graph is drawn for various values of μ at a given β. In certain instances, it was again found necessary to determine $|\Sigma'_{max}|$ at frequencies near π and its multiples by use of Equation 13.

DISCUSSION OF RESULTS

The results obtained from the computer program as outlined above are generally in agreement with those quoted in the A. D. Little report[1] except for values of the normalized maximum dynamic stress, $|\Sigma'_{max}|$, corresponding to nondimensional frequencies, ω', near or equal to 3.142. The computation of $|\Sigma'_{max}|$ at $\omega = \pi$ according to Equation 13 gave results which compare favorably with those obtained from the computer program. A comparison of three typical results is given in Table I.

It should be noted that the value of $|\Sigma'_{max}|$ computed from Equation 13 is not necessarily the peak value, since resonance will occur at nondimensional frequencies other than π depending upon the values of β and μ. When μ approaches zero, the resonant frequencies approach π, 2π, 3π, etc, and the value of $|\Sigma'_{max}|$ as determined from Equation 13 may then be interpreted as the maximum value. This can be seen to be true by inspection of Figures 15 through 22.

Table I. Comparison of Typical Values of $|\Sigma'_{max}|$ as Computed by Digital Computer Program and as Calculated From Equation 13

β	μ	$\lvert\Sigma'_{max}\rvert$ Computed by Digital Computer Program	$\lvert\Sigma'_{max}\rvert$ Calculated from Equation 13	Percentage Difference
0.50	0.10	112.1	110.1	1.80
1.00	0.10	142.32	139.5	2.01
5.00	0.10	514.09	503.5	2.10

The parameters β and μ are representative of the damping and the ratio of the weight of the cable to the virtual mass of the load respectively. As was noted in the A. D. Little report, the variations of $|\Sigma'_{max}|$ with ω', β, and μ are in agreement with known results for simpler systems. As the mass of the load is decreased, i.e., $\mu \to \infty$, the system reduces to that of a free-ended spring, with the resonant frequencies approaching $\pi/2$ and $3\pi/2$, etc. As the mass is increased, $\mu \to 0$, the resonant frequencies approach π, 2π, etc., which agrees with the case of a fixed-ended spring.

The damping parameter, β, has a slight effect on the resonant frequencies but a far more important effect on the amplitude of $|\Sigma'_{max}|$ at resonance. A conclusion in the A. D. Little report indicated that the maximum dynamic stress amplitude at resonance increases when the damping is increased beyond a certain value. From the above calculations it can be seen that the amplitude at resonance increases generally with increased damping; i.e., there is no minimum amplitude as implied by the above conclusion. This result is compatible with the concept that as the damping increases, the system becomes equivalent to a fixed-ended spring giving resonances at π, 2π, etc., and amplitudes tending to infinity, restricted only by internal and external damping of the cable. This argument considers the damping effects, a function of β, to be divorced from the inertial effects, which are dependent upon μ.

In view of the dependence of the maximum dynamic stress amplitude on β, and since β depends on the parameters of the load — i.e., the cross-sectional area, the mass, and the density of sea water, which are fixed — and on the coefficient of drag, the value of C_D assumed for a given load configuration is of particular importance. This can be seen from the results given above where a change of β from 1.00 to 3.00 results in a change in $|\Sigma'_{max}|$ at resonances from 142 to 370. If $|\Sigma'_{max}|$ is interpreted as an allowable stress which when exceeded results in an unsafe condition for the operation, as implied in the design procedure which follows, then the value of C_D used in the calculation of β becomes critical. For poor hydrodynamic shapes such as blunt bodies or open frameworks, it is not possible within the present state of development of theoretical fluid dynamics to calculate C_D from the basic equations of fluid flow. The alternative, therefore, is

to resort to an experimental determination of the coefficients of drag for the particular load configuration in question, for both steady and oscillatory motions. There exists little experimental data on the appropriate coefficients of drag applicable to typical load shapes being lowered to the deep ocean floor. A series of experiments directed toward obtaining such data thus appears justified.

Similar arguments also apply to the values assumed for the coefficient of added mass, C_m. Summaries of information pertinent to the determination of the drag and added mass coefficients are presented in Appendixes D and E respectively.

The shape of each curve determined from Equations 7, 8, 9, and 10 differs from those obtained for linear systems in that a second peak in the normalized maximum dynamic stress occurs at nondimensional frequencies on the order of 0.10 to 0.40. The significance of such a secondary peak, which is termed herein a subharmonic response, is more easily discussed in relation to a specific design example. Two such examples are given below following a proposed design procedure.

PROPOSED DESIGN PROCEDURE

The parameters required in the design procedure are those applicable to the load and the cable. They may be tabulated as follows:

Load Parameters

M = mass of the load

A = cross-sectional area of the load in the direction of motion (ft^2)

C_D = coefficient of drag applicable to the load

C_m = coefficient of added mass applicable to the load

Cable Parameters

L_{max} = maximum length of cable (ft)

w = weight of cable per unit length (lb/ft)

E = modulus of elasticity for the cable ($lb/in.^2$)

Σ_{ult} = ultimate tensile strength of the cable ($lb/in.^2$)

F = safety factor for maximum operating stress in the cable

ρ = density of sea water (lb/ft^3)

From the above parameters, the following may be determined:

$$\Sigma_d = \frac{\Sigma_{ult}}{F} - \Sigma_{static} \tag{1}$$

where Σ_{static} equals the static stress in the cable, including that due to the cable itself at L_{max}, and Σ_d equals the operational maximum dynamic stress allowable with a cable of ultimate tensile stress, Σ_{ult}, and a safety factor of F.

$$c = \sqrt{\frac{E}{\rho_c}} \tag{2}$$

the velocity of sound in the cable in feet per second; and

$$k = \frac{4 C_D \rho A}{3 \pi C_m M} \tag{3}$$

a constant. Since the cable length varies from zero to L_{max} and because the design must be valid for all lengths, several values of L should be chosen ($L = L_n$, where $n = 1, 2, 3, \ldots$) between zero and L_{max}. Hence, values of $\mu_n = wL_n/C_m M$ may be calculated.

Values of $|U_o|$, the amplitude of the cable support-point oscillation, may be selected as $|U_o| = 1.0, 2.0, 5.0, 10.0$ feet. A table may then be set up, as illustrated by Table II, for each μ_n corresponding to the selected L_n.

Table II. Outline of Table for Computation of Relationship Between Frequency and Amplitude of Oscillations, Given μ, L, c, and k

(For $\mu = \mu_1$, $L = L_1$, $c/L = c/L_1$)

Column 1	Column 2	Column 3	Column 4	Column 5
$\lvert U_o \rvert$ (ft)	$\beta = k\lvert U_o \rvert$	$\left\lvert \Sigma'_{max} \right\rvert = \frac{L \Sigma_d}{\lvert U_o \rvert E}$	ω'	$\omega = \frac{\omega' c}{L}$
1.0 2.0 5.0 10.0 15.0				

The use of the table is as follows. Column 1 consists of the amplitudes of the cable support-point oscillations as selected above, and from this, Column 2 may be calculated by multiplying by k derived previously. Column 3 is computed for the given L, Σ_d, $|U_o|$, and E values appertaining to the cable. For polypropylene or nylon cables, it may not be possible to determine Σ_d and E directly. Manufacturers' tables generally allow the computation of S Σ_d and S E, where S is the material cross section of the cable. Hence, the constant ratio Σ_d/E may be determined and used in Column 3.

Column 4 is obtained from the curves of Figures 2 to 7, 8 to 13, 15 to 22, and 25 to 32 for the particular values of μ and β given in the table. Column 5 is evaluated from Column 4 for the particular ratio of c/L_n. Thus, from Columns 1 and 5 a curve relating the allowable amplitude of oscillation to the frequency of that oscillation may be drawn for the particular cable length used. The process may then be repeated for other cable lengths. A judicious choice of cable length can serve to reduce the numerical calculation to a minimum.

It may be assumed that operating conditions lying on or below the curve are safe, with the safety factor, F, as defined, and that operating conditions lying above, to the right of, the curve are unsafe.

In line with comments raised in the Discussion of Results, the unknown parameters are C_D and C_m. With existing deficiencies in data giving C_D and C_m for various load configurations, they must of necessity be estimated. See Appendixes D and E.

If it should occur in a design problem that the ranges of ω', β, or μ are not covered in the graphs developed in this study, then the appropriate curves may be calculated for specific values, or ranges of values, of those parameters by use of the digital computer program used in obtaining the results quoted herein. Details of this program are given in Appendix C.

Two examples of the application of the above design procedure are given below.

APPLICATION OF PROPOSED DESIGN PROCEDURE TO TWO PROTOTYPE EXAMPLES

The application of the proposed design procedure to two hypothetical prototype examples is demonstrated below for polypropylene and steel cable respectively. The parameters used in these examples are such as to enable the design procedure to be carried out using the curves presented previously in the results.

Design Example Using Polypropylene Cable

The parameters of the load are given as

$$M = 5.0 \text{ tons} = 10,000 \text{ lb}$$

$$A = 12 \text{ ft} \times 12 \text{ ft} = 144 \text{ ft}^2$$

$$C_D = 2.0$$
$$C_m = 1.5$$

The cable parameters chosen are

$$L_{max} = 20,000 \text{ ft}$$
$$w = 0.90 \text{ lb/ft}$$
$$SE = 240,000 \text{ lb}$$
$$S\Sigma_d = 10,000 \text{ lb}$$
$$c = \left(\frac{E}{\rho_c}\right)^{1/2} = \left(\frac{SE}{w}\right)^{1/2} = 2,930 \text{ ft/sec}$$
$$k = \frac{4 C_D \rho A}{3\pi C_m M} = 0.50$$

and, therefore, $\beta = 0.50 |U_o|$.

The cable data used herein was obtained from the August 1964 "Braided Rope and Cordage Catalog" of the Samson Cordage Works, Boston, Mass. It is now convenient to select cable lengths such that values of μ, where $\mu = wL/M_a$, coincide with those used in deriving the curves presented previously in the results. These values are given in Table III.

Table III. Cable Lengths Used in Design Example for Polypropylene Cable

L (ft)	μ	c/L
16,660	1.00	0.1758
8,330	0.50	0.3516
1,660	0.10	1.7580
833	0.05	3.5160
166	0.01	17.5800

It is now possible to set up Table IV corresponding to Table II given in the proposed design procedure by specifying that input amplitudes of oscillation, $|U_o|$, of 1.0, 2.0, 6.0, 10.0, and 14.0 feet will be considered. Knowing that $\beta = k |U_o|$, Column 2 of Table IV may be calculated. The values of $|\Sigma'_{max}| = L\Sigma_d / |U_o| E$ can be derived for appropriate values of L and $|U_o|$ as shown in Column 3 of the table.

From inspection of the table, it can be seen that in view of the relationship between the various cable lengths chosen, values of $|\Sigma'_{max}|$ at these different lengths are quite simply related — thus facilitating the design calculations.

Values of the nondimensional frequency, ω', are then entered in Column 4 by the use of Figures 2 to 13, 15 to 22, and 25 to 32. That is, for a particular μ and β, the value of ω' corresponding to $|\Sigma'_{max}|$ may be found. Hence, the circular frequency, ω, can be calculated and entered in Column 5. From the completed table, the relationship as a function of cable length, can be drawn between input amplitude of oscillation, $|U_o|$, and the allowable circular frequency, ω, of that amplitude — i.e., the circular frequency at which the oscillation can occur such that the maximum dynamic stress in the cable is less than or equal to the design dynamic stress. Figure 33 shows this relationship for the computation given in Table IV. The significance of these results is discussed below together with that of the following design example.

Design Example Using Steel Cable

The relevant load parameters are given as follows:

$$M = 20 \text{ tons} = 40,000 \text{ lb}$$

$$A = 600 \text{ ft}^2$$

$$C_D = 2.0$$

$$C_m = 1.5$$

The appropriate cable parameters were chosen to be

$$L_{max} = 20,000 \text{ ft}$$

$$\rho_c = 550 \text{ lb/ft}^3$$

$$w = 7.64 \text{ lb/ft}$$

$$E = 15 \times 10^6 \text{ psi}$$

$$\Sigma_d = 40,000 \text{ psi}$$

$$c = 11,200 \text{ ft/sec}$$

$$k = \frac{4 C_D \rho A}{3 \pi C_m M} = 0.50$$

and, therefore, $\beta = 0.50 |U_o|$.

Table IV. Design Calculations for 10,000-Pound Load to 20,000 Feet Using Polypropylene Cable

U_o (ft)	β	$\Sigma = \frac{L\Sigma_d}{\lvert U_o \rvert E}$	ω'	ω	$\Sigma = \frac{L\Sigma_d}{\lvert U_o \rvert E}$	ω'	ω	$\Sigma = \frac{L\Sigma_d}{\lvert U_o \rvert E}$	ω'	ω
		$L = 16,660$ ft $\mu = 1.00$ $c/L = 0.1758$			$L = 8,330$ ft $\mu = 0.50$ $c/L = 0.3516$			$L = 1,660$ ft $\mu = 0.10$ $c/L = 1.758$		
1	0.50	694.2	7.75π	4.281	347.1	3.88π	4.286	69.42	0.995π	5.496
2	1.00	347.1	4.88π	2.695	173.5	2.50π	2.762	34.71	0.980π	5.414
6	3.00	115.7	1.95π	1.077	57.85	0.995π	1.099	11.51	0.925π	5.109
10	5.00	69.42	1.20π	0.663	34.71	0.782π	0.864	6.942	0.880π	4.861
14	7.00	49.58	0.990π	0.547	24.79	0.725π	0.800	4.958	0.835π	4.613
		$L = 833$ ft $\mu = 0.05$ $c/L = 3.516$			$L = 166$ ft $\mu = 0.01$ $c/L = 17.58$			$L = 83.3$ ft $\mu = 0.005$ $c/L = 35.16$		
1	0.50	34.71	0.975π	10.77	6.94	0.875π	48.34	3.47	0.76π	83.95
2	1.00	17.35	0.945π	10.44	3.47	0.76π	41.98	1.735	0.57π	62.97
6	3.00	5.79	0.855π	9.44	1.15	0.0780	1.371	0.579	0.0295	1.037
10	5.00	3.47	0.750π	8.285	0.694	0.0410	0.721	0.347	0.0180	0.633
14	7.00	2.48	0.68π	7.511	0.496	0.0280	0.492	0.248	0.0130	0.457

As in the first example, cable lengths are chosen to give values of μ coincident with those used in the calculation of Figures 2 to 13, 15 to 22, and 25 to 32. These lengths and the corresponding values of μ and c/L are given in Table V.

Table V. Cable Lengths Used in Design Example for Steel Cable

L (ft)	μ	c/L
15,700.0	2.000	0.713
7,850.0	1.000	1.426
3,925.0	0.500	2.850
1,963.0	0.250	5.600
785.0	0.100	14.260
393.0	0.050	28.500
236.0	0.030	47.500
78.5	0.010	142.600
39.3	0.005	285.000

A similar table to that derived in the previous design example may now be set up and the numerical computations performed as above. These calculations are summarized in Table IV, and the relationship between the input amplitude of oscillation, $|U_o|$, and the allowable circular frequency, ω, of that amplitude is illustrated in Figure 34.

DISCUSSION OF RESULTS OF THE APPLICATION OF THE PROPOSED DESIGN PROCEDURE

Figures 33 and 34 show the results obtained in the application of the proposed design procedure to the two hypothetical cases described above.

In any load-lowering operation, the cable used will have a certain known ultimate load at which the cable could be expected to break. With repeated use of a particular cable, this ultimate load will decrease. Hence, for any lowering operation a safety factor must be chosen defining a load, or corresponding stress, which should not be exceeded. This allowable working stress is assumed to include static stress due to both the load and cable — the latter being negative in the case of a buoyant cable such as polypropylene — and the dynamic stress.

This discussion and the design procedure proposed earlier in the report are based on the assumption that a particular maximum dynamic stress is given which should not be exceeded during the lowering or raising operation.

Figures 33 and 34 indicate the allowable frequency of an input oscillation at various amplitudes of this oscillation as a function of the cable length, such that the stipulated maximum dynamic stress is not exceeded. Alternatively, they indicate the maximum amplitude of an input oscillation at a particular frequency such that a maximum dynamic stress is not exceeded.

One of the most important problems in the interpretation of these graphs is the selection of appropriate input conditions, $|U_o|$ and ω, corresponding to the response of the vessel used for the lowering or raising operation of the sea state in which the operation is carried out.

It is apparent that the frequency range given in Figures 33 and 34 is far greater than that which would be expected under operational conditions. Data is available in the literature (Kaplan and Putz,[2] Pierson and Holmes[3]) on the response of the Cuss-I drilling barge to various sea states. In sea state 5, the range of frequencies of oscillation in heave is 0.40 to 1.40 radians per second with root-mean-square values of heave of 1.8 and 1.3 feet at headings of 90 degrees and 0 degrees to the wind respectively. These values imply expected maximum amplitudes of oscillation of 7.2 and 5.2 feet during a 4-hour period on station (Pierson and Holmes). It should be noted, however, that combinations of heave and roll oscillations could easily produce oscillations greater than this if the load-lowering operation is carried out using the boom over the side of the vessel. The above values are used here to illustrate the interpretation of Figures 33 and 34.

Referring to Figure 33 for the design example using a polypropylene cable, it can be seen that for a heave amplitude of 7.2 feet at frequencies of 1.40 and 0.40 radians per second — to cover the entire frequency range — the design dynamic stress will be exceeded at a cable length of less than 200 feet for $\omega = 1.40$. For frequencies less than 1.40 radians per second down to 0.40 radian per second, it is estimated from the curves that the design dynamic stress will be exceeded at cable lengths which gradually decrease from 200 feet. Thus the operation will be unsafe relative to the prescribed maximum dynamic stress for a cable length of less than 200 feet. This condition has been fully recognized in the design of various lowering operations conducted by this laboratory. The dynamic stress will then be less than the design stress until the length of the cable reaches a value of approximately 5,000 feet. According to the results obtained above the operation will then become unsafe, if the frequency is 1.40 radians per second and the amplitude is 7.2 feet.* For a frequency of 1.00 radian per second the operation becomes unsafe at a depth of 7,000 feet. The reasons for this result are difficult to visualize, but may be explained from both the mathematical and physical points of view. In terms of the numerical computations carried out as shown in Table VI, the regression of the curves given in Figures 33 and 34 is due to the fact that when the maximum dynamic stress,

* These comments are based on an approximate interpolation between the curve labeled 6 feet and 10 feet in Figure 33 for $|U_o| = 7.2$ feet.

$|\Sigma'_{max}|$, increases, say doubles, due to an increase in the cable length of L to twice L, the appropriate nondimensional frequency, ω', at the corresponding value of μ is not twice the ω' at the shorter length. This results in a lower circular frequency, ω, at the longer cable length. This applies to the larger values of $|\Sigma'_{max}|$ corresponding to these lengths. A similar argument applies at cable lengths lower than 200 feet. For intermediate cable lengths a relatively small variation in $|\Sigma'_{max}|$ results in a significant increase in ω', resulting in an increase in the circular frequency, ω. This applies to a range of ω' from 0.4π to 0.8π — i.e., to values of $|\Sigma'_{max}|$ larger than those corresponding to the first peak in Figures 2 to 13 and 15 to 22, but less than those associated with the peak responses occurring at ω' approximately equal to 3.142. As ω' values tend toward this value, significant changes in $|\Sigma'_{max}|$ result in larger variations in circular frequency for different cable lengths due to the influence of the c/L ratio in computing the latter. Hence the variation of cable stress with cable length depends upon the shapes of the computed curves relating $|\Sigma'_{max}|$ to ω'.

The physical behavior of the cable assembly may be described by reviewing the significant results obtained by Little[1] and by Whicker.[4] The latter is a rather simplified (i.e., no damping) theoretical analysis of the effect of ship motion on mooring cables in deep water. On Figure 33, values of ω' corresponding to $\pi/2$ and π are indicated, as well as the roots of the equations $\tan\omega' = \mu/\omega'$ and $\tan\omega' = -\mu/\omega'$. The case of the fixed-ended spring for zero damping ($\beta = 0.0$) is shown by Whicker and by Little to have resonant frequencies of $\omega' = \pi, 2\pi, \ldots n\pi$ when the relative mass, μ, of the cable and payload is decreased infinitely (i.e., the payload mass increases indefinitely). The case of the free-ended spring for zero damping ($\beta = 0.0$) is represented by:

1. Values of ω' equal to $\pi/2, 3\pi/2 \ldots n\pi/2$ when the relative mass is increased indefinitely. When the damping $\beta = 0.0$, it is shown by Little that values of ω' equal to $\pi/2, 3\pi/2 \ldots n\pi/2$ result in infinite dynamic stress for infinitely large values of μ.

2. Values of ω' corresponding to the roots of the equation $\tan\omega' = -\mu/\omega'$. Whicker shows that for finite values of μ, the least root of the above equation results in infinite total stress.

In addition, Little shows that for finite values of μ, and for zero damping, infinite total stress will result when the roots of the equation $\tan\omega' = \mu/\omega'$ are satisfied. This is in contrast to the results given by Whicker, yet both formulations appear to be correct. Thus, it would appear that the Little and Whicker results are compatible for long cable lengths, but that the Whicker results are not applicable for short lengths, since all of recorded data supports Little's conclusions. In any event, the least of the roots of the above equation lies between 0 and $\pi/2$. As μ is increased indefinitely, the roots of the above equation approach $\pi/2, 3\pi/2 \ldots n\pi/2$. There is no comparable analogy with the well-known results of simpler systems.

Table VI. Design Calculations for 40,000-Pound Load to 20,000 Feet Using Steel Cable

U_o (ft)	β	$\Sigma = \frac{L\Sigma_d}{\lvert U_o \rvert E}$	ω'	ω	$\Sigma = \frac{L\Sigma_d}{\lvert U_o \rvert E}$	ω'	ω	$\Sigma = \frac{L\Sigma_d}{\lvert U_o \rvert E}$	ω'	ω
		L = 15,700 ft μ = 2.00 c/L = 0.713			L = 7,850 ft μ = 1.00 c/L = 1.426			L = 3,925 ft μ = 0.50 c/L = 2.850		
1	0.50	41.85	2.75π	6.16	20.93	1.40π	6.27	10.46	0.95π	8.50
2	1.00	20.93	1.71π	3.83	10.46	0.98π	4.39	5.23	0.87π	7.77
6	3.00	6.98	0.935π	2.09	3.49	0.807π	3.66	1.74	0.56π	5.01
10	5.00	4.18	0.840π	1.88	2.09	0.656π	2.92	1.05	0.17π	1.54
14	7.00	2.99	0.755π	1.69	1.49	0.465π	2.08	0.747	0.095π	0.850
		L = 1,963 ft μ = 0.25 c/L = 5.60			L = 785 ft μ = 0.10 c/L = 14.26			L = 393 ft μ = 0.05 c/L = 28.50		
1	0.50	6.280	0.89π	15.68	2.093	0.62π	27.80	1.046	0.1653	4.710
2	1.00	3.140	0.765π	13.49	1.046	0.203	2.895	0.523	0.1140	3.250
6	3.00	1.047	0.350	1.960	0.349	0.100	1.436	0.174	0.0505	1.439
10	5.00	0.628	0.185	1.035	0.209	0.062	0.884	0.105	0.0320	0.897
14	7.00	0.449	0.130	0.727	0.149	0.045	0.642	0.075	0.0230	0.656
		L = 236 ft μ = 0.03 c/L = 47.5			L = 78.5 ft μ = 0.01 c/L = 142.6			L = 39.3 ft μ = 0.005 c/L = 285.0		
1	0.50	0.6276	0.1020	4.840	0.2093	0.0385	5.490	0.1046	0.0205	5.840
2	1.00	0.3138	0.0715	3.396	0.1046	0.0255	3.636	0.0523	0.0125	3.560
6	3.00	0.1044	0.0305	1.448	0.0349	0.0100	1.426	0.0174	0.0030	0.854
10	5.00	0.0628	0.0190	0.903	0.0209	0.0050	0.713	0.0105	0.0019	0.542
14	7.00	0.0448	0.0140	0.665	0.0149	0.0040	0.570	0.0075	0.0015	0.428

Beginning with large lengths, the cable assembly behaves as a fixed-ended spring, and the role of damping, which is dependent on the input amplitudes, is to provide an additional margin of safety. Thus higher frequencies for the same length at constant input amplitudes can be tolerated without danger of breaking the cable.

As the length decreases, a transition occurs and the cable assembly takes on the characteristics of a free-ended spring. Again the role of damping is to provide an additional margin of safety against failure.

Finally at very short cable lengths, the cable appears to behave like a rigid connection between source and load rather than as a "spring." In this case, the role of damping (drag) is reversed in that, for constant input amplitudes, smaller frequencies can be tolerated than for the case when $\beta = 0.0$.

All of the above trends are confirmed by the calculations for both the damped and undamped cases as the length L approaches zero, as indicated by Figure 33. For comparative purposes, a few results obtained by applying the method developed by Whicker for a free-ended cable are included. The mathematical formulation by Whicker does not include the damping term. Thus a direct comparison of the effect of damping is available.

It is recognized that the analysis used for this investigation — that given in the report by A. D. Little, Inc. — does not accurately describe the prototype situation by virtue of the linearization required in the drag term $|\partial u/\partial t'|(\partial u/\partial t')$, which is necessary in order to solve the basic equation of motion. In the present state of the art concerning nonlinearly damped oscillations there appears to be no alternative to the linearization. Further theoretical analysis is considered necessary and justified in order to resolve the question of safety of lowering systems as the length of the cable increases. Such an analysis would consider the use of analogue computations to allow retention of the nonlinear $|\partial u/\partial t'|(\partial u/\partial t')$ term.

Similar interpretations regarding the safety of a load-lowering operation may well apply at greater depths for lower frequencies if the curves presented in Figure 33 were extended. From the general shape of the curve shown and for a given input amplitude oscillation there is a limiting input frequency below which the operation is safe (the maximum dynamic stress is not exceeded) down to a certain depth. For a particular lowering operation it may be possible to use a working vessel which has little or no response to excitations above this limiting frequency. Alternatively, the operation may be carried out in a lower sea, but this does not necessarily imply a maximum frequency of input oscillation, although it does imply a diminished amplitude of oscillation which would render the operation safe.

A similar discussion may also be applied to Figure 34 for the case of a steel cable, although an unsafe condition is not likely to occur until depths of 20,000 feet even with input amplitudes of 14 feet. In this case, however, an additional factor must be considered, namely the very significant increase in static stress due to the weight of the cable. As far as the dynamic stress is concerned, it may be concluded that the operation may be safe for cable lengths greater than 100 feet when input

amplitudes are less than 6 feet at a maximum frequency of 1.40 radians per second. As the cable length diminishes to zero it would appear that the design dynamic stress will be exceeded by an increasingly large amount. From Figures 33 and 34 it is seen that for both examples at shorter lengths of cable, a greater amplitude of oscillation is relatively less safe than a small amplitude, as expected. Further calculations are required to determine the form of the curves as the cable length approaches zero.

On 13 April 1965, a Submersible Test Unit (STU) loaded with racks of specimens was lowered to a depth of 2,500 feet by the Deep Ocean Engineering Division of NCEL. The record of cable tensions during the lowering operation is shown on Figure 35. The weight of the load in water was approximately 5,500 pounds, the structure being in the form of an open truss, its base consisting of two flat plates with a total cross-sectional area of approximately 150 square feet. The load was lowered on a 1.3-inch-diameter polypropylene cable. From a depth of 450 feet the descent was carried out at a steady rate of 132 feet per minute. At depths shallower than 450 feet the lowering operation was intermittent. The wave excitation was estimated to be in the form of a 6- to 10-foot swell with periods of 10 to 12 seconds. A brief discussion of various properties of the record in the light of the calculations given above is pertinent. The parameters of the cable and load were approximately those used for the first design example, although values of the coefficients of drag and virtual mass do not necessarily agree.

The record shows an expected decrease of dynamic stress with increasing depth. The immediate reduction in the mean load at point B of approximately 2,000 pounds corresponds to a drag force on the structure with a coefficient of drag equal to 2.76 at a vertical velocity of 132 feet per minute. Since the load consisted of racks of specimens orientated parallel to the flow, this drag coefficient is not necessarily that corresponding to form drag alone; however, the contribution of tangential drag on the cable can be shown to be negligible. The steady reduction of mean load from 450 to 2,500 feet is due to the gradual removal of the weight of a 2,500-foot-long steel cable suspended from the base of the STU to the ocean floor.

From the design example given previously the expected maximum dynamic stresses in the lowering cable were calculated at cable lengths of 83, 830, and 1,660 feet assuming that $|U_o|$ equals 6.0 feet. Table VII summarizes these computations which were carried out for each cable length by determining the period of the cyclic stress from the record. Values of $|\Sigma'_{max}|$ were then found from the curves given in the results, for the appropriate β and μ values. Hence, the maximum dynamic stresses were determined as shown in Table VII and superposed on the stress record as given in Figure 35.

In view of the uncertainty with respect to values of C_D, C_m, and $|U_o|$ for the operation represented by Figure 35, the comparison of the calculated dynamic stresses with those determined experimentally is considered to be fair. It is noted that at 830 and 1,660 feet the stresses recorded exceed those calculated by a factor of 2. As the load is lowered, only one variable changes, that being the cable length.

However, the frequency and amplitude of the cyclic stress change with cable length. This may well result in a significant change in the coefficient of drag and mass since the amplitude and velocities of vertical oscillation will vary. This is possibly one cause of the discrepancies noted.

Table VII. Summary of Calculations for STU Lowering Operation to 2,500 Feet

Cable Length, L	83.0 ft	830.0 ft	1,660.0 ft
Parameter, μ	0.005	0.05	0.10
Parameter, β	3.00	3.00	3.00
c/L	0.0283	0.283	0.566
Period of Oscillation, T	5.45 sec	8.00 sec	9.23 sec
Frequency of Oscillation, ω	1.153 rads/sec	0.786 rad/sec	0.681 rad/sec
$\omega' = \frac{\omega L}{c}$	0.0326	0.222	0.385
$\left\|\Sigma'_{max}\right\|$ From Curves	0.660	1.165	1.225
$S\Sigma_d$ - Dynamic Load	±3,752.0 lb	±707.4 lb	±371.9 lb
Static Load	5,500 lb	3,400 lb	3,100 lb
Static + Max Dynamic Load	9,252 lb	4,107 lb	3,472 lb
Static - Max Dynamic Load	1,748 lb	2,693 lb	2,728 lb

From the record given in Figure 35 there also appears to be a somewhat irregular, long-period reinforcement of the dynamic stress amplitude. During the lowering operation it was not possible to record the actual motions of the load, and thus any departure from purely vertical motions are unknown. At a lowering velocity of 132 feet per minute it is quite possible that the load motion will become unstable and that sidewise oscillations will occur, giving rise to complex lift forces on the structure with resulting variations in the cable tensions. There is no evidence in Figure 35 to support the result shown in Figure 34 that dynamic stresses may increase at greater depths, because of the limited depth of 2,500 feet to which the STU was lowered. There is a pressing need for a load-lowering operation to be carried out in which both the cable tensions and the load motions are recorded, thus allowing a more definite analysis of the results. Preferably this full-scale experiment would be carried out with a formalized body shape so that coefficients of drag and mass could be more accurately estimated.

FINDINGS

As a result of the investigation described above, it was found that:

1. The theoretical analysis presented by Arthur D. Little, Inc., in Project Trident Technical Report No. 1370863 of the Bureau of Ships[1] was readily adaptable to a design procedure for heavily loaded cables for deep ocean emplacement or recovery operations.

2. This design procedure is relatively straightforward, but the results of its application require confirmation by prototype measurements.

3. The most important unknowns in the input parameters for the design procedure are the coefficients of drag and virtual mass, which at this stage must of necessity be estimates, again requiring confirmation by prototype measurements.

4. For the two prototype examples given, the operations are unsafe with respect to the specified maximum allowable dynamic stresses when the load is between zero and approximately 200 feet below the ocean surface.

5. Using polypropylene cable, there exists a possibility that under certain conditions of motion of the working vessel the operation will again become unsafe at depths on the order of 5,000 feet and greater. The reason is not difficult to visualize. As the length increases the natural period also increases, eventually corresponding to periods of the exciting waves. If the damping is small, very large stresses may be induced by relatively small input amplitudes.

CONCLUSIONS

It is concluded that the proposed design procedure is applicable to heavily loaded cables in deep ocean emplacement or recovery operations. However, the results of its application may not be considered rigorous in view of the estimates of values of coefficients of drag and mass required for the calculations. In order to make the design procedure applicable to a prototype situation with a greater degree of confidence, it is considered necessary to make measurements of cable tensions and load and ship motions during a full-scale operation to provide a basis for comparison between theory and prototype.

ACKNOWLEDGMENTS

Acknowledgment is made to NCEL personnel for their assistance in the preparation of this report: to Mr. W. L. Wilcoxson for assistance in the analysis given in Appendix B; to Mr. R. E. Jones for valuable discussions in relation to the practicalities involved in lowering heavy loads to the deep ocean floor; to Mr. B. J. Muga for overall guidance of the task effort and the preparation of Appendix D; and to Mr. Richard Tu for preparation of Appendix E.

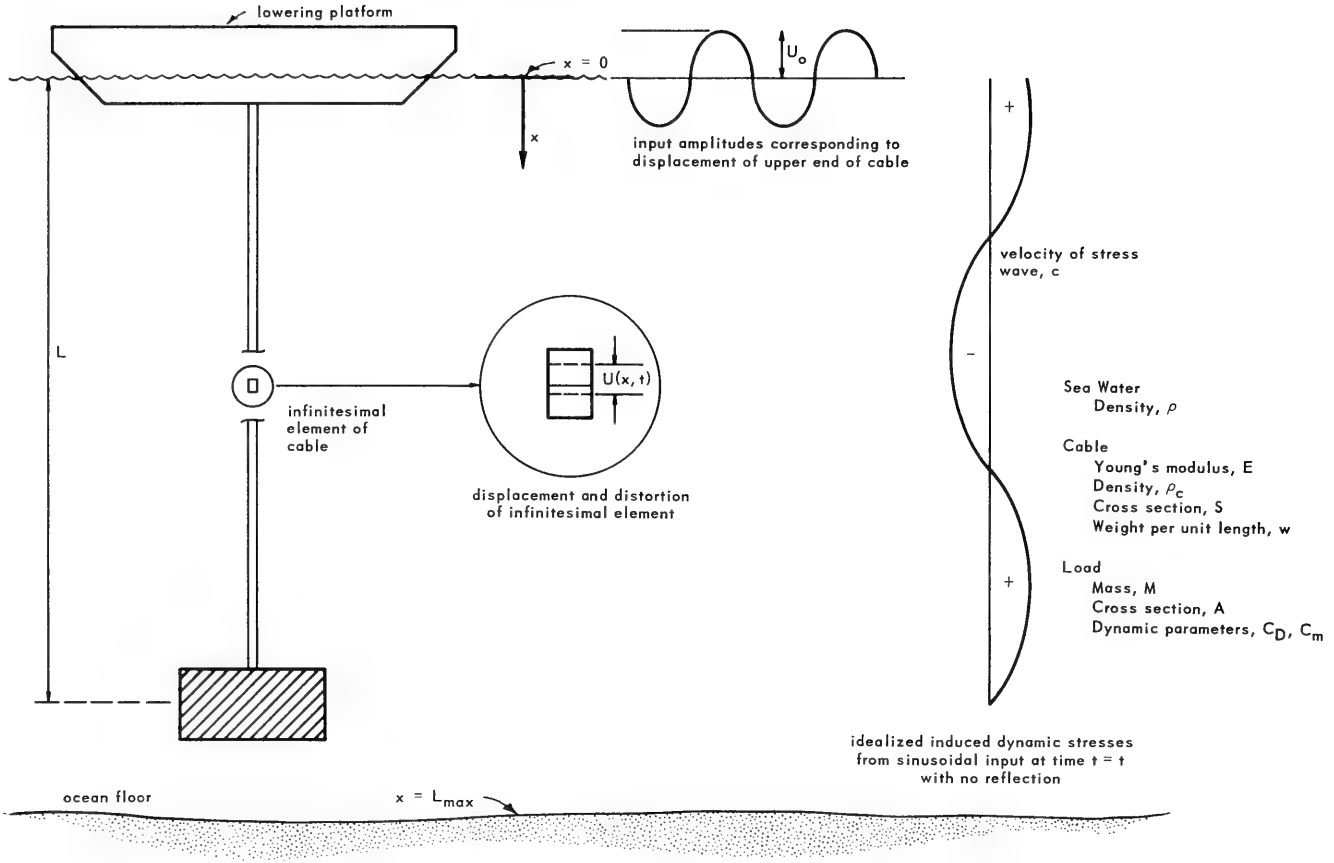

Figure 1. Definition sketch of lowering or raising operation.

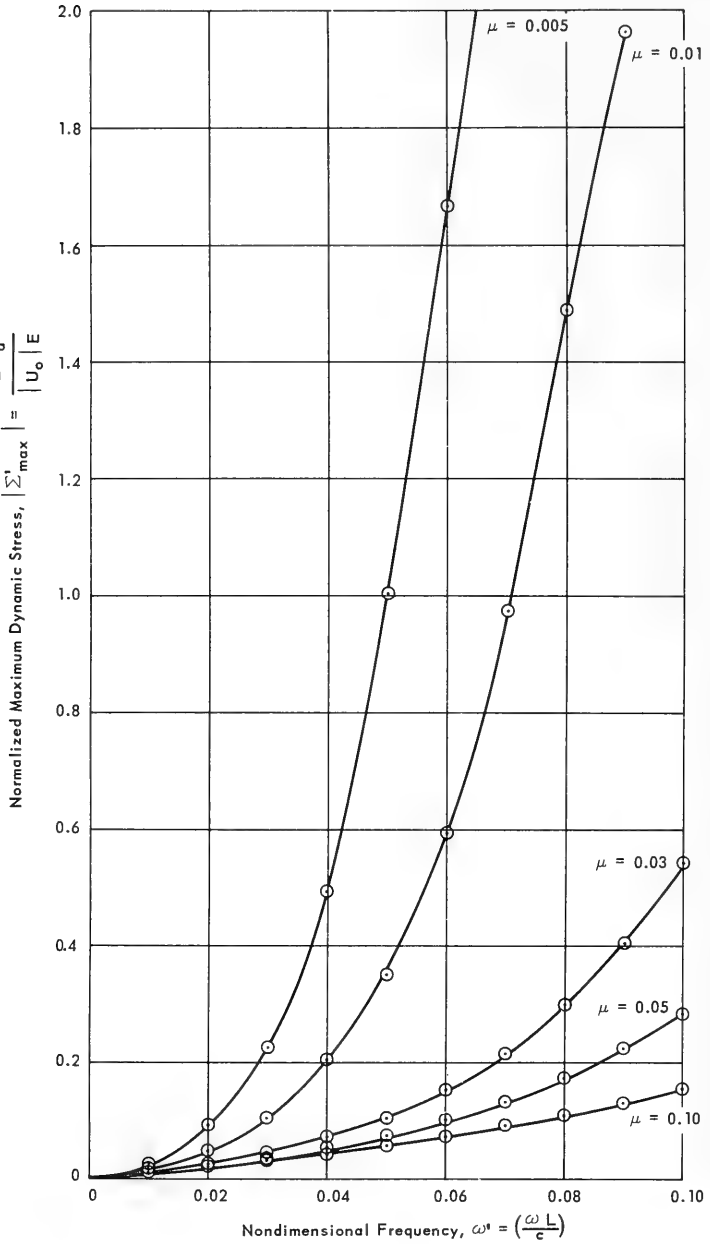

Figure 2. Variation of normalized maximum dynamic stress, $|\Sigma'_{max}|$, with nondimensional frequency, ω', for $\beta = 0.25$ over the range $0 \leq \omega' \leq 0.10$ for values of μ as indicated.

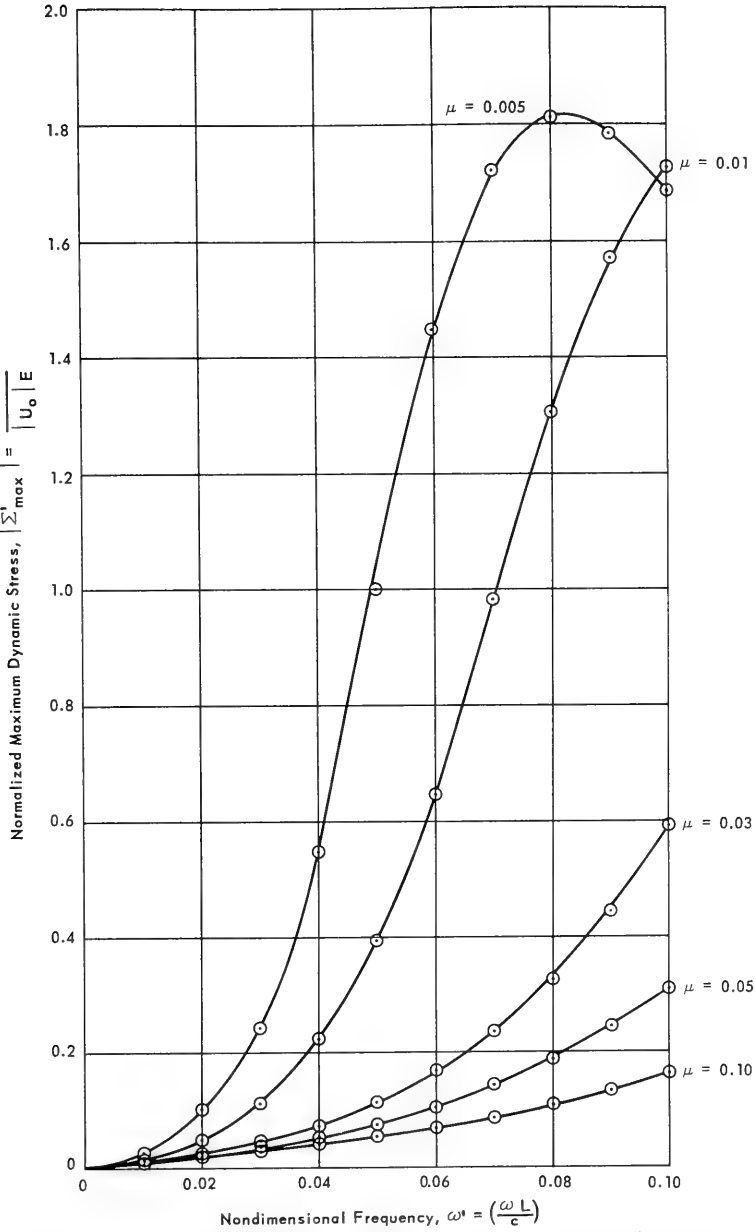

Figure 3. Variation of normalized maximum dynamic stress, $|\Sigma'_{max}|$, with nondimensional frequency, ω', for $\beta = 0.50$ over the range $0 \leq \omega' \leq 0.10$ for values of μ as indicated.

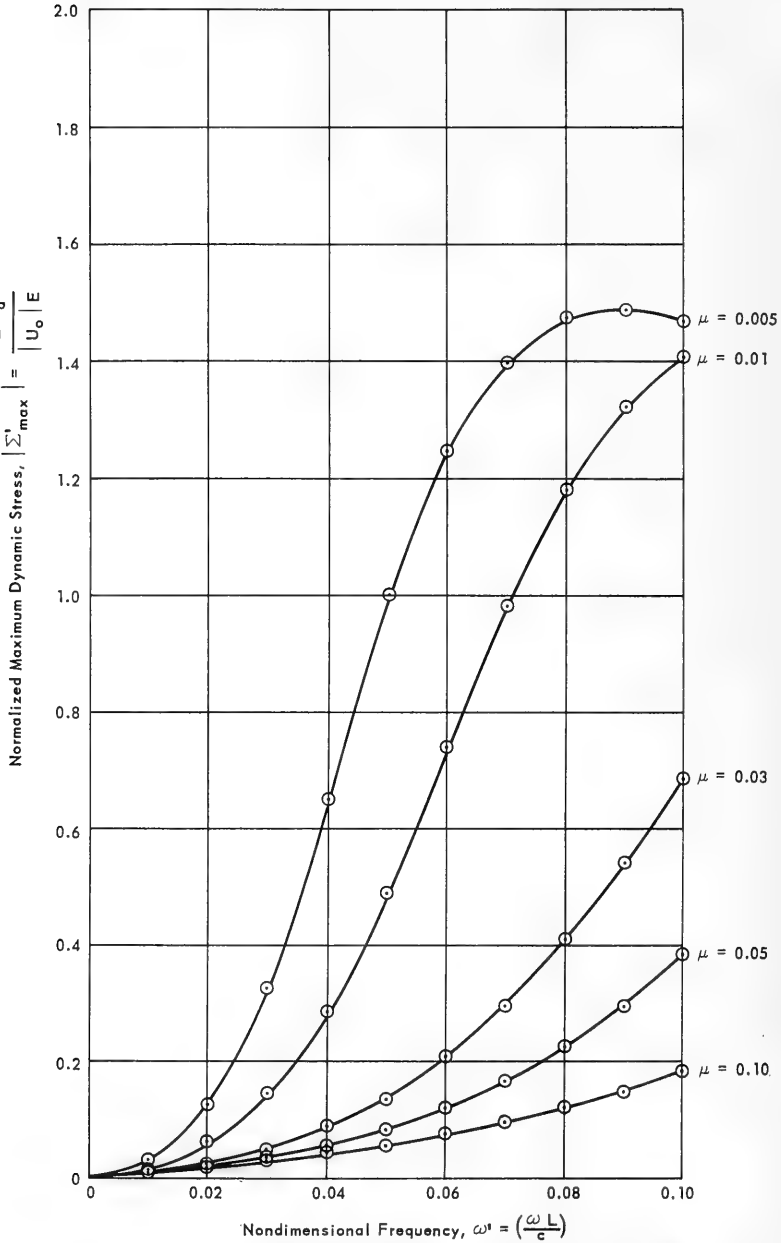

Figure 4. Variation of normalized maximum dynamic stress, $|\Sigma'_{max}|$, with nondimensional frequency, ω', for $\beta = 1.00$ over the range $0 \le \omega' \le 0.10$ for values of μ as indicated.

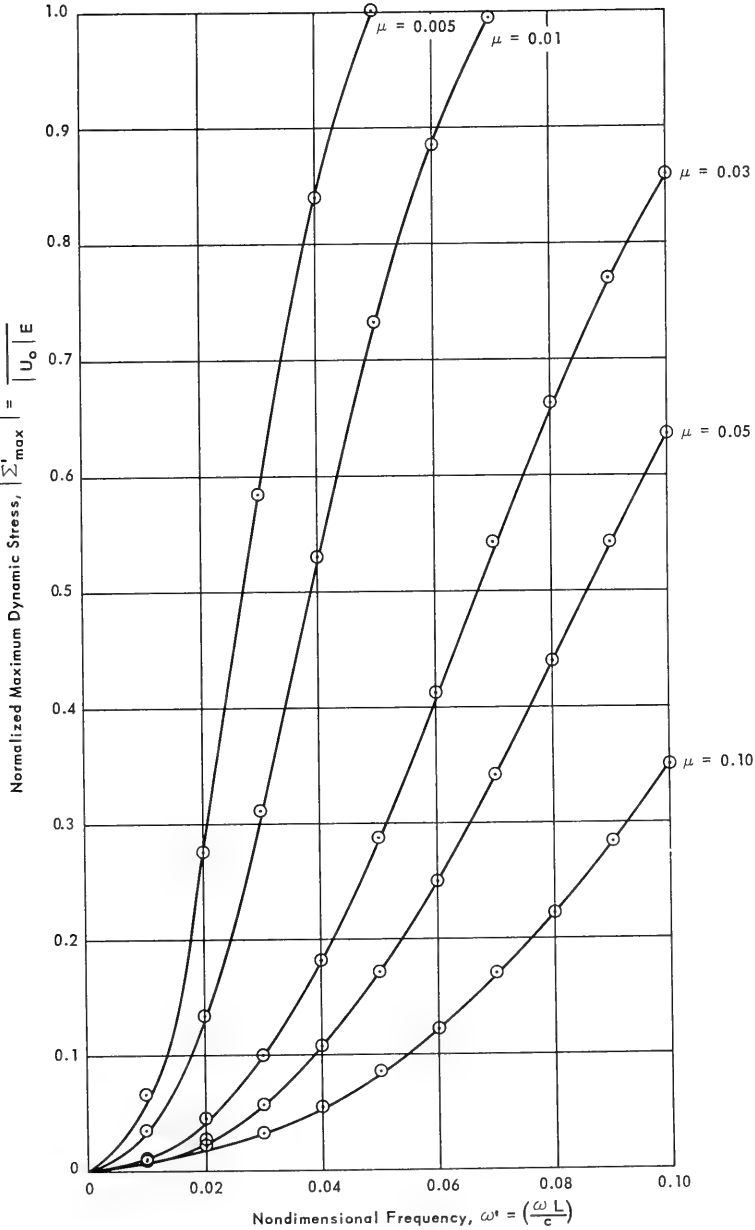

Figure 5. Variation of normalized maximum dynamic stress, $|\Sigma'_{max}|$, with nondimensional frequency, ω', for $\beta = 3.00$ over the range $0 \leq \omega' \leq 0.10$ for values of μ as indicated.

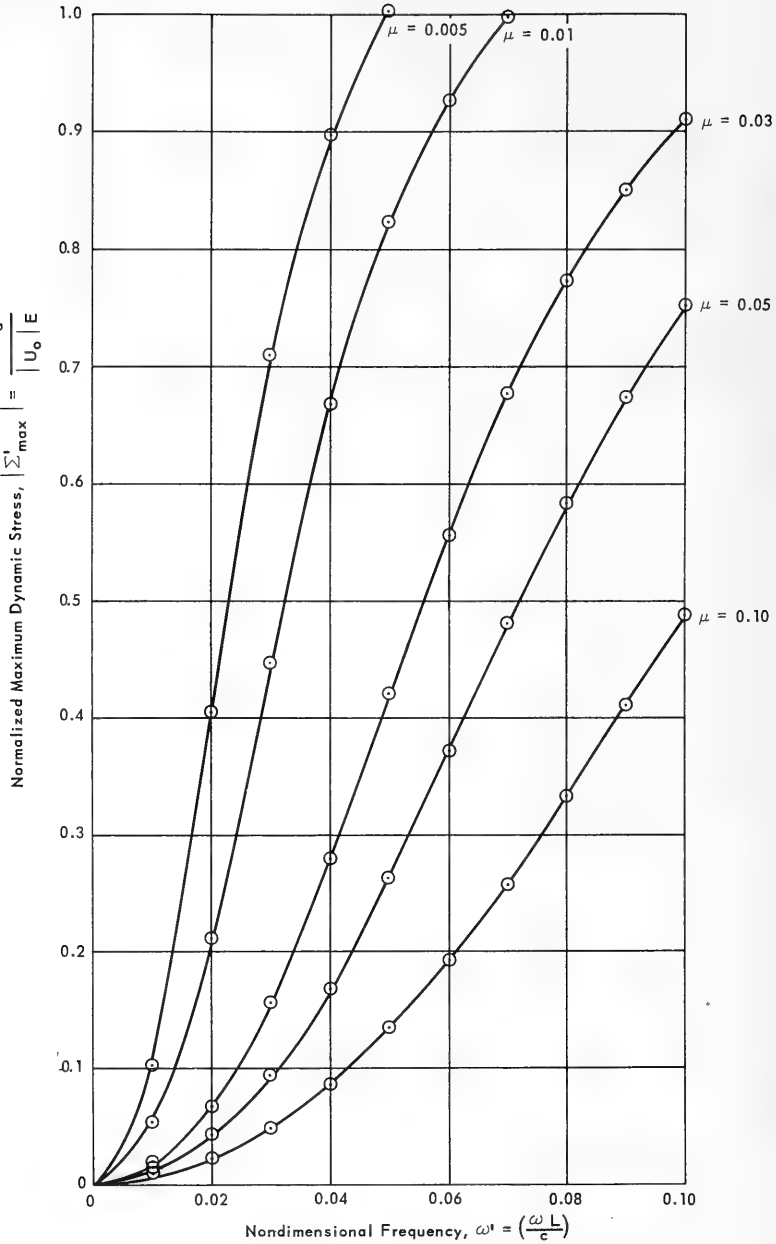

Figure 6. Variation of normalized maximum dynamic stress, $|\Sigma'_{max}|$, with nondimensional frequency, ω', for $\beta = 5.00$ over the range $0 \leq \omega' \leq 0.10$ for values of μ as indicated.

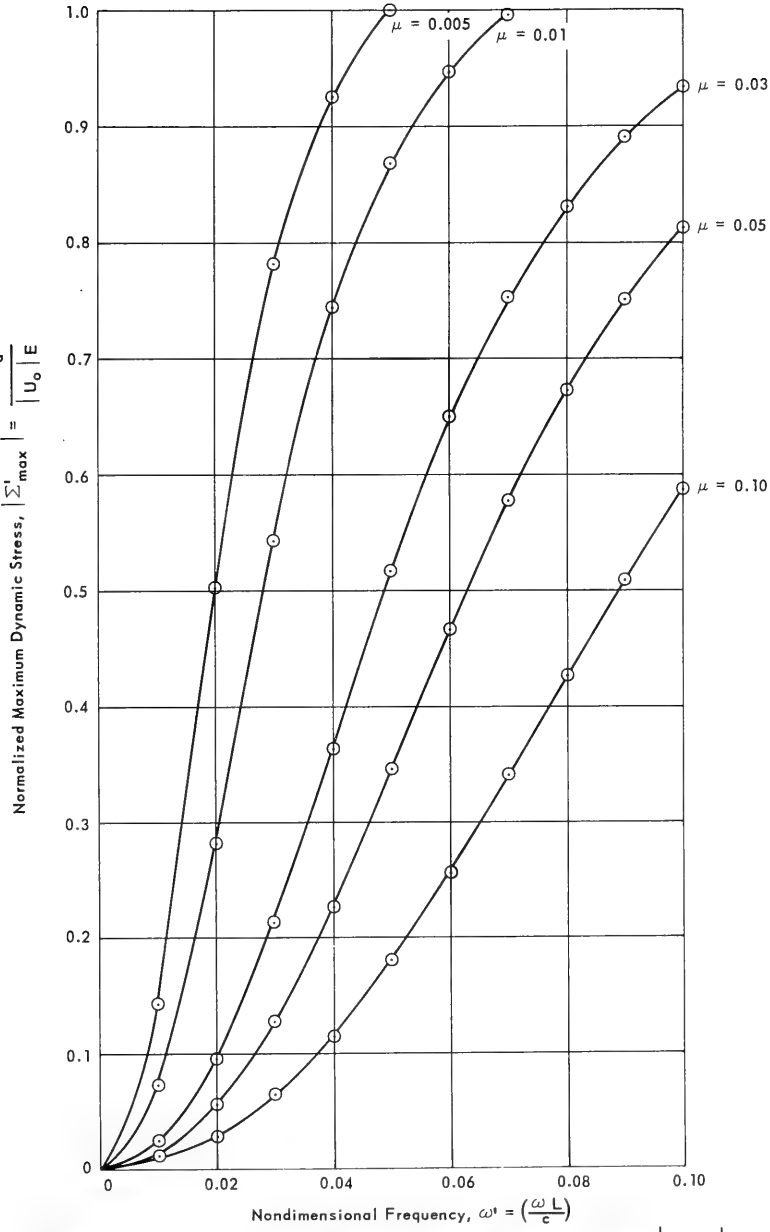

Figure 7. Variation of normalized maximum dynamic stress, $\left|\Sigma'_{max}\right|$, with nondimensional frequency, ω', for $\beta = 7.00$ over the range $0 \leq \omega' \leq 0.10$ for values of μ as indicated.

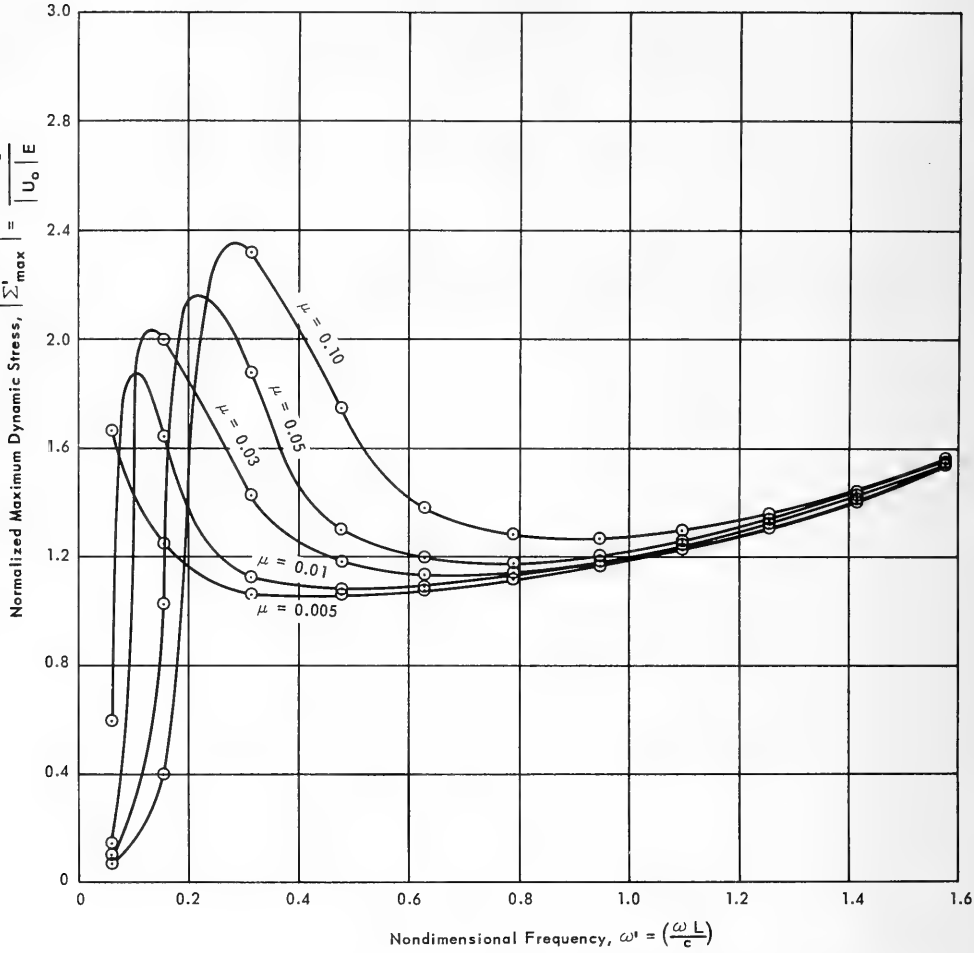

Figure 8. Variation of normalized maximum dynamic stress, $|\Sigma'_{max}|$, with nondimensional frequency, ω', for $\beta = 0.25$ over the range $0 \leq \omega' \leq \pi/2$ for values of μ as indicated.

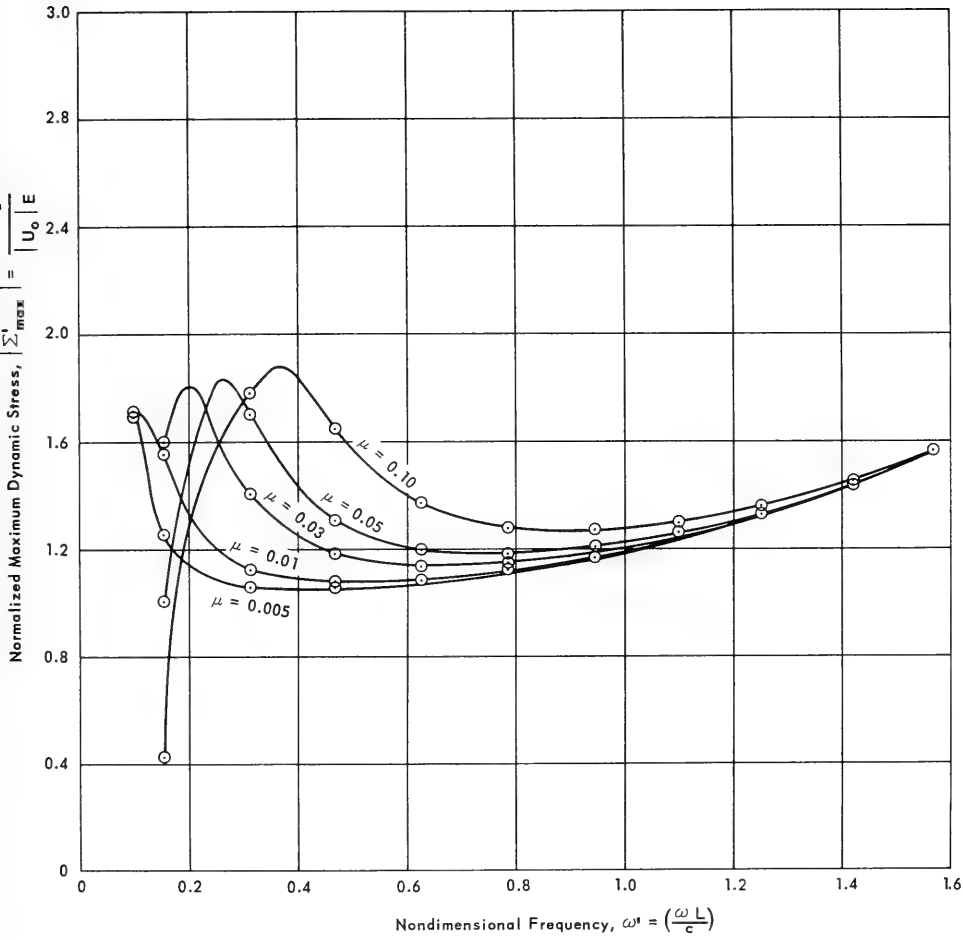

Figure 9. Variation of normalized maximum dynamic stress, $|\Sigma'_{max}|$, with nondimensional frequency, ω', for $\beta = 0.50$ over the range $0 \leq \omega' \leq \pi/2$ for values of μ as indicated.

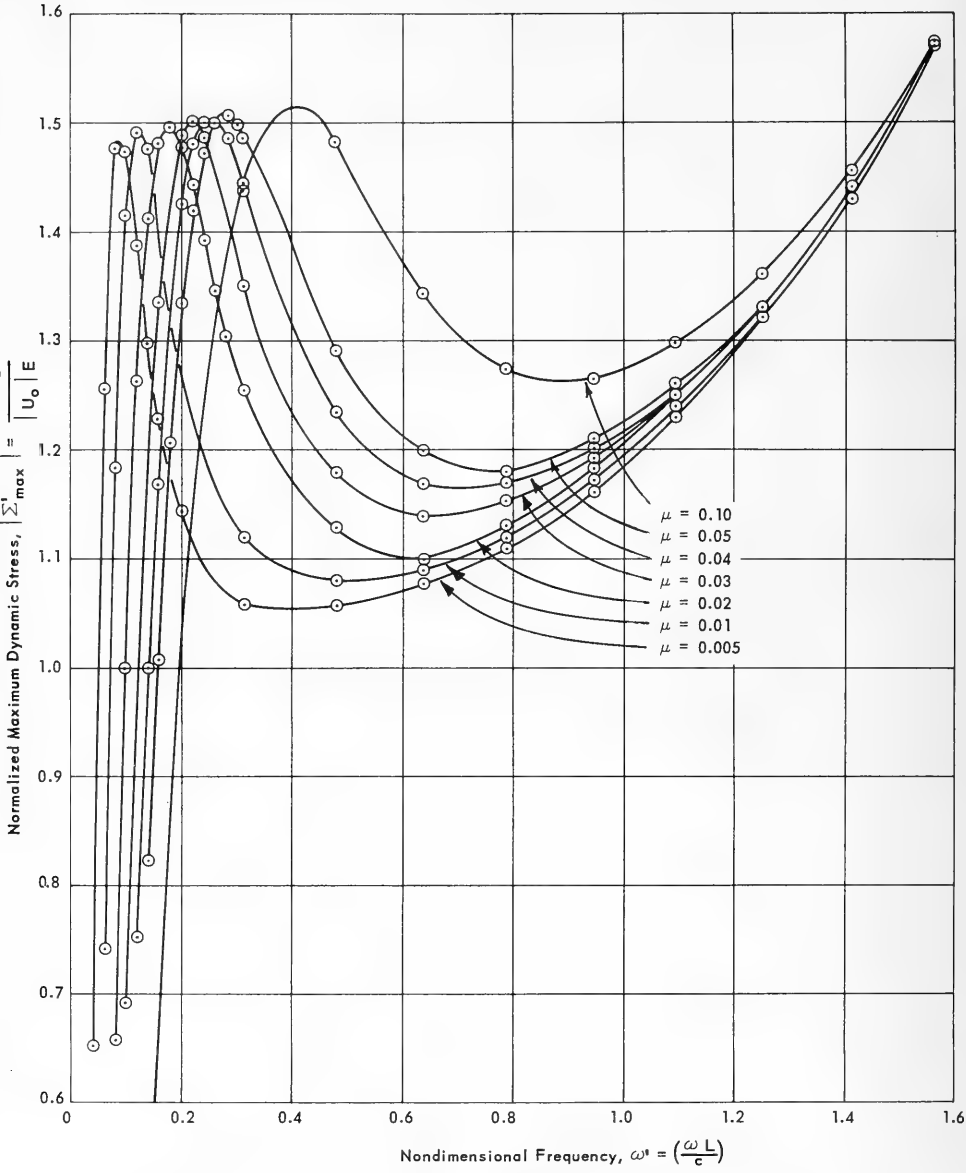

Figure 10. Variation of normalized maximum dynamic stress, $|\Sigma'_{max}|$, with nondimensional frequency, ω', for $\beta = 1.00$ over the range $0 \leq \omega' \leq \pi/2$ for values of μ as indicated.

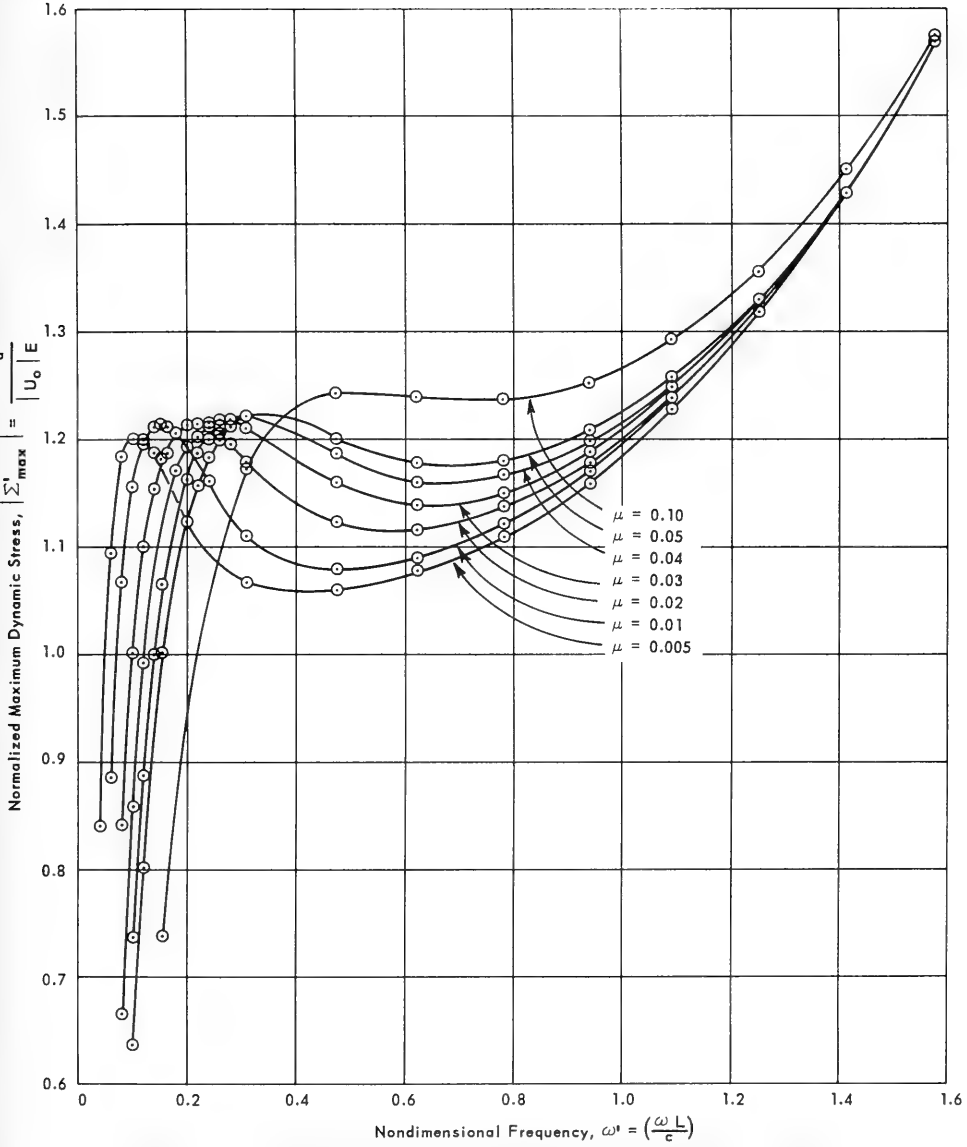

Figure 11. Variation of normalized maximum dynamic stress, $|\Sigma'_{max}|$, with nondimensional frequency, ω', for $\beta = 3.00$ over the range $0 \leq \omega' \leq \pi/2$ for values of μ as indicated.

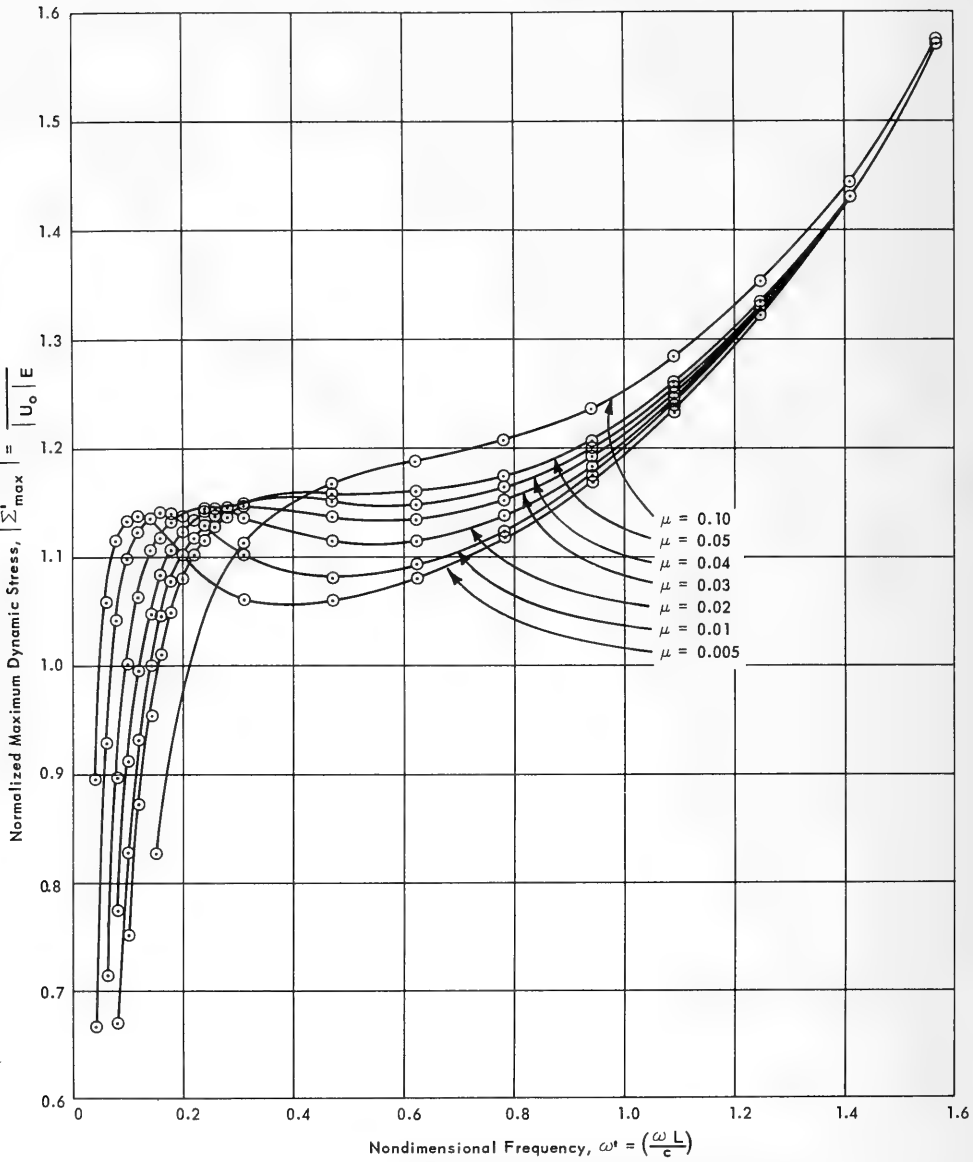

Figure 12. Variation of normalized maximum dynamic stress, $\left|\Sigma'_{max}\right|$, with nondimensional frequency, ω', for $\beta = 5.00$ over the range $0 \leq \omega' \leq \pi/2$ for values of μ as indicated.

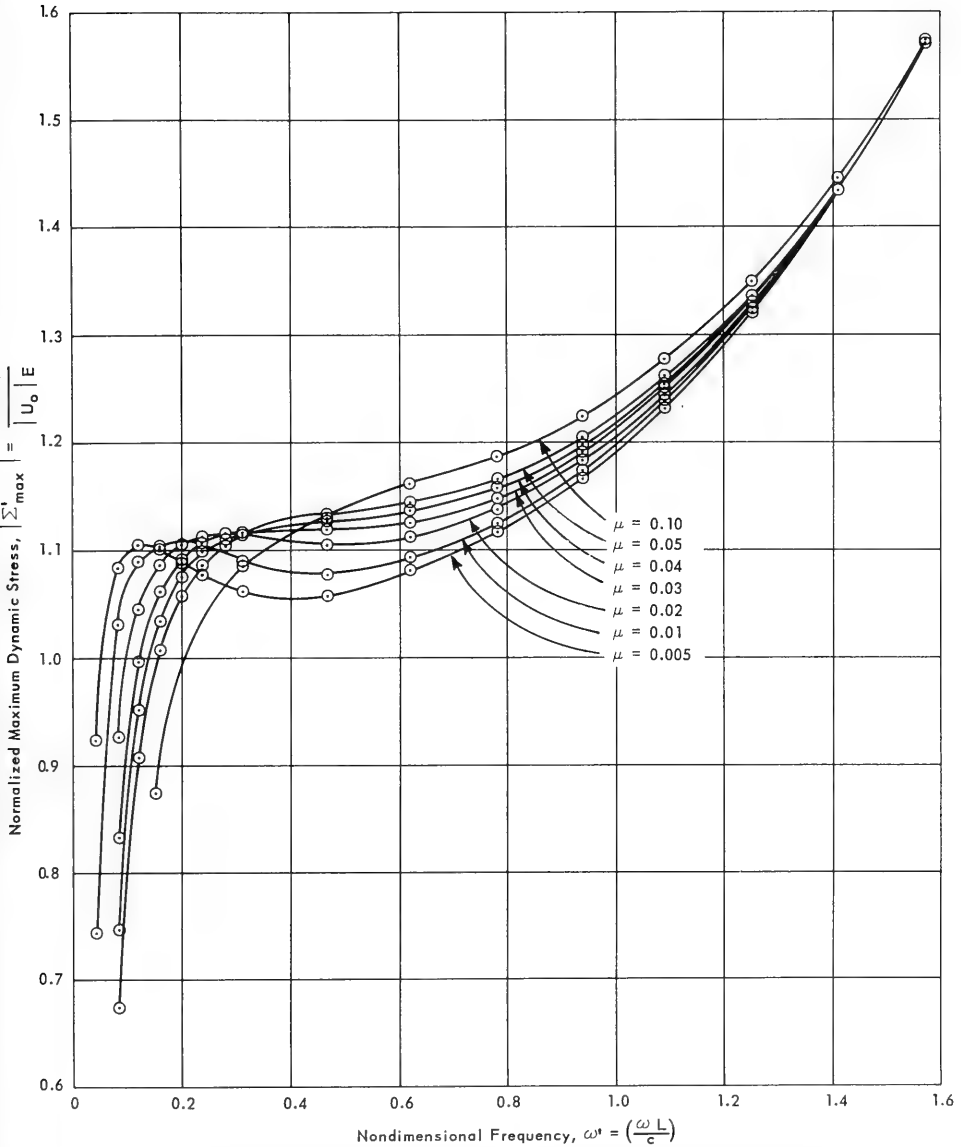

Figure 13. Variation of normalized maximum dynamic stress, $|\Sigma'_{max}|$, with nondimensional frequency, ω', for $\beta = 7.00$ over the range $0 \leq \omega' \leq \pi/2$ for values of μ as indicated.

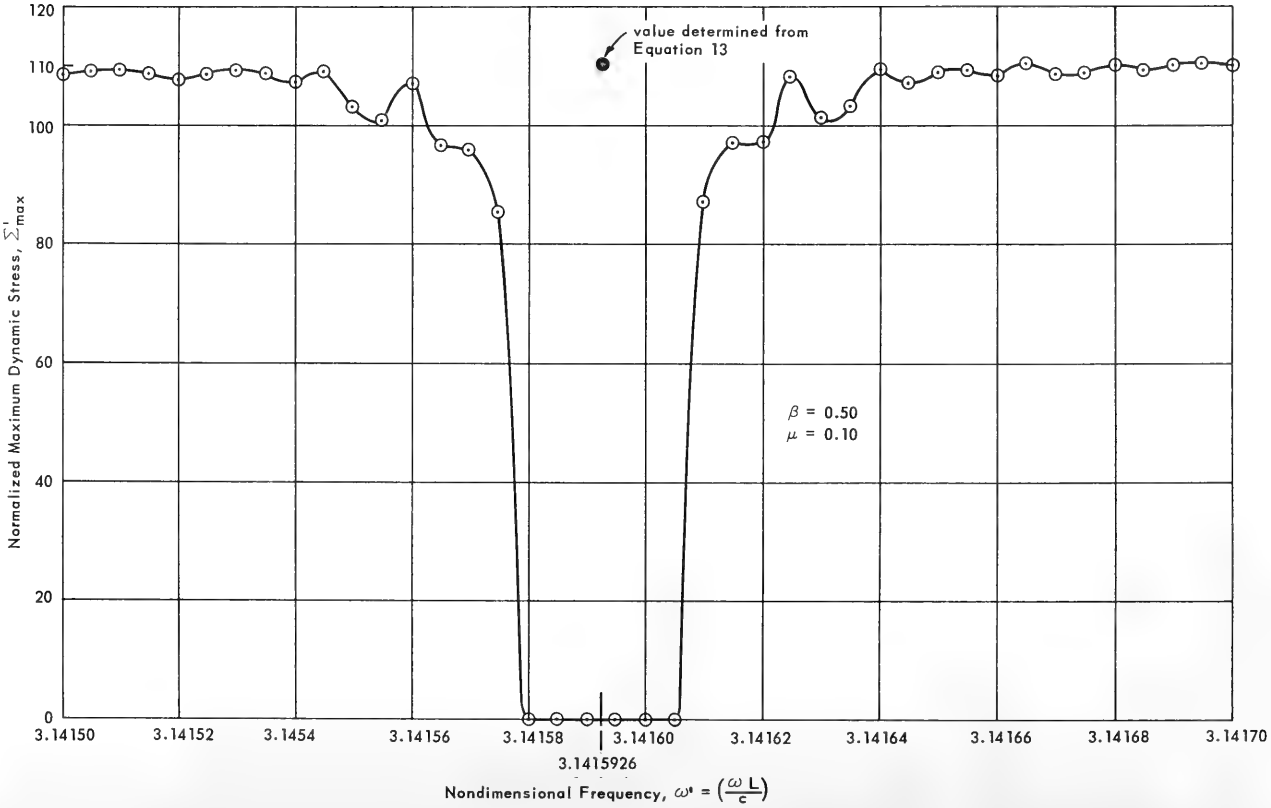

Figure 14. Illustration of rounding off errors in the computer program.

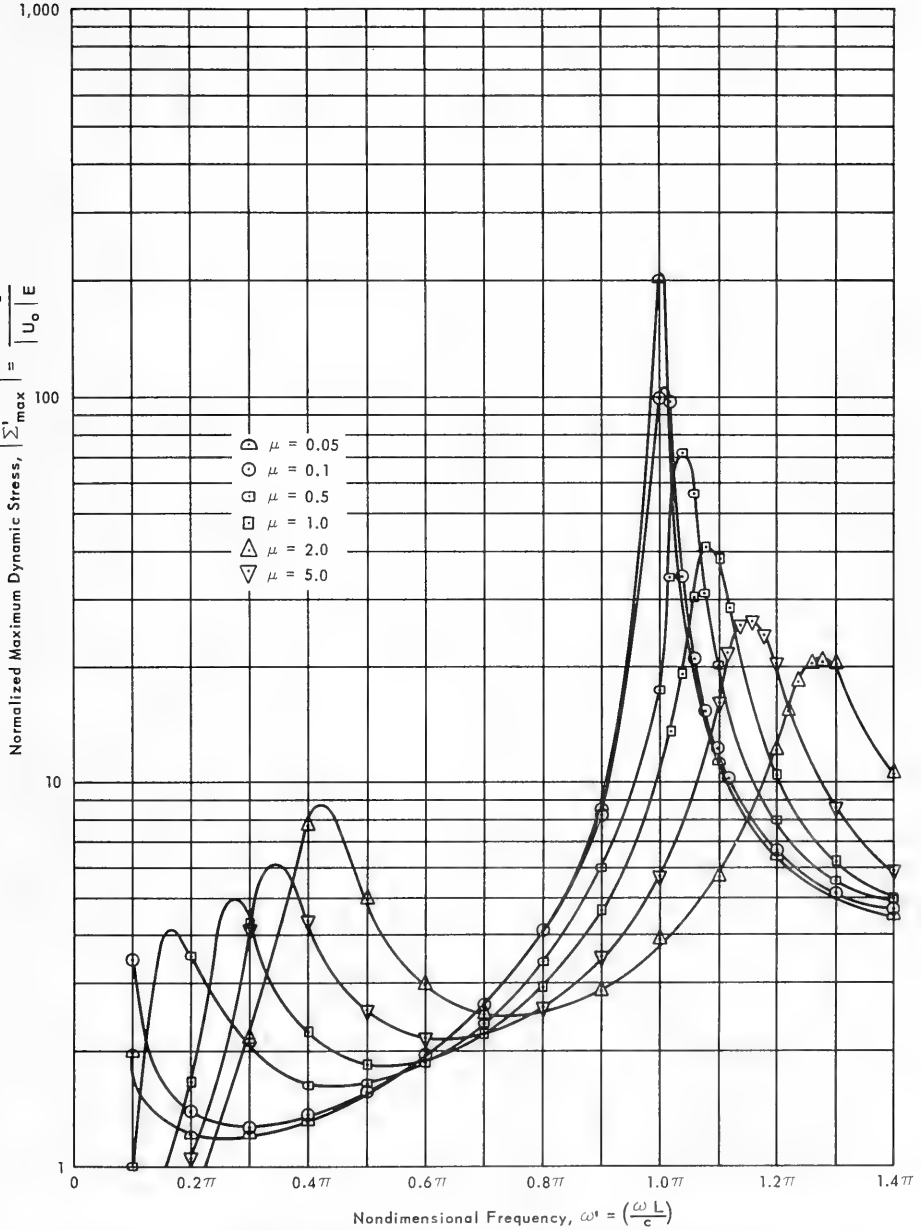

Figure 15. Variation of normalized maximum dynamic stress, $|\Sigma'_{max}|$, with nondimensional frequency, ω', for $\beta = 0.10$ over the range $\pi/10 \leq \omega' \leq 1.4\pi$ for values of μ as indicated.

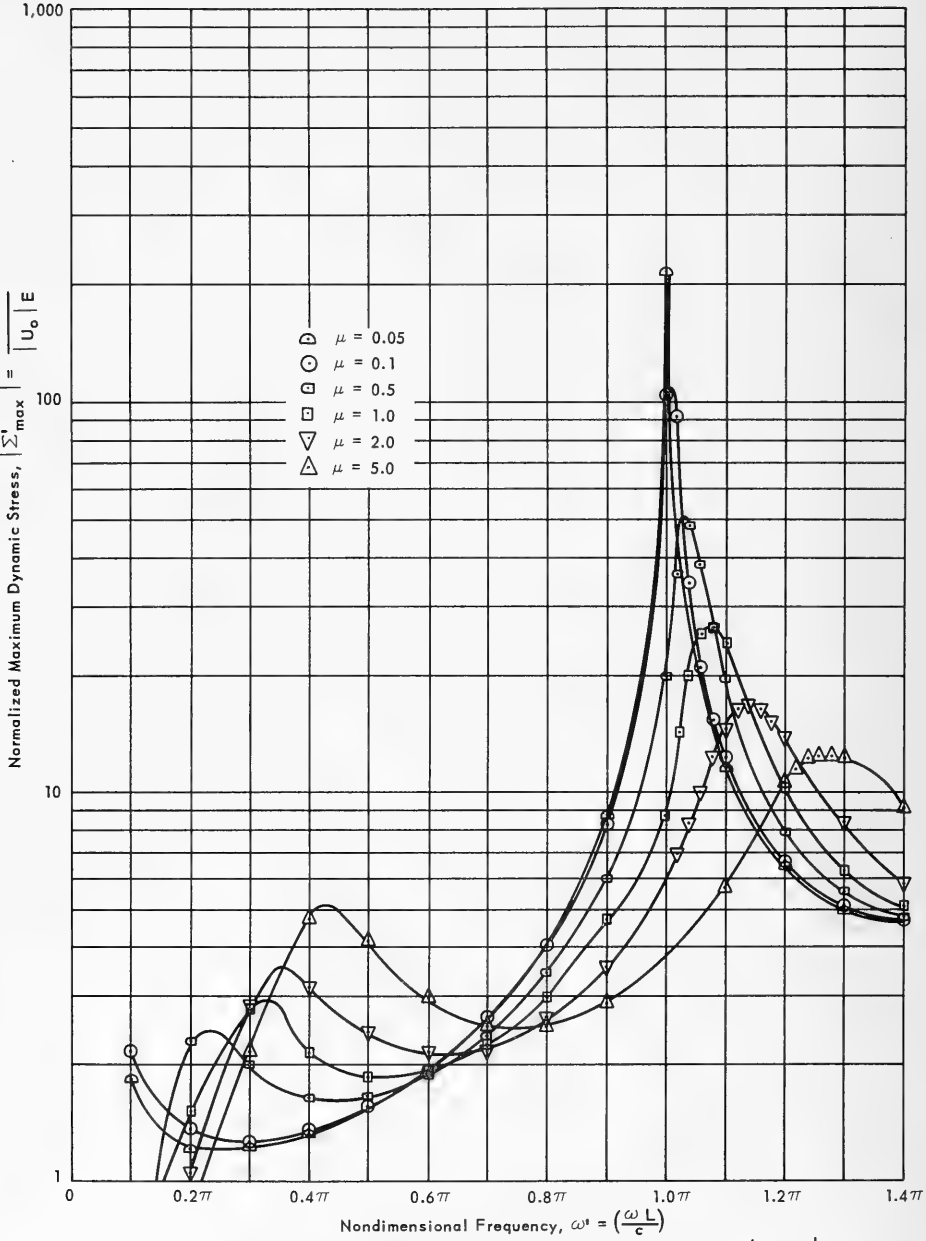

Figure 16. Variation of normalized maximum dynamic stress, $\left|\Sigma'_{max}\right|$, with nondimensional frequency, ω', for $\beta = 0.30$ over the range $\pi/10 \leq \omega' \leq 1.4\pi$ for values of μ as indicated.

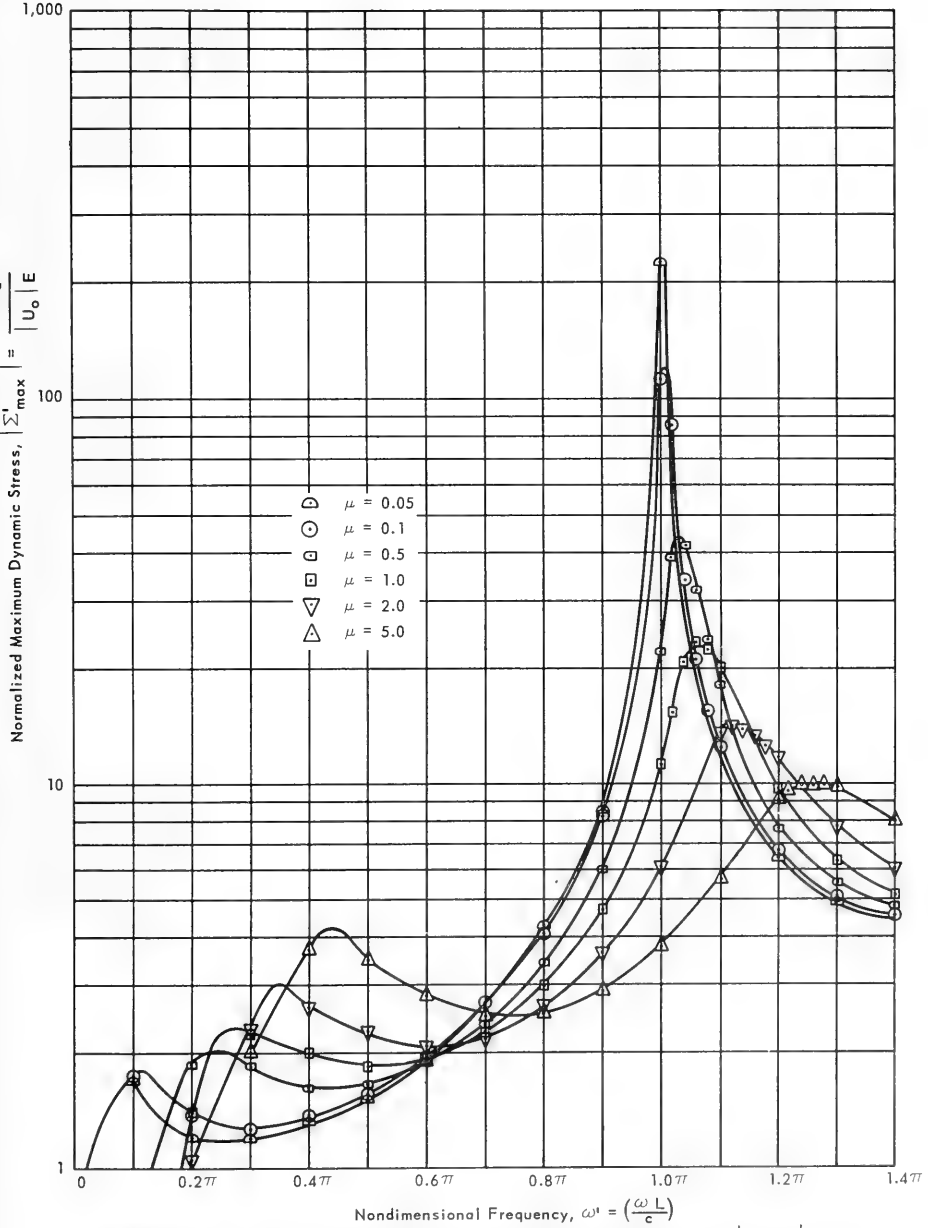

Figure 17. Variation of normalized maximum dynamic stress, $|\Sigma'_{max}|$, with nondimensional frequency, ω', for $\beta = 0.50$ over the range $\pi/10 \leq \omega' \leq 1.4\pi$ for values of μ as indicated.

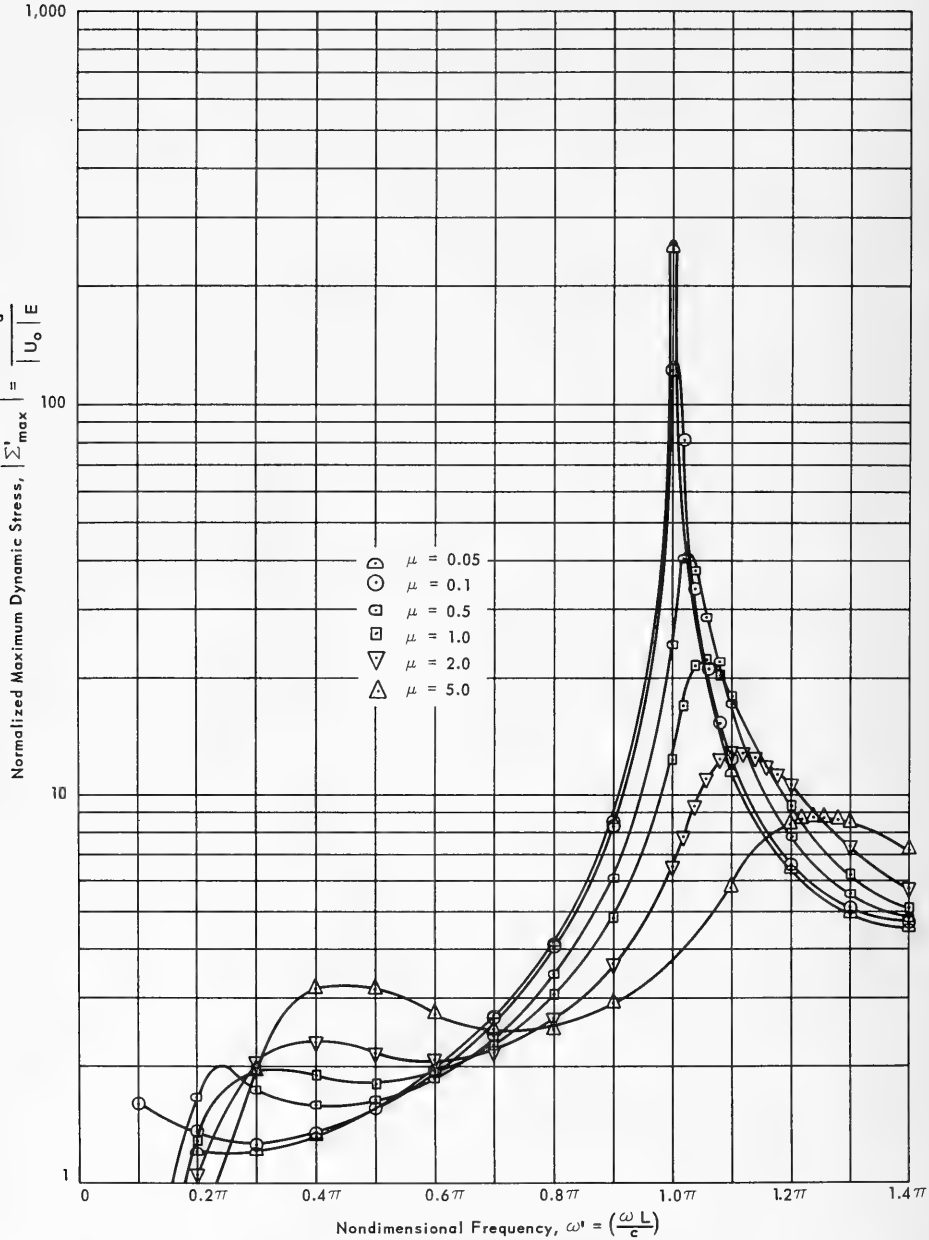

Figure 18. Variation of normalized maximum dynamic stress, $|\Sigma'_{max}|$, with nondimensional frequency, ω', for $\beta = 0.70$ over the range $\pi/10 \leq \omega' \leq 1.4\pi$ for values of μ as indicated.

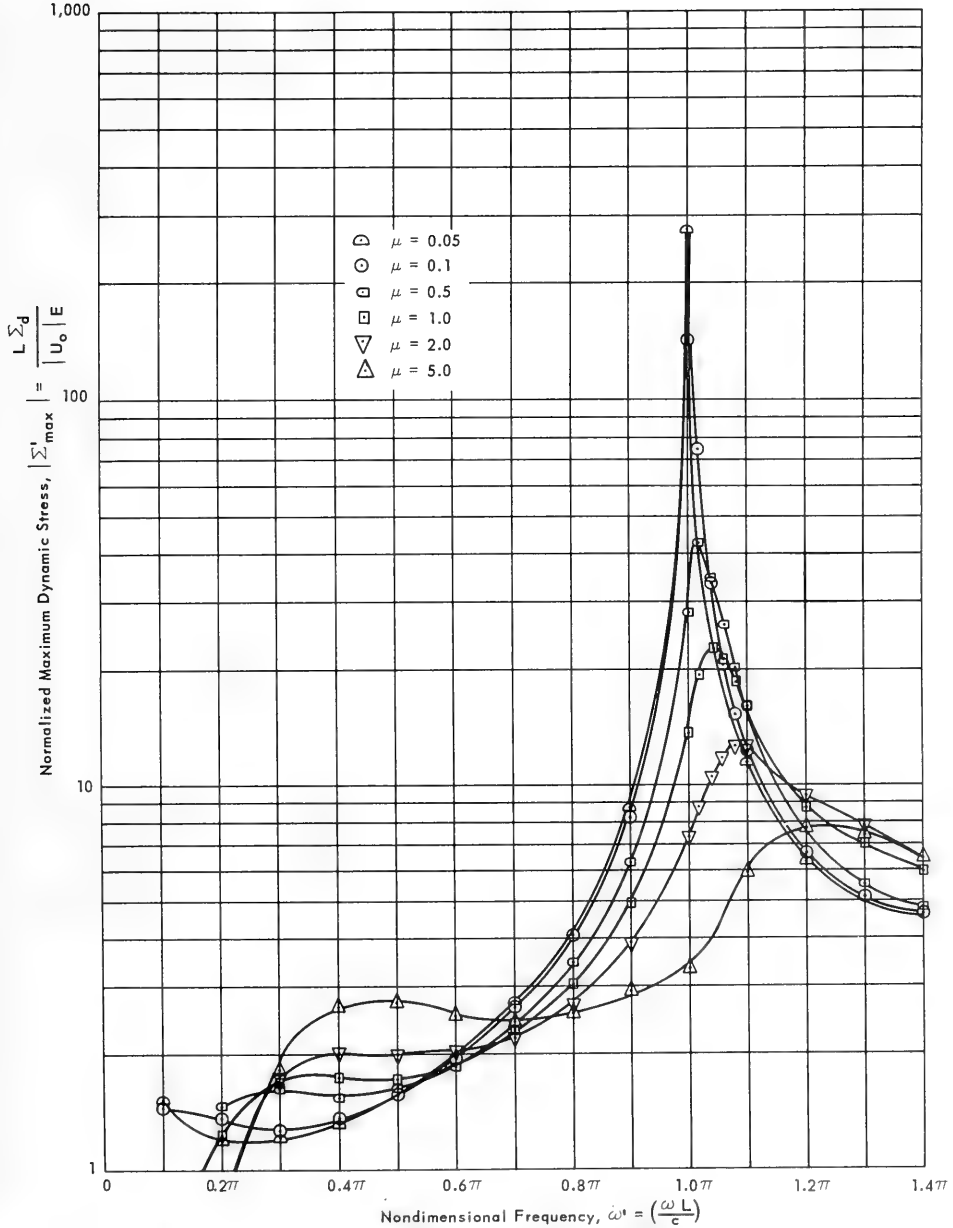

Figure 19. Variation of normalized maximum dynamic stress, $\left|\Sigma'_{max}\right|$, with nondimensional frequency, ω', for $\beta = 1.00$ over the range $\pi/10 \leq \omega' \leq 1.4\pi$ for values of μ as indicated.

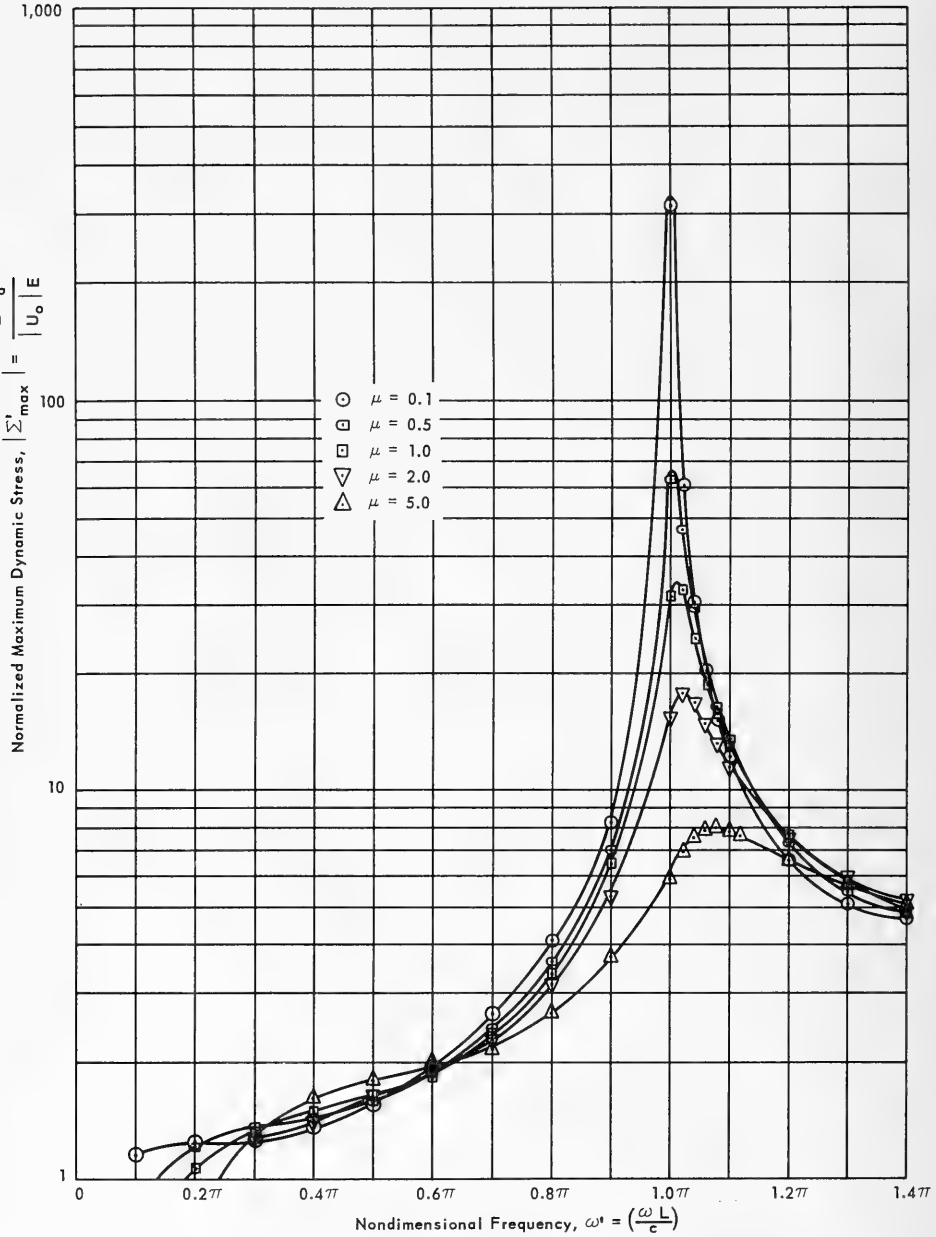

Figure 20. Variation of normalized maximum dynamic stress, $|\Sigma'_{max}|$, with nondimensional frequency, ω', for $\beta = 3.00$ over the range $\pi/10 \leq \omega' \leq 1.4\pi$ for values of μ as indicated.

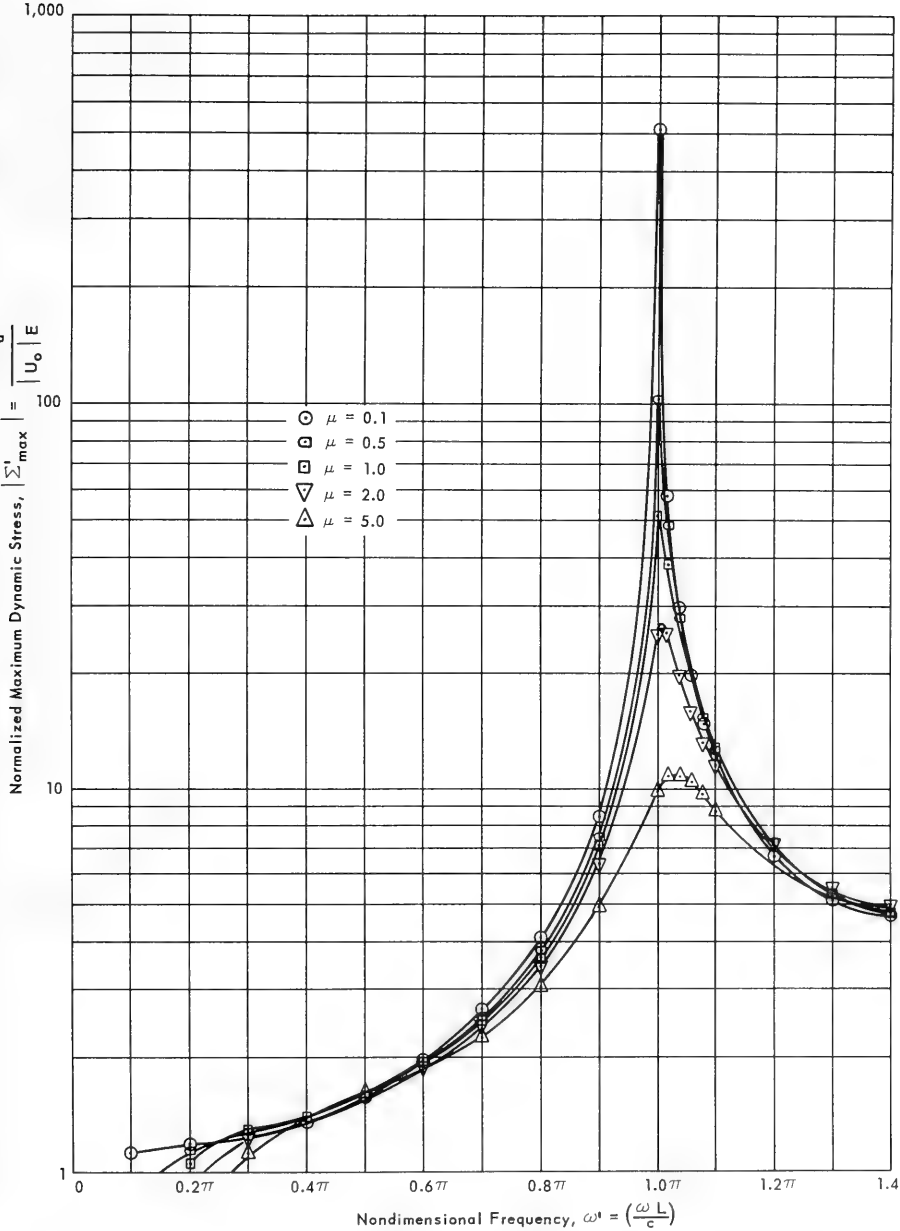

Figure 21. Variation of normalized maximum dynamic stress, $\left|\Sigma'_{max}\right|$, with nondimensional frequency, ω', for $\beta = 5.00$ over the range $\pi/10 \leq \omega' \leq 1.4\pi$ for values of μ as indicated.

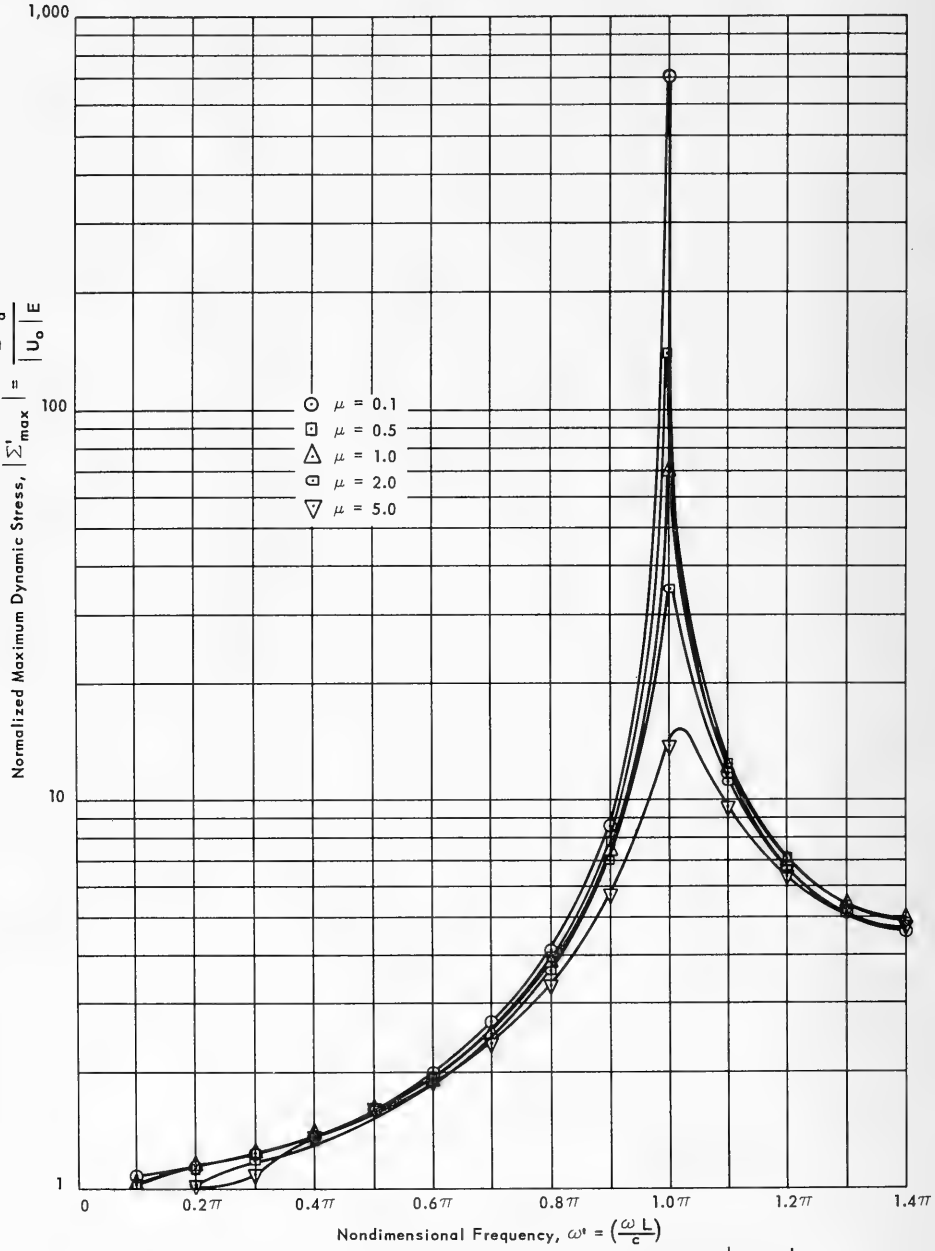

Figure 22. Variation of normalized maximum dynamic stress, $|\Sigma'_{max}|$, with nondimensional frequency, ω', for $\beta = 7.00$ over the range $\pi/10 \leq \omega' \leq 1.4\pi$ for values of μ as indicated.

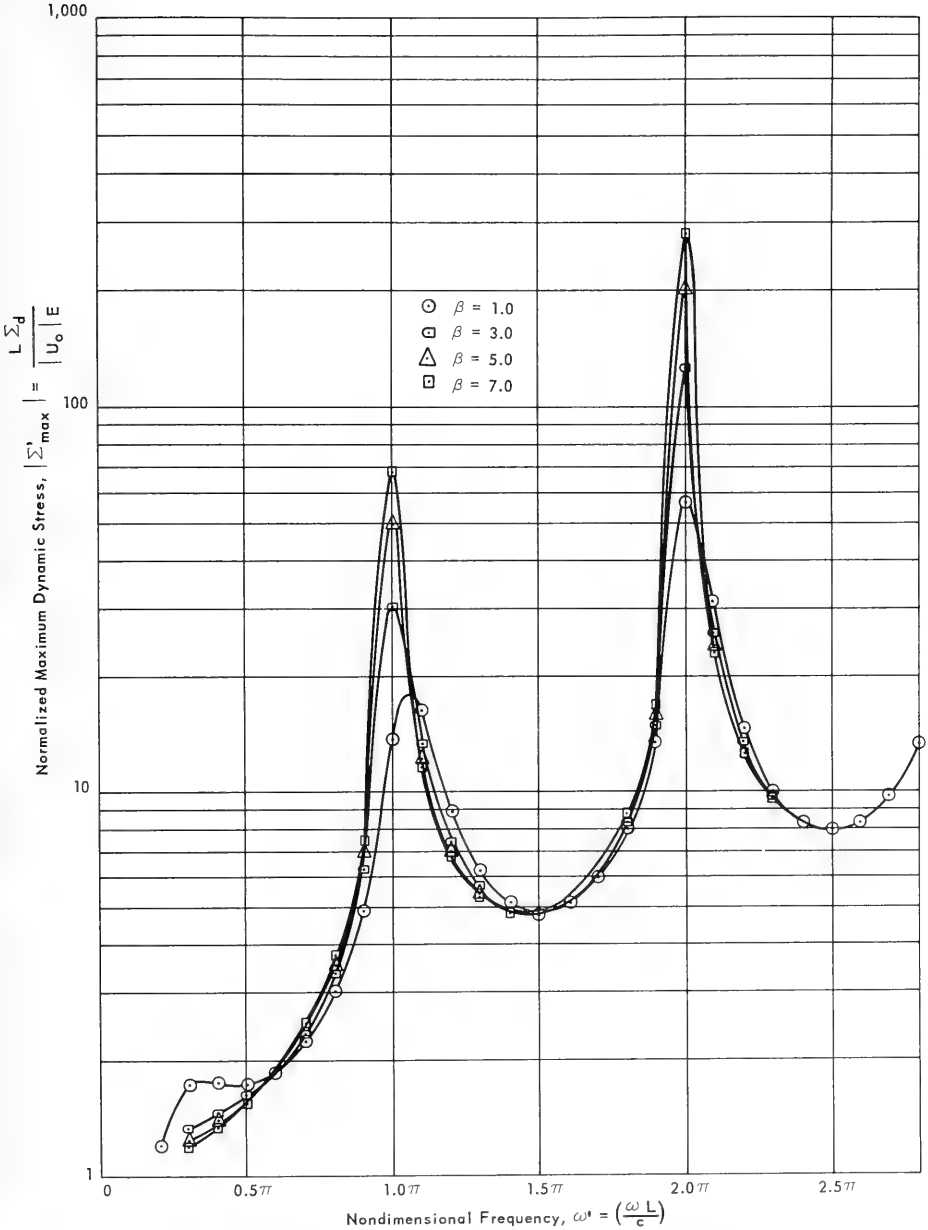

Figure 23. Variation of $\left|\Sigma'_{max}\right|$ with β for a particular μ.

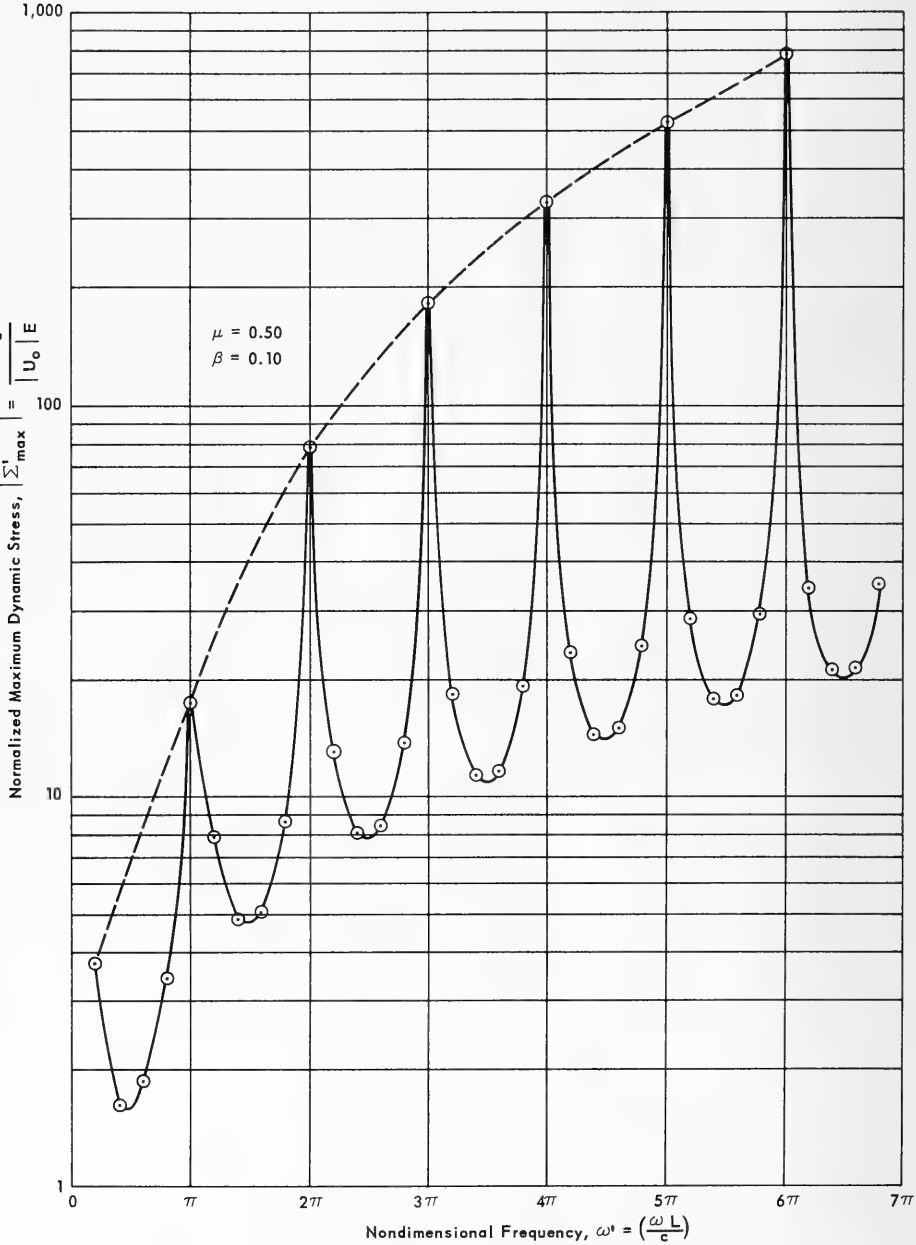

Figure 24. Variation of $|\Sigma'_{max}|$ over a wide range of ω'. Dashed line illustrates approximation used.

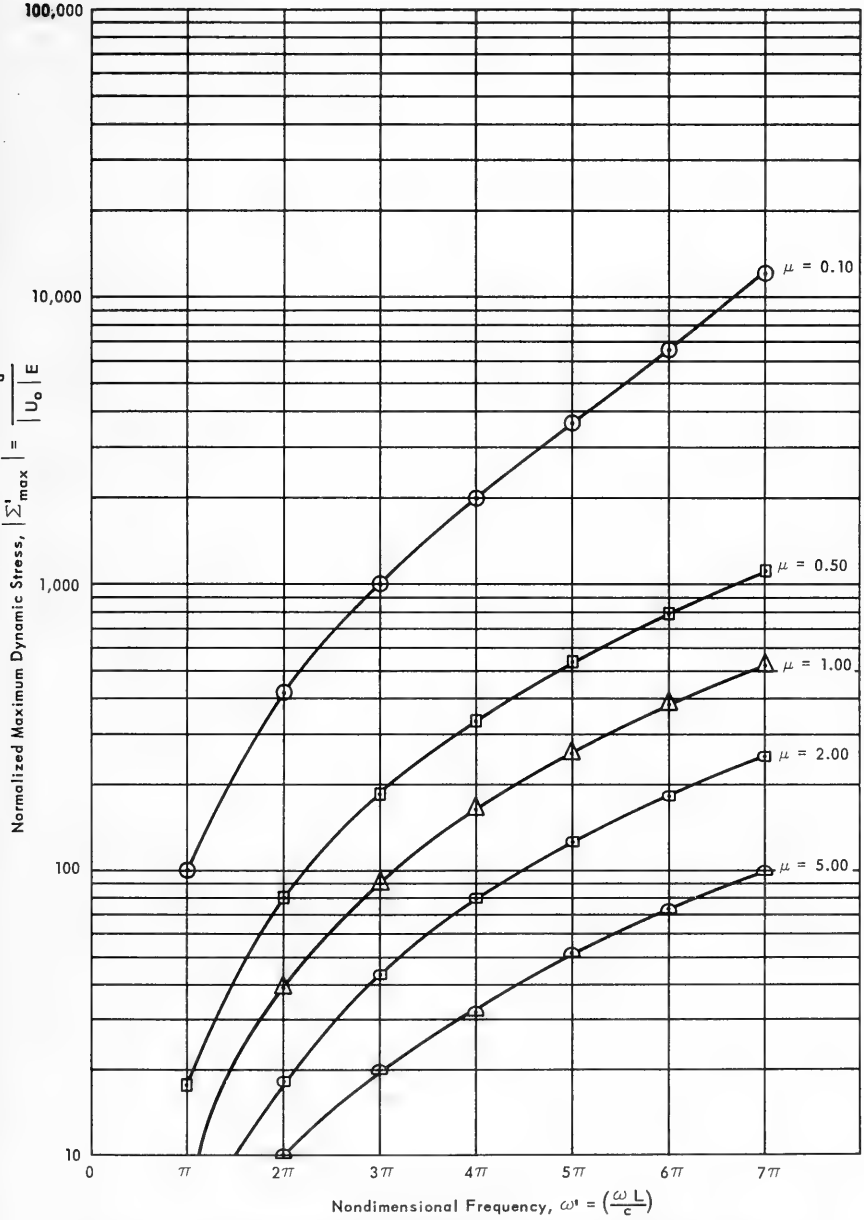

Figure 25. Variation of normalized maximum dynamic stress, $|\Sigma'_{max}|$, with nondimensional frequency, ω', for $\beta = 0.10$ over the range $\pi/5 \leq \omega' \leq 7.0\pi$ for values of μ as indicated.

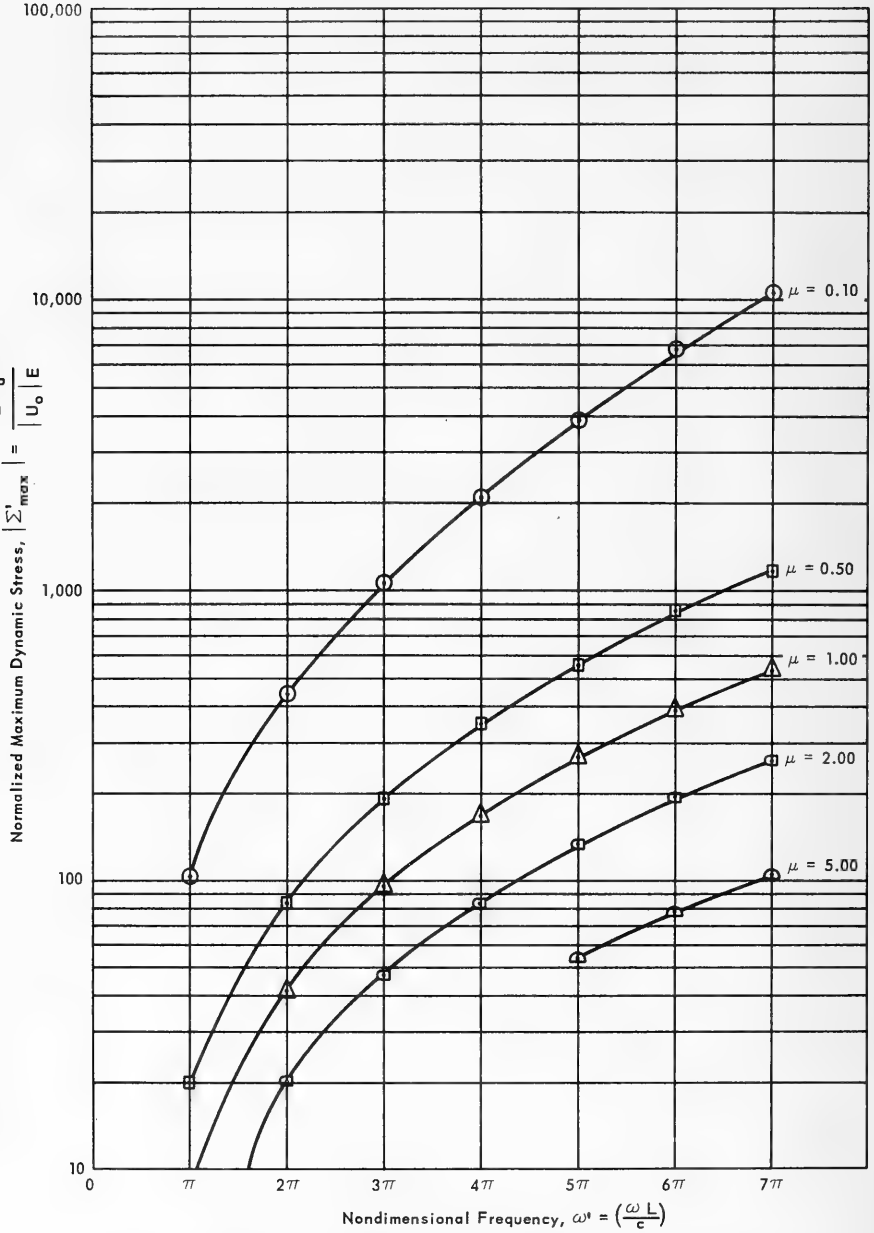

Figure 26. Variation of normalized maximum dynamic stress, $|\Sigma'_{max}|$, with nondimensional frequency, ω', for $\beta = 0.30$ over the range $\pi/5 \leq \omega' \leq 7.0\pi$ for values of μ as indicated.

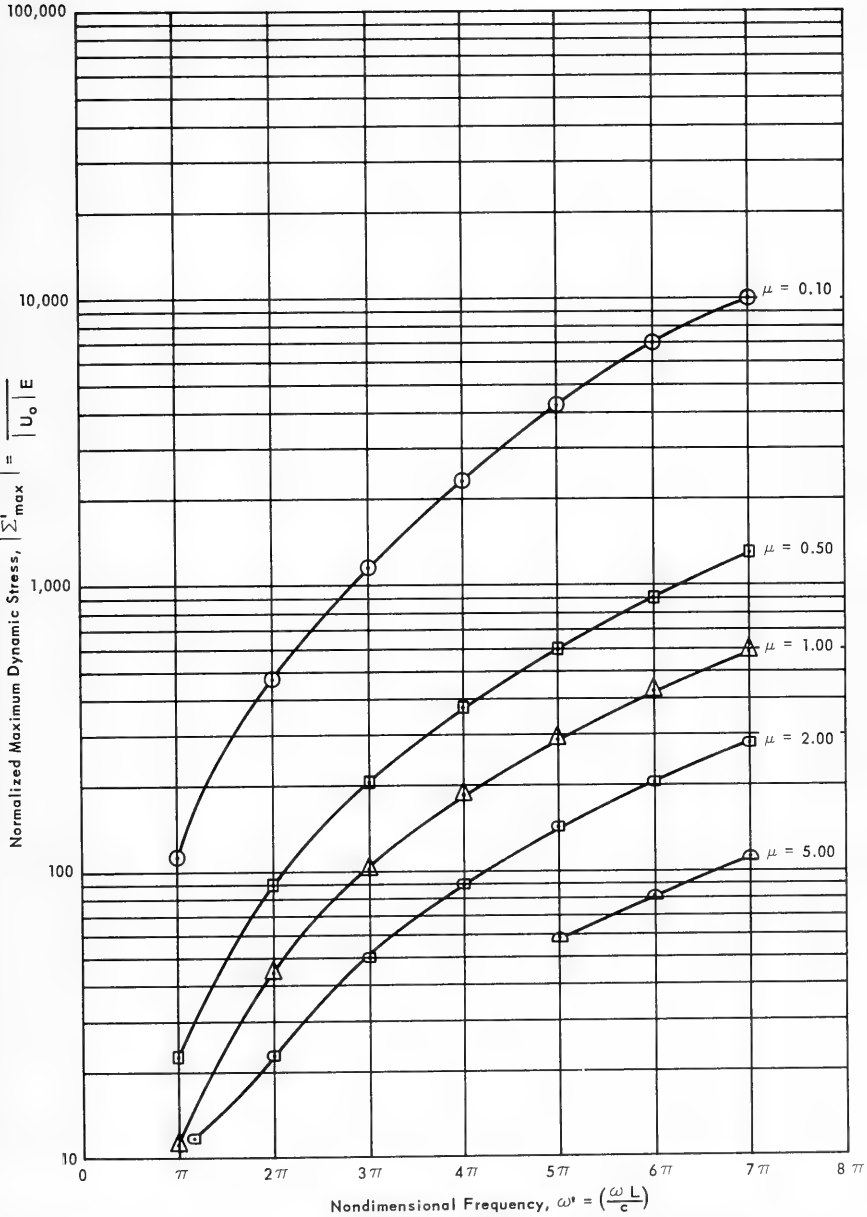

Figure 27. Variation of normalized maximum dynamic stress, $|\Sigma'_{max}|$, with nondimensional frequency, ω', for $\beta = 0.50$ over the range $\pi/5 \leq \omega' \leq 7.0\pi$ for values of μ as indicated.

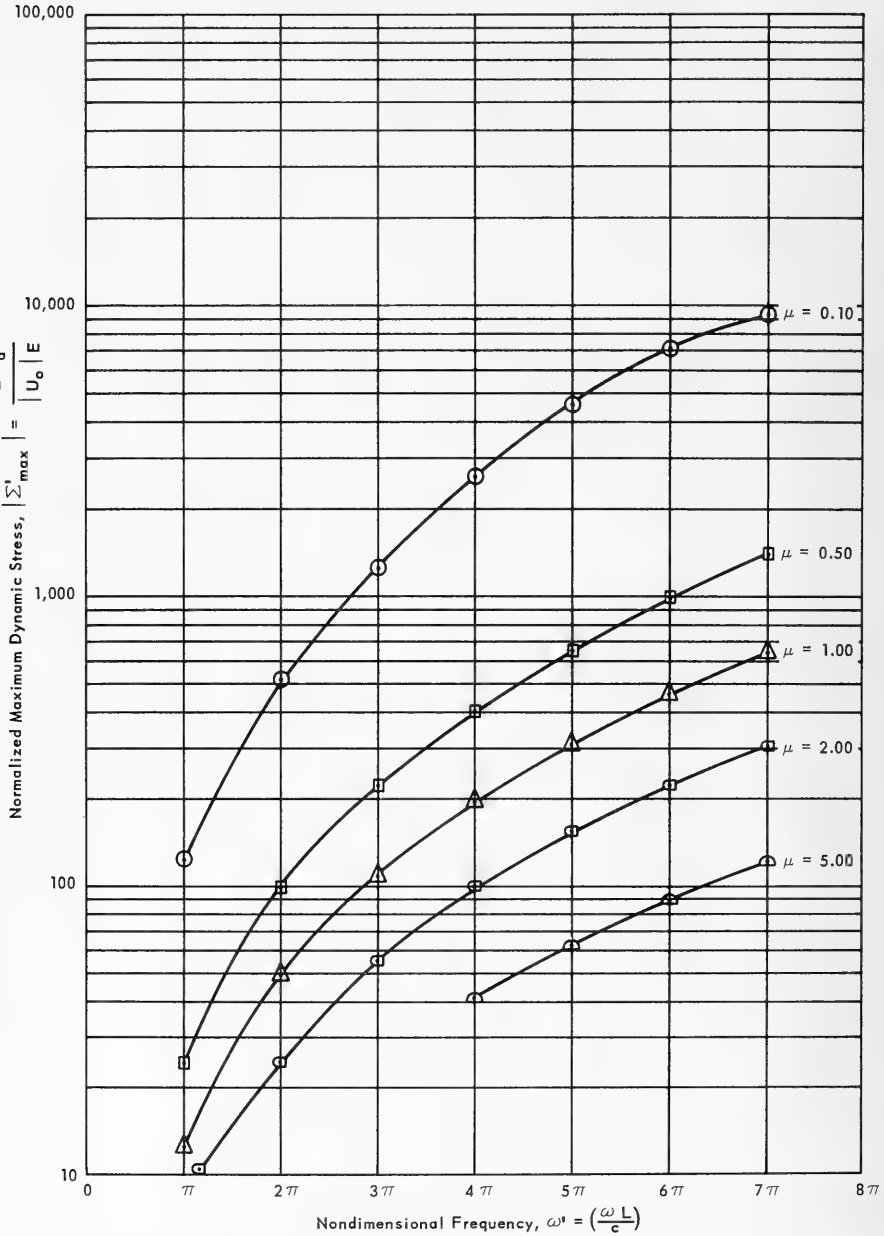

Figure 28. Variation of normalized maximum dynamic stress, $|\Sigma'_{max}|$, with nondimensional frequency, ω', for $\beta = 0.70$ over the range $\pi/5 \leq \omega' \leq 7.0\pi$ for values of μ as indicated.

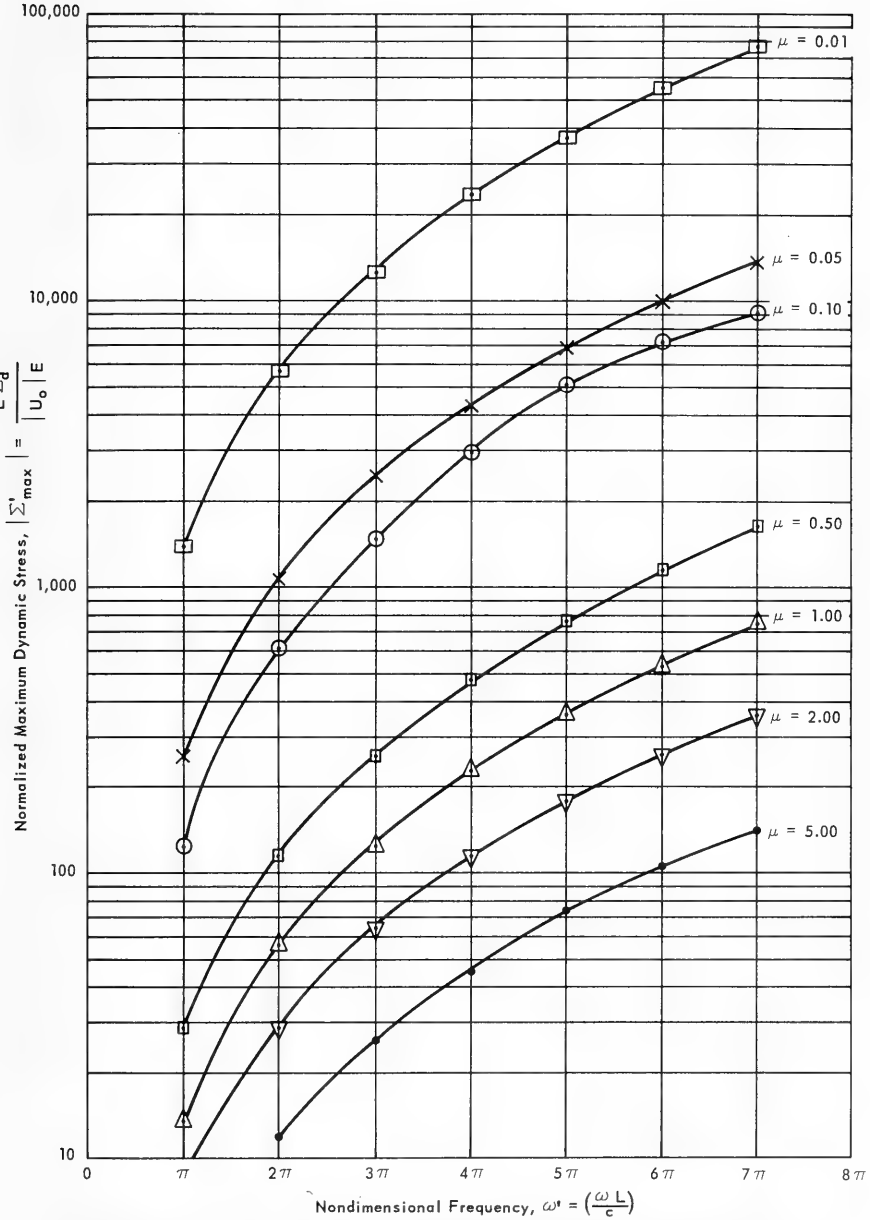

Figure 29. Variation of normalized maximum dynamic stress, $\left|\Sigma'_{max}\right|$, with nondimensional frequency, ω', for $\beta = 1.00$ over the range $\pi/5 \leq \omega' \leq 7.0\pi$ for values of μ as indicated.

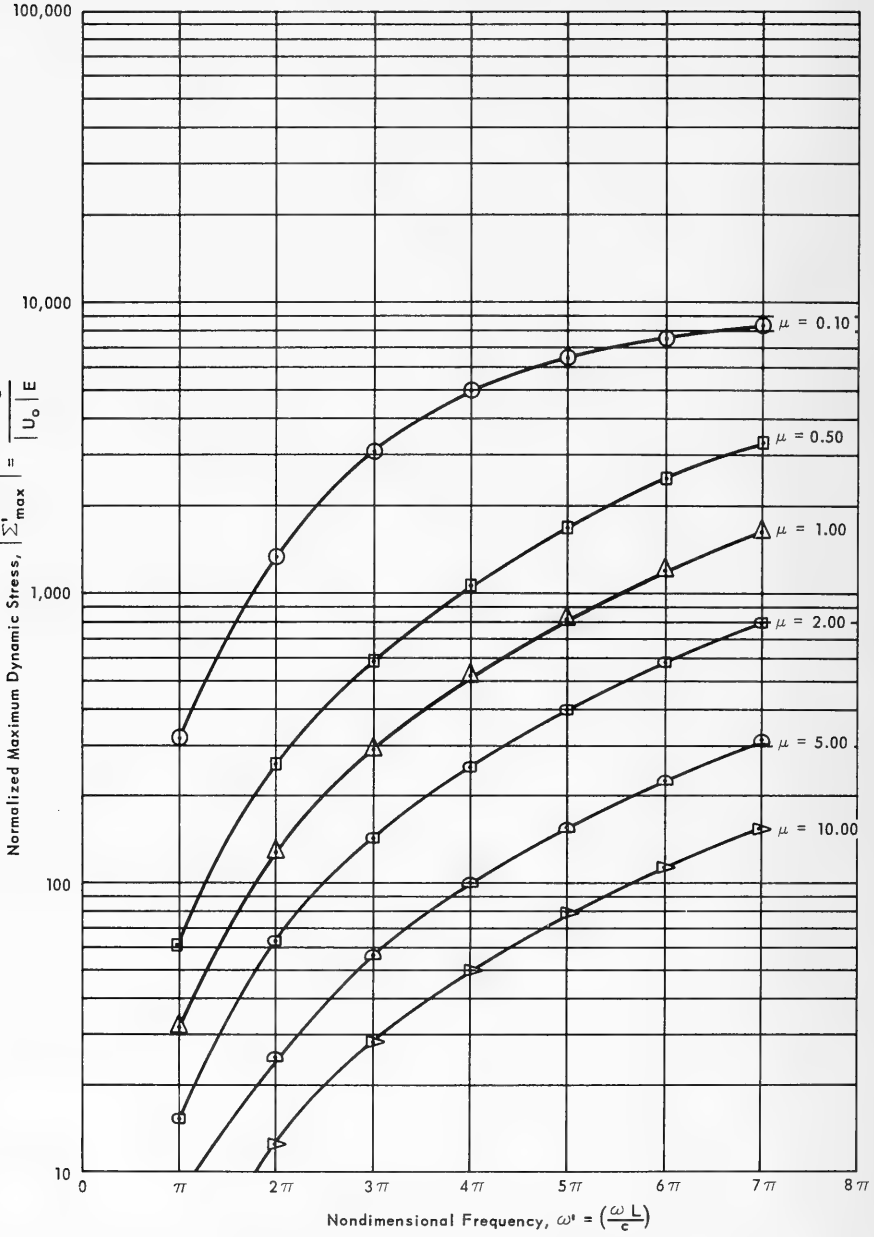

Figure 30. Variation of normalized maximum dynamic stress, $|\Sigma'_{max}|$, with nondimensional frequency, ω', for $\beta = 3.00$ over the range $\pi/5 \leq \omega' \leq 7.0\pi$ for values of μ as indicated.

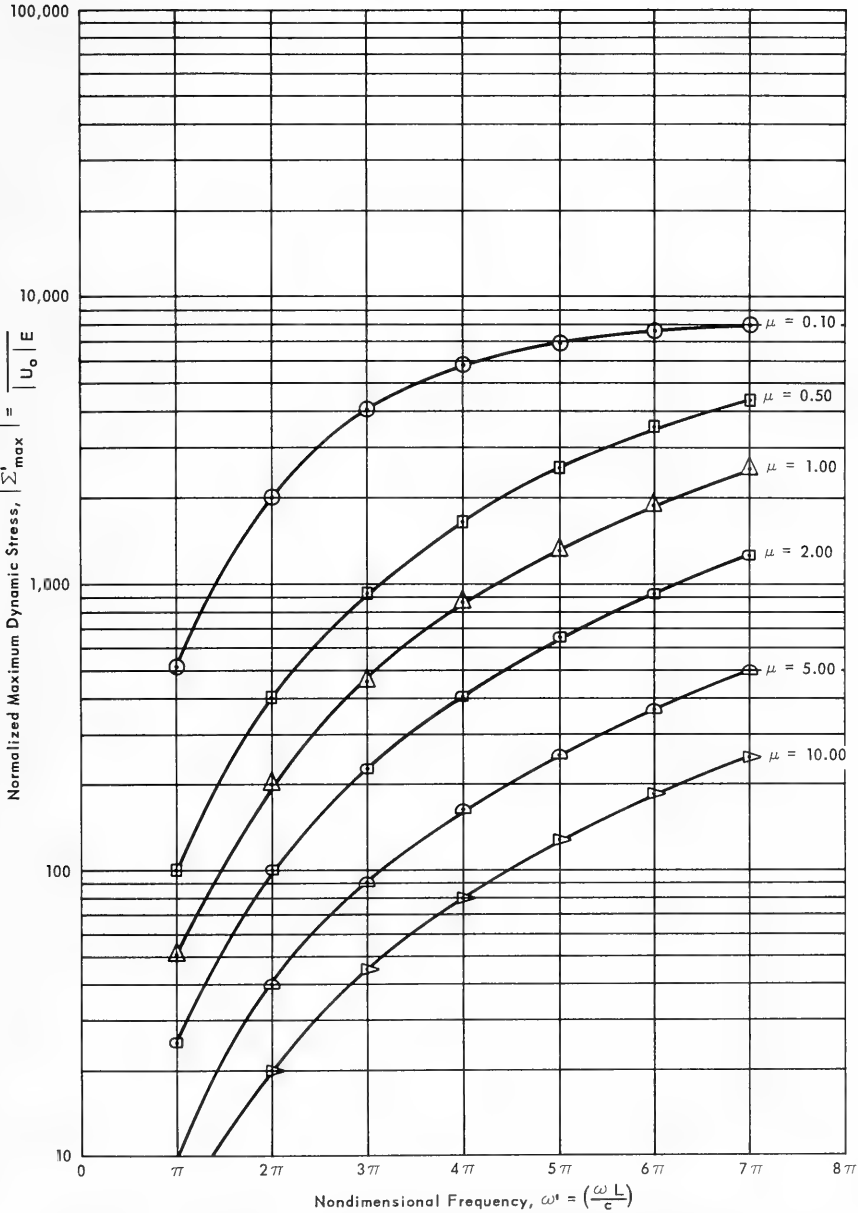

Figure 31. Variation of normalized maximum dynamic stress, $\left|\Sigma'_{max}\right|$, with nondimensional frequency, ω', for $\beta = 5.00$ over the range $\pi/5 \leq \omega' \leq 7.0\pi$ for values of μ as indicated.

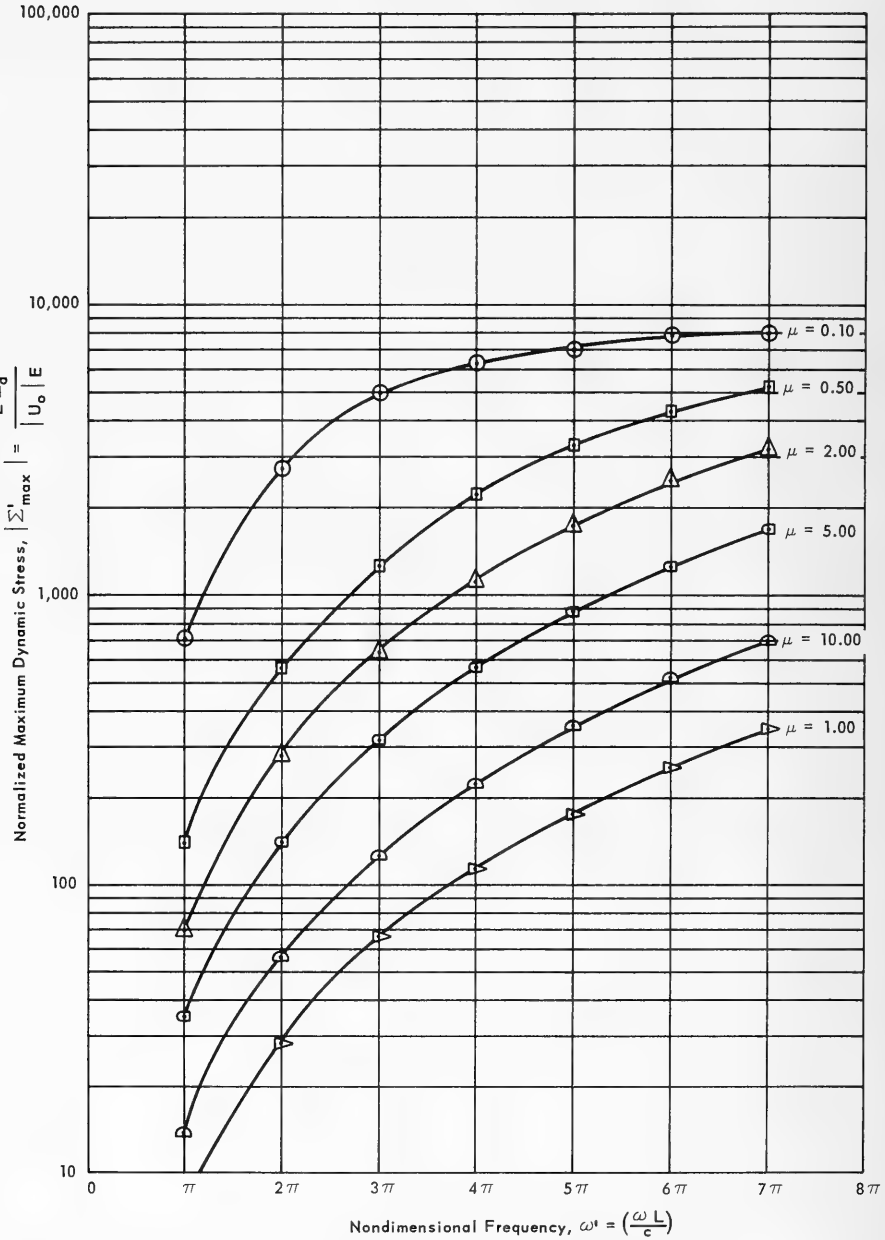

Figure 32. Variation of normalized maximum dynamic stress, $|\Sigma'_{max}|$, with nondimensional frequency, ω', for $\beta = 7.00$ over the range $\pi/5 \leq \omega' \leq 7.0\pi$ for values of μ as indicated.

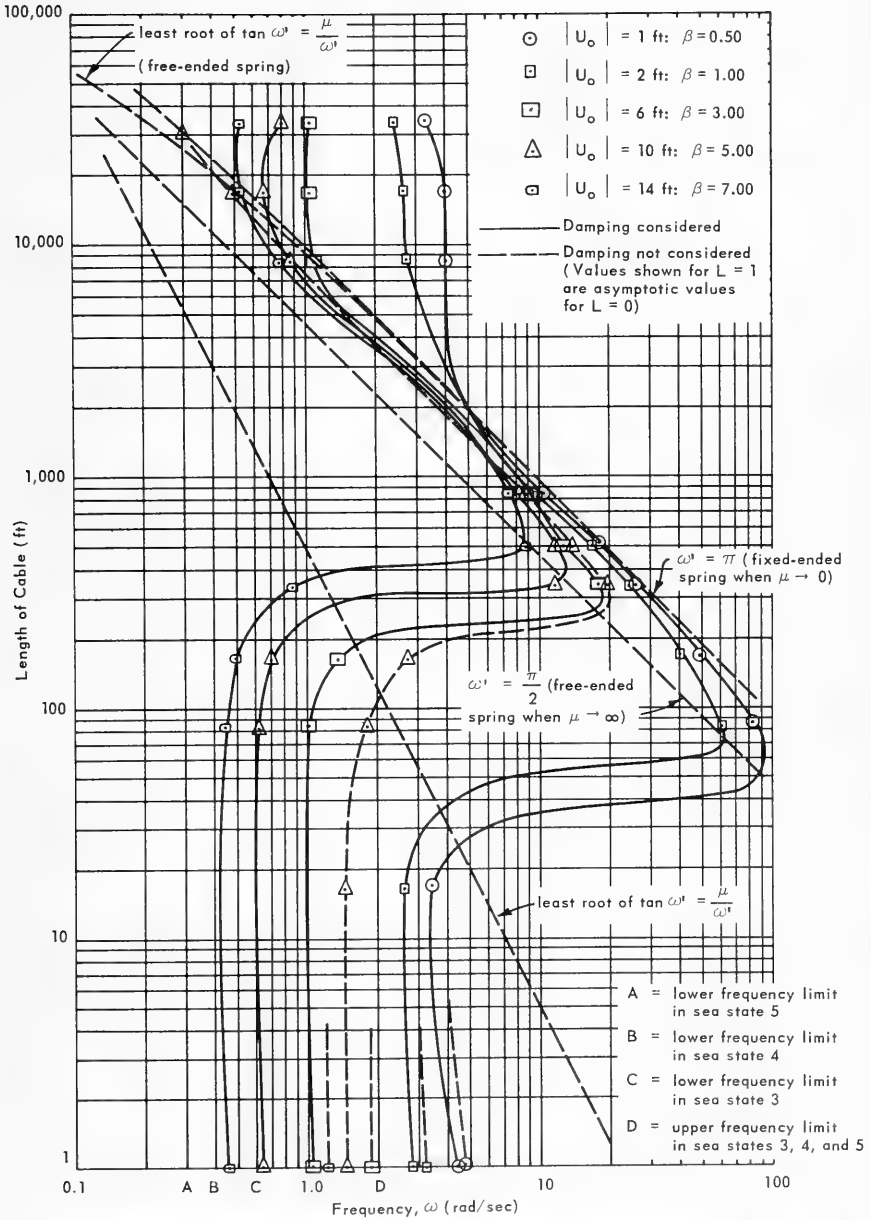

Figure 33. Results for design example using polypropylene cable.

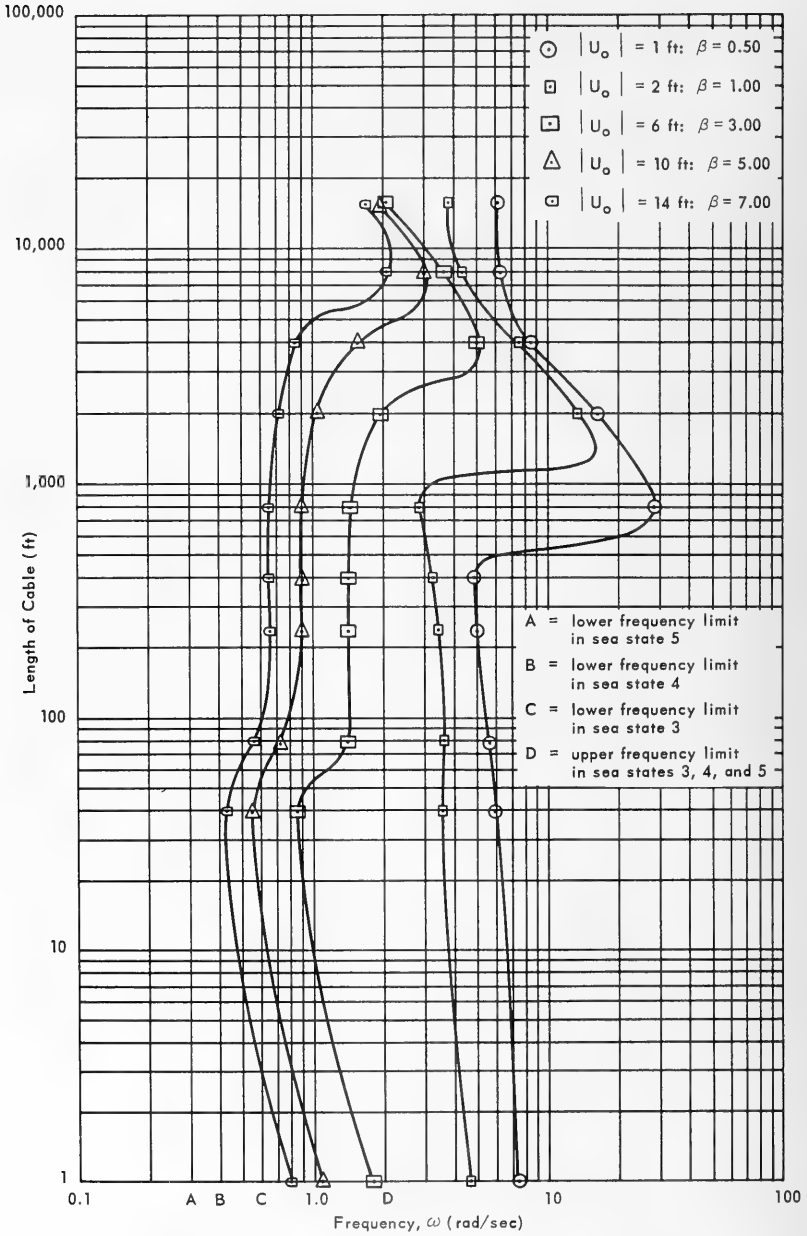

Figure 34. Results for design example using steel cable.

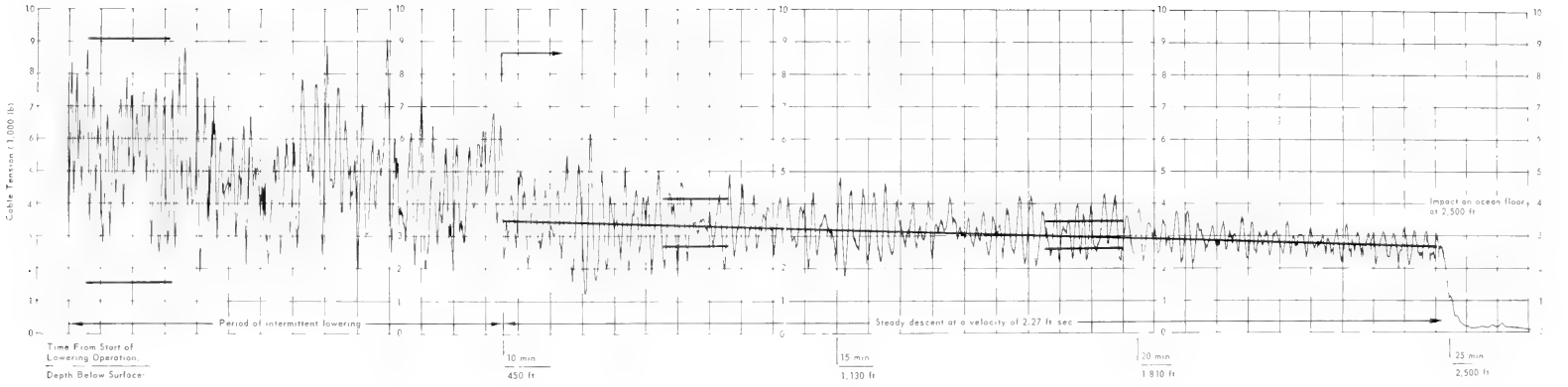

Figure 35. Record of cable tension during STU lowering operation. Comparison with calculated maximum dynamic stresses.

Appendix A

ANALYSIS OF CABLE AND PAYLOAD DYNAMICS FOR RAISING AND LOWERING LOADS IN THE DEEP OCEAN

The analysis presented here is essentially that given in BuShips Technical Report No. 1370863, "Stress Analysis of Ship-Suspended Heavily Loaded Cables for Deep Underwater Emplacements," by Arthur D. Little, Inc. [1]

The cable and load are considered to be in a vertical position as shown in Figure 1; i.e., the deflection of the cable due to currents is small. Any displacement of the cable support point will cause the dynamic displacement $u(x, t)$ at time t of an element of cable originally located at x; see Figure 1. Displacement $u(x, t)$ is of a form which satisfies the equation for the propagation of waves in the cable:

$$\rho_c S \frac{\partial^2 u}{\partial t^2} = SE \frac{\partial^2 u}{\partial x^2} - K \frac{\partial u}{\partial t} \tag{A-1}$$

where ρ_c = density of the cable

S = material cross section of the cable

E = modulus of elasticity of the cable

K = constant of friction on the cable due to the surrounding water

In an actual lowering or raising operation, the length of the cable, L, varies with time. However, it is assumed that L may be considered constant over short periods of time; i.e., the net vertical motion of the load and cable does not influence the dynamic displacements due to the cable support-point oscillations.

The following nondimensional variables and parameters may then be defined:

$$x' = \frac{x}{L}, \qquad t' = \frac{tc}{L} \tag{4d, e}$$

$$c^2 = \frac{E}{\rho_c}, \qquad \beta_c = \frac{KL}{\rho_c c S} \tag{4c, a}$$

and Equation A-1 becomes

$$\frac{\partial^2 u}{(\partial t')^2} + \beta_c \frac{\partial u}{\partial t'} = \frac{\partial^2 u}{(\partial x')^2} \tag{1}$$

The boundary conditions at the upper end of the cable is the specification that u at x' = 0. The boundary condition at the load, when x = L, is given by

$$M_a \frac{\partial^2 u}{\partial t^2} + ES \frac{\partial u}{\partial x} + \frac{1}{2} C_D \rho A \left|\frac{\partial u}{\partial t}\right| \frac{\partial u}{\partial t} = 0 \qquad \text{(A-2)}$$

where M_a = dynamic mass of the array

C_D = drag coefficient of the array

A = horizontal cross section of the load

By defining the parameters

$$\mu = \frac{\rho_c S L}{M_a}, \qquad B = \frac{C_D \rho A}{2 M_a} \qquad \text{(4b, f)}$$

Equation A-2 may be reduced to

$$\frac{\partial^2 u}{(\partial t')^2} + \mu \frac{\partial u}{\partial x'} + B \left|\frac{\partial u}{\partial t'}\right| \frac{\partial u}{\partial t'} = 0 \qquad (2)$$

at x' = 1.0.

The difficulty of applying this boundary condition, Equation A-2, arises from the nonlinear term $B\,|\partial u/\partial t'\,|\,(\partial u/\partial t')$, which represents the drag on the load. To avoid the complexities arising from this nonlinear term, an approximation was made in the reference report by replacing the $|\partial u/\partial t'|$ term by $(8/3\pi)\omega U_1$, where U_1 is the amplitude of the load displacement, which is assumed to be sinusoidal. This selection results in the same energy dissipation when u is sinusoidal in the third term of Equation 2. It is demonstrated in the report that this approximation leads to errors on the order of 20% in the drag term.

Defining a normalized displacement amplitude U' equal to U divided by $|U_o|$ and noting that U'_1 is the value of U' at the load, a solution for U' as a function of x' is given by

$$U' = U'_1 \cos \omega' y' + C \sin \omega' y' \qquad (5)$$

where y' = 1 - x' and

$$\omega' = \frac{\omega L}{c} \qquad (6b)$$

This solution satisfies the governing equation, Equation 1, provided the friction of water on the cable may be neglected. In Appendix A of the reference report it is shown that this assumption is valid for the frequency range of interest.

Substituting Equation 5 into Equation 2 and incorporating the boundary conditions, the unknown complex constant C is determined as

$$C = \frac{\omega'}{\mu} U_1' (-1 + i\beta U_1') \tag{A-3}$$

and hence, Equation 5 reduces to

$$U' = U_1' \sec\varphi \cos(\omega' y' + \varphi) + i\beta (U_1')^2 \tan\varphi \sin\omega' y' \tag{A-4}$$

where

$$\tan\varphi = \frac{\omega'}{\mu}, \qquad 0 \le \varphi \le \frac{\pi}{2} \tag{A-5}$$

In requiring that $|U'|$ at $y' = 1$ be equal to 1, U_1' is determined to be

$$(U_1')^2 = \frac{\cos^2(\omega' + \varphi)}{2\beta^2 \sin^2\varphi \sin^2\omega'} \left\{ \left[1 + \frac{\beta^2 \sin^2\omega' \sin^2 2\varphi}{\cos^4(\omega' + \varphi)} \right]^{1/2} - 1 \right\} \tag{8}$$

If the amplitude of the dynamic stress is denoted by Σ and a normalized stress amplitude, Σ', is defined equal to $L\Sigma/|U_o|E$, the distribution of Σ' is given by

$$\Sigma' = \omega' U_1' \sec\varphi \sin(\omega' y' + \varphi) - i\omega\beta (U_1')^2 \tan\varphi \cos\omega' y' \tag{A-6}$$

Hence the normalized amplitude of the maximum dynamic stress $|\Sigma'_{max}|$ is of the form

$$(\Sigma'_{max})^2 = (\omega')^2 (U_1')^2 [1 + \tan\varphi (\tan\Psi + \sec\Psi)] \tag{7}$$

where

$$(U_1')^2 = \frac{\cos^2(\omega' + \varphi)}{2\beta^2 \sin^2\varphi \sin^2\omega'} \left\{ \left[1 + \frac{\beta^2 \sin^2\omega' \sin^2 2\varphi}{\cos^4(\omega' + \varphi)} \right]^{1/2} - 1 \right\} \tag{8}$$

$$\varphi = \arctan\frac{\omega'}{\mu}, \qquad 0 \le \varphi \le \frac{\pi}{2} \tag{9}$$

$$\Psi = \arctan\left[\frac{1}{2}\beta^2 (U_1')^2 \tan\varphi - \cot 2\varphi\right], \qquad -\frac{\pi}{2} \le \Psi \le \frac{\pi}{2} \tag{10}$$

Equation 7 together with Equations 8, 9, and 10 was evaluated by use of a computer program as given in Appendix C, in which $|\Sigma'_{max}|$ was determined as a function of ω' for various ranges of β and μ.

Appendix B

EVALUATION OF THE NORMALIZED AMPLITUDE OF THE MAXIMUM DYNAMIC STRESS AS $\omega' \to n\pi$

As noted in the main text in the Discussion of results, the normalized amplitude of the maximum dynamic stress, $|\Sigma'_{max}|$, is particularly sensitive to variations of ω'. For particular values of ω', given specific values of β and μ, it is desirable to evaluate the peak in $|\Sigma'_{max}|$ more precisely than by an interpolation of the computer output. This essentially requires the derivation of $d\Sigma'_{max}/d\omega'$ from Equation 7, equating this to zero, and solving for ω' as a function of β and μ. Inspection of Equation 7 indicates the complexity of this derivation, which is unilluminating in terms of a proposed design procedure. As an alternative, Equation 7 was evaluated in the limit as ω' approaches $n\pi$, where $n = 1, 2, 3, \ldots$ In certain cases, this corresponds to the peak in the maximum dynamic stress $|\Sigma'_{max}|$. The analysis was carried out in order to determine the inaccuracies involved in interpolating the computer output, and is repeated here for completeness.

Given Equations 7, 8, 9, and 10 below, it is required to determine the value of $|\Sigma'_{max}|$ as ω' approaches $n\pi$, where $n = 1, 2, 3, \ldots$

$$(\Sigma'_{max})^2 = (\omega')^2 (U'_1)^2 [1 + \tan\varphi(\tan\Psi + \sec\Psi)] \tag{7}$$

$$(U'_1)^2 = \frac{\cos^2(\omega' + \varphi)}{2\beta^2 \sin^2\varphi \sin^2\omega'} \left\{ \left[1 + \frac{\beta^2 \sin^2\omega' \sin^2 2\varphi}{\cos^4(\omega' + \varphi)} \right]^{1/2} - 1 \right\} \tag{8}$$

$$\varphi = \arctan \frac{\omega'}{\mu}, \qquad 0 \le \varphi \le \frac{\pi}{2} \tag{9}$$

$$\Psi = \arctan \left[\frac{1}{2} \beta^2 (U'_1)^2 \tan\varphi - \cot 2\varphi \right], \qquad -\frac{\pi}{2} \le \Psi \le \frac{\pi}{2} \tag{10}$$

From Equation 9, when $\omega' \to n\pi$,

$$\tan\varphi = \frac{\omega'}{\mu} = \frac{n\pi}{\mu} \tag{B-1}$$

$$\cot 2\varphi = \frac{1 - \tan^2\varphi}{2\tan\varphi} = \frac{1 - \left(\frac{n\pi}{\mu}\right)^2}{2\left(\frac{n\pi}{\mu}\right)} \tag{B-2}$$

From Equations 10, B-1, and B-2,

$$\tan\Psi = \left\{ \frac{1}{2}\beta^2 (U_1')^2 \frac{n\pi}{\mu} - \left[\frac{1 - \left(\frac{n\pi}{\mu}\right)^2}{2\left(\frac{n\pi}{\mu}\right)} \right] \right\} \tag{B-3}$$

As $\omega' \to n\pi$, $\sin^2\omega' \to 0$

$$\cos^2(\omega' + \varphi) \to \cos^2\varphi \tag{B-4}$$

$$\cos^4(\omega' + \varphi) \to \cos^4\varphi \tag{B-5}$$

By defining $C = (\beta^2 \sin^2 2\varphi)/\cos^4\varphi$, Equation 8 becomes

$$(U_1')^2 = \frac{\cos^2\varphi}{2\beta^2 \sin^2\varphi \sin^2\omega'} \left[(1 + C\sin^2\omega')^{1/2} - 1 \right] \tag{B-6}$$

In Equation B-6,

$$\lim_{\omega' \to n\pi} \left[\frac{(1 + C\sin^2\omega')^{1/2} - 1}{\sin^2\omega'} \right] = \lim_{\omega' \to n\pi} \left[\frac{\frac{1}{2} C\, 2\sin\omega'\cos\omega'}{(1 + C\sin^2\omega')^{1/2}} \right] \left(\frac{1}{2\sin\omega'\cos\omega'} \right)$$

$$= \lim_{\omega' \to n\pi} \left[\frac{\frac{1}{2} C}{(1 + C\sin^2\omega')^{1/2}} \right] = \frac{1}{2} C$$

Therefore, from Equation B-6,

$$\lim_{\omega' \to n\pi} (U_1')^2 = \frac{1}{2} C \left(\frac{\cos^2\varphi}{2\beta^2 \sin^2\varphi} \right)$$

$$= \frac{1}{2}\left(\frac{\beta^2 \sin^2 2\varphi \cos^2\varphi}{\cos^4\varphi\, 2\beta^2 \sin^2\varphi}\right)$$

$$= \frac{1}{4}\left(\frac{\sin^2 2\varphi}{\cos^2\varphi \sin^2\varphi}\right) = 1$$

That is,

$$\lim_{\omega' \to n\pi} (U_1')^2 = 1 \tag{B-7}$$

Thus, from Equation B-3,

$$\tan\Psi = \left\{ \frac{1}{2}\beta^2 \frac{n\pi}{\mu} - \left[\frac{1 - \left(\frac{n\pi}{\mu}\right)^2}{2\left(\frac{n\pi}{\mu}\right)}\right] \right\} \tag{B-8}$$

But $\sec\Psi = \pm\sqrt{1 + \tan^2\Psi}$, and since $-\pi/2 \le \Psi \le \pi/2$,

$$\sec\Psi = +\sqrt{1 + \tan^2\Psi} \tag{B-9}$$

From Equations 7, B-1, B-7, and B-9,

$$\lim_{\omega' \to n\pi} (\Sigma'_{max})^2 = (n\pi)^2 \left\{ 1 + \frac{n\pi}{\mu}\left[\tan\Psi + (1+\tan^2\Psi)^{1/2}\right] \right\} \tag{B-10}$$

or

$$= (n\pi)^2 \left\{ 1 + \frac{n\pi}{\mu} \left[\frac{1}{2}\beta^2 \frac{n\pi}{\mu} - \left[\frac{1 - \left(\frac{n\pi}{\mu}\right)^2}{2\left(\frac{n\pi}{\mu}\right)}\right] + \left[1 + \left\{ \frac{1}{2}\beta^2 \frac{n\pi}{\mu} - \left[\frac{1 - \left(\frac{n\pi}{\mu}\right)^2}{2\left(\frac{n\pi}{\mu}\right)}\right] \right\}^2 \right]^{1/2} \right] \right\} \tag{B-11}$$

and letting $K = n\pi/\mu$,

$$\lim_{\omega' \to n\pi} (\Sigma'_{max})^2 = (n\pi)^2 \left\{ \left\{ 1 + K \left\{ \frac{1}{2}\beta^2 K - \frac{1}{2K} - \frac{K}{2} + \left[1 + \left(\frac{1}{2}\beta^2 K + \frac{1}{2K} - \frac{K}{2} \right)^2 \right]^{1/2} \right\} \right\} \right. \tag{13}$$

Values of $\left|\Sigma'_{max}\right|$, evaluated from Equation 13, are given in the Results section of the main report for various ranges of β and μ.

Appendix C

COMPUTER PROGRAM FOR THE EVALUATION OF THE NORMALIZED AMPLITUDE OF THE MAXIMUM DYNAMIC STRESS, $|\Sigma'_{max}|$

The program evaluates the normalized amplitude of the maximum dynamic stress, $|\Sigma'_{max}|$, according to Equations 7, 8, 9, and 10 given in Appendix A and is written for use on an IBM 1620 digital computer. A flow chart for the program is given in Figure C-1, followed by the FORTRAN source program.

Input parameters are read as follows in format (2F10.2, 2F10.8, 2F5.2, F10.8):

CAY = parameter equal to $\frac{4 C_D \varphi A}{3 \pi M_a} = k$

UM = parameter equal to $\frac{w L}{M_a} = \mu$

SFR = increment on nondimensional frequency scale, $\Delta\omega'$

FMAX = maximum nondimensional frequency, ω'_{max}

STU = increment on input displacement amplitude $|U_o|$, ΔU_o

UMAX = maximum input displacement amplitude, $|U_o|_{max}$

FZER = initial nondimensional frequency, ω'_o

The computed output is presented on punched cards in the following form. The values of k, μ, β, and $|U_o|$ are given followed by the input parameters as defined above. The computed values of $|\Sigma'_{max}|$ are then tabulated at each value of the nondimensional frequency, according to format (E15.8, 3X, F8.4) for a particular $|U_o|$. The process is then repeated for each value of $|U_o|$ up to $|U_o|_{max}$, at which point a new set of input data is required.

The initial frequency is used as an input parameter in order that specific ranges on the nondimensional frequency axis may be investigated; e.g., relatively small increments in frequency may be used over a range of frequency corresponding to peak values in $|\Sigma'_{max}|$. There is a limit to the smallest allowable increment in frequency resulting from the rounding-off errors inherent to the program, which results in $|\Sigma'_{max}|$ equaling 0 at ω' near to π. These errors are discussed in the main text under Discussion of Results.

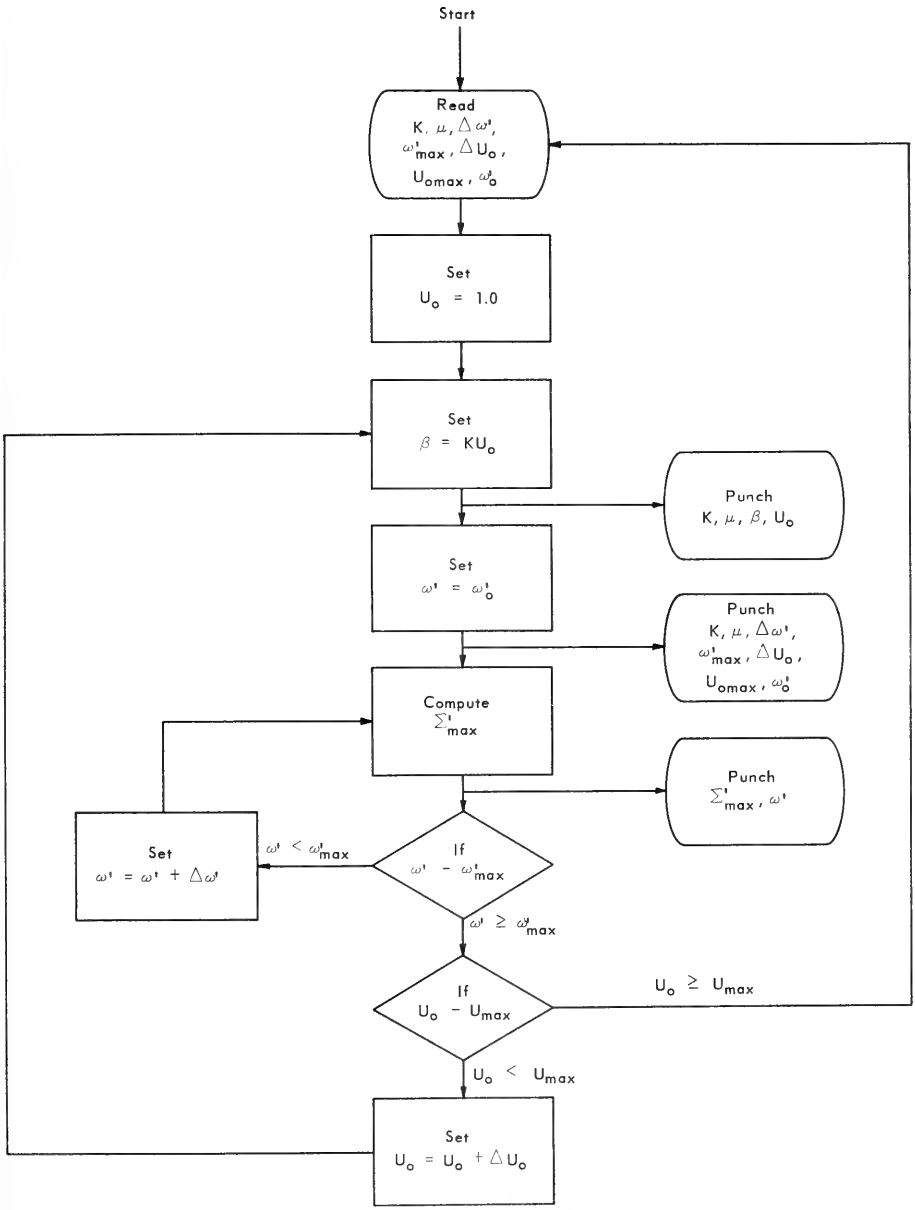

Figure C-1. Flow chart for computer program to evaluate $\left|\Sigma'_{max}\right|$.

```
C       STRESS IN CABLE LOWERING LOADS TO DEEP OCEAN.
C       CAY=CONSTANT,K,  UM=PARAMETER,  SFR=STEP IN FREQUENCY.
C       FMAX=MAXIMUM FREQUENCY,  STU=STEP IN U-ZERO,
C       UMAX=MAXIMUM U-ZERO,  FZER=INITIAL FREQUENCY.
    1 READ 100,CAY,UM,SFR,FMAX,STU,UMAX,FZER
      UO=1.0
    8 BETA=CAY*UO
      PUNCH 101
      PUNCH 102,CAY,UM,BETA,UO
      FREQ=FZER
      PUNCH 111,CAY,UM,SFR,FMAX,STU,UMAX,FZER
      PUNCH 109
    5 PHI=ATAN(FREQ/UM)
      ALPH=2.*PHI
      DELT=FREQ+PHI
      UONS=(COS(DELT))**2/(2.*BETA**2*SIN(PHI)**2*SIN(FREQ)**2)
      TERM=(1.+((BETA**2*SIN(FREQ)**2*SIN(ALPH)**2)/COS(DELT)**4))
      TERM=TERM**0.5
      TERM=TERM-1.
      UON=UONS*TERM
      U=UON**0.5
      TPSI=((0.5*BETA**2.*UON)*SIN(PHI)/COS(PHI))-(COS(ALPH)/SIN(ALPH))
      PSI=ATAN(TPSI)
      STRS=(1.+SIN(PHI)/COS(PHI)*(SIN(PSI)/COS(PSI)+1./COS(PSI)))
      STRS=STRS*UON*(FREQ**2.)
      STR=STRS**0.5
      PUNCH 110,STR,FREQ
      IF(FREQ-FMAX)3,4,4
    3 FREQ=FREQ+SFR
      GO TO 5
    4 IF(UO-UMAX)6,1,1
    6 UO=UO+STU
      GO TO 8
  100 FORMAT(2F10.2,2F10.8,2F5.2,F10.8)
  101 FORMAT(8X,9H CONSTANT,4X,3H UM,10X,5H BETA,8X,7H U-ZERO)
  102 FORMAT(3X,F10.2,3X,F10.2,3X,F10.2,3X,F10.2)
  109 FORMAT(7H STRESS,10X,10H FREQUENCY)
  110 FORMAT(E15.8,3X,F8.4)
  111 FORMAT(2F10.2,2F10.5,2F5.2,F10.5)
      END
```

Appendix D

SUMMARY OF DRAG COEFFICIENTS

INTRODUCTION

In an analysis of the motions of a body through water, whether the body is falling freely or being lowered by cable, one of the most important effects which must be considered is the resistance, or drag, experienced by the body.

The purpose of this appendix is to summarize existing information on drag forces and indicate areas of work which must be covered in order that such forces may be included in calculating the motions of a load being lowered to the deep ocean.

DRAG IN UNIFORM FLOW

On the front of every solid body moving through water, there is at least one point where there is no relative motion between the water particles and the body; i.e., there is a stagnation point. The pressure at this point, termed the dynamic pressure, is given as

$$P_{stag} = \frac{1}{2}\rho V^2 \tag{D-1}$$

where ρ is the density of water and V is the relative velocity of the body to the water. It is convenient to express the total drag due to pressure forces relative to this stagnation pressure by defining

$$D = C_D\left(\frac{1}{2}\rho V^2\right)S \tag{D-2}$$

where D is the drag force due to pressure, C_D is the coefficient of drag, and S is a representative area of the body — either its frontal or cross-sectional area. Equation D-2 is essentially a definition of C_D.

The total drag on any body consists of the "pressure drag," defined above, plus drag forces due to skin friction. However, for angular bodies such as those envisaged as loads to be lowered to the deep ocean floor, the skin friction drag may be assumed small compared to the pressure drag.

According to Reynolds' Similarity Law, the flow pattern around the drag coefficients on two similar bodies (identical in shape but dissimilar in size) moving through a body of water are similar if their Reynolds numbers, R_e, are identical:

$$R_e = \frac{V d \rho}{\mu} = \frac{V d}{\nu} \tag{D-3}$$

where V is the velocity of the body relative to the water, ρ is the density of the water, μ is its absolute viscosity, ν is its kinematic viscosity (μ/ρ), and d is a characterizing dimension of the body.

Hence it is possible to determine the appropriate C_D for a body moving through water from the results of experiments performed on an identically shaped body of a different scale and possibly in a different fluid, provided the Reynolds numbers are equal.

The kinematic viscosity of sea water at normal temperatures and pressures is on the order of 1.5×10^{-5} square feet per second. If a load to be lowered to the deep ocean has a typical dimension of 15 feet, and moves at a velocity on the order of 1 foot per second, the Reynolds number, R_e, equals 10^6. It appears that relatively little information is available from the literature on the variation of coefficients of drag at Reynolds numbers greater than 10^6 to 10^7. Figure D-1 with inserts show the variation of C_D with R_e for spheres and cylinders respectively, and summarizes some, though by no means all, existing data on the coefficients of drag applicable to bodies of different shapes.

Although objects to be dropped or lowered to the deep ocean floor may not be spherical or cylindrical, a brief investigation of the dynamics of a sphere is illuminating. Consider a body held stationary in water and which is then allowed to fall freely. During the initial motions, the velocity is small and the body will accelerate under its own weight minus a buoyancy force due to the weight of water displaced, the drag force being negligible at this stage. This net vertical force acts on the mass of the body plus a certain fraction of its mass which is included to account for the water contained in the body, if any, and an effective mass of water to which accelerations are imparted due to the motion of the body. The latter terms are usually called the "apparent added mass"; the total mass (body mass and apparent added mass) being termed the "virtual mass." Values of the apparent added mass vary from 40% to 150% of the mass of the body.

As the velocity increases from zero, the drag force opposing the motion becomes significant, and at a particular time $t = t_1$ this force is given by

$$F_D = C_D \left(\frac{1}{2} \rho V_1^2\right) S \tag{D-4}$$

where V_1 is the velocity at $t = t_1$, and C_D is the appropriate coefficient of drag. After a given time the velocity of the falling body attains a terminal velocity, V_T, in which condition the drag force balances the body weight minus the buoyancy force; i.e.,

$$(W_B - F_B) = F_D = (C_D)_T \left(\frac{1}{2} \rho V_T^2\right) S \qquad \text{(D-5)}$$

where $(C_D)_T$ is the coefficient of drag at the Reynolds number corresponding to a velocity of V_T. Equation D-5 may be rewritten as

$$(W_B - F_B) = F_D = f\left(\frac{V_T L}{\mu}\right) \left(\frac{1}{2} \rho V_T^2\right) S \qquad \text{(D-6)}$$

The function $f(V_T L/\mu)$ is not known and cannot be defined analytically, and Equation D-6 cannot be solved explicitly for the terminal velocity, V_T, without the prior assumption of a particular C_D.

However, starting from zero initial velocity, it is possible to determine the motion of a particular body by considering the acceleration and velocities attained over small increments of time. A simple computer program was written to accomplish this. At $t = 0$ the velocity is zero, there is no drag force, and the body will accelerate under the force $(W_B - F_B)$. At $t = t_1$ the velocity is finite and the appropriate Reynolds number may be calculated together with the corresponding C_D. For the purpose of these calculations, C_D was specified at increments of R_e, and a simple interpolation was made to determine the specific C_D corresponding to R_e at $t = t_1$. Hence the drag and out-of-balance force may be calculated at $t = t_1$ together with the instantaneous acceleration at this point. The process can be repeated to determine the velocity of the body at time increments from $t = 0$ to $t = T$, where T is the time taken to attain a terminal velocity.

For an up-to-date complete treatment of hydrodynamic drag, the excellent treatise prepared and published by Dr. Sighard F. Hoerner[5] should be consulted.

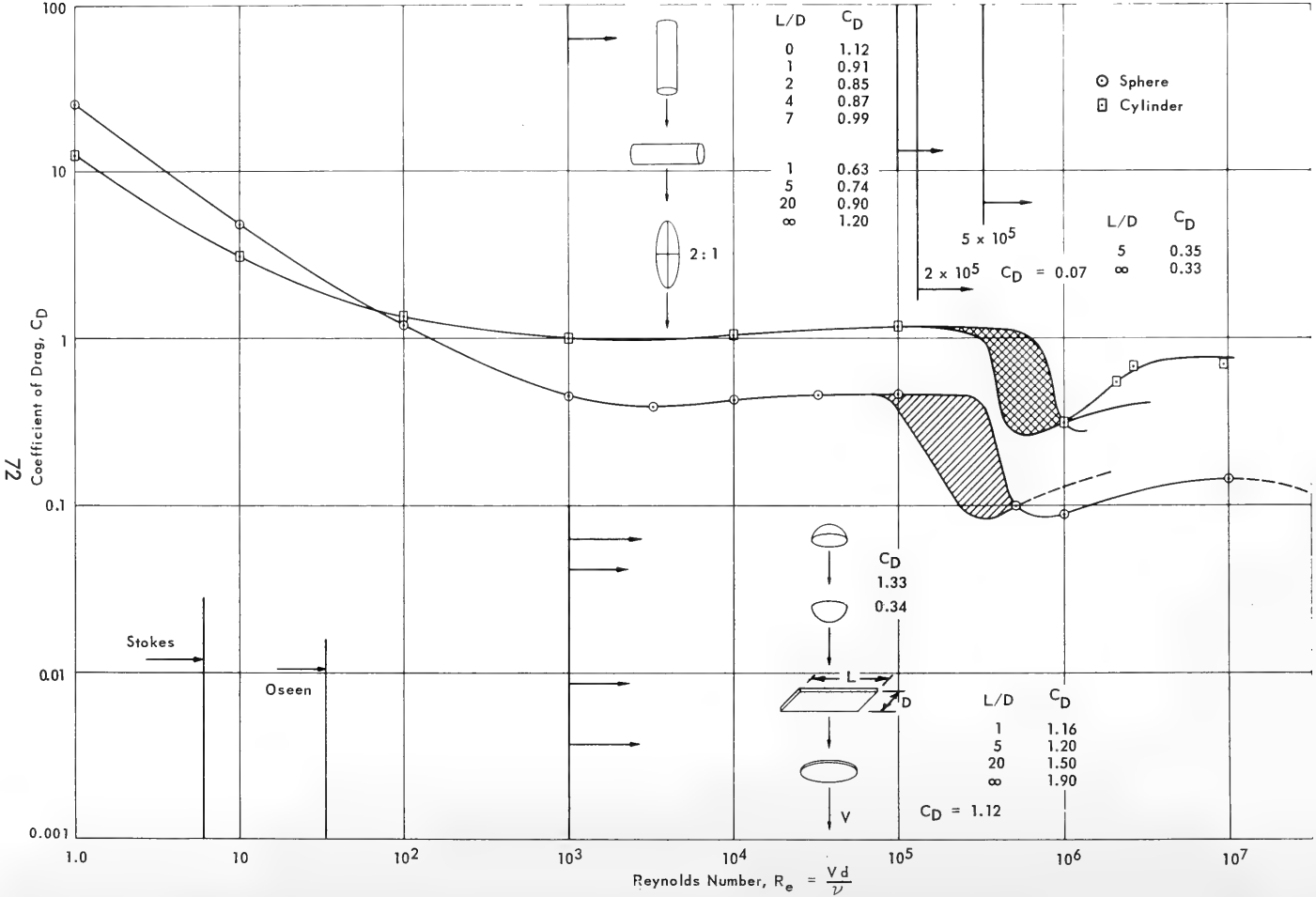

Figure D-1. Variation of C_D with Reynolds number.

Appendix E

SUMMARY OF ADDED MASS COEFFICIENTS

The concept of added mass is well known in fluid mechanics. The physical explanation of this phenomenon is that when a body is subjected to an unbalanced force, not only must the mass of the body be accelerated, but also that of the added fluid mass surrounding the body. The ratio of this added fluid mass to the body mass is the added mass coefficient, C_m.

The added mass depends on the dimensions and shape of the body and the density and viscosity of the fluid. In general, measurements of the apparent added mass have been obtained under two fundamentally different flow situations. In one the motion is oscillatory in that an immersed body is vibrated. In the other the motion is unidirectional in that an immersed body is accelerated rectilinearly. The exact analytical description of fluid resistance to the acceleration of an arbitrarily shaped submerged solid is not known, hence the exact added mass coefficient for various shapes of objects is not known. The following reports are the results of different experiments under different conditions, but they are quite consistent: T. E. Stelson and F. T. Mavis,[6] E. Silberman,[7] T. Sarpkaya,[8] N. L. Ackermann and A. Arbhabhirama,[9] O. C. Zienkiowicz and B. Nath.[10] A summary of most of the important results obtained from these references is presented in Figure E-1.

The coefficients, C_m, have been arranged in terms of a common dimension, namely the ratio of the added mass to the mass of fluid displaced. The results obtained from oscillatory motion are as follows:

1. Spheres: $C_m = 0.51$. This compares with a value of 0.50 obtained from ideal fluid theory for rectilinear motion.
2. Cubes: $C_m = 0.67$ ("broadside-on" or "edge-on").
3. Circular Cylinders: See Figure E-1. The abscissa is the ratio of length to diameter. The motion is in the direction perpendicular to the circular cross section.
4. Rectangular Plates: See Figure E-1. The abscissa is the ratio of length to width. The motion is in the broadside-on direction. The ratio of thickness to width is limited to values less than 0.04.
5. Square Prisms: See Figure E-1. The abscissa is the ratio of length to width of the square sides. The motion is in the direction perpendicular to the square cross section.

6. Symmetrical Lenses: See Figure E-1. These lenses are two intersecting or separated spheres:

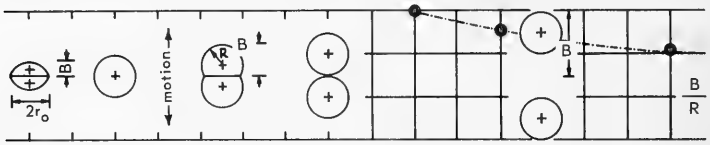

The abscissa is the ratio of B/R. The motion is in the direction shown.

7. Two Parallel Rectangular and Square Plates: See Figure E-1. The abscissa is the ratio of spacing between two plates to width, where the spacing is measured from center to center of the plates. The ratio of length to width of the plates are over 17 to 1. The motion is in a direction parallel to the thickness of the plates.

For all of the oscillatory motion cases the experiments were conducted at low velocities and high accelerations. Thus the total resistance force to the moving object is largely due to the added mass which is dependent on the acceleration. At higher velocities, the total resistance force is due to a velocity-dependent drag term as well as to the added mass term. That part of the resistance to motion due to viscous and form drag and that part due to added mass are difficult to separate. Stelson and Mavis[6] and Silberman[7] realized the difficulties. From experiments on a sphere the measured added mass increased by approximately 1% above the values obtained from ideal fluid theory. Thus it was concluded that viscosity did not seriously affect the experimental values for the added mass.

A recent method (Zienkiewicz and Nath[10]) of measuring the added mass is worth mentioning here. Using an electric analogy method, the virtual mass as well as the pressure distribution around a rigid body accelerating in an incompressible fluid can be determined. In the following table, the results are compared with the known added mass coefficients obtained from other sources. Agreement is excellent.

Object	Added Mass Coefficient	
	Obtained by Zienkiewicz[10]	From Indicated Source
Infinitely long vertical plate	1.03	1.04 (Riabouchinsky[10])
Infinitely long cylinder	0.98	1.00 (H. Lamb[11])
Thin circular disc	0.61	0.636 (H. Lamb[11])
Cube	0.62	0.67 (Stelson[6])

These values are measured for an infinitely large submergence depth. At small depths the measured added mass decreased. This agrees with the physical explanation of the added mass phenomenon. The experiments were conducted for small-amplitude motions and no separation occurred, hence the boundary effect is not considered. This method can be used for rotary acceleration of a body. This experimental method has important implications since it can be set up in a deep ocean simulating tank to measure the added mass as well as the pressure distribution of any arbitrarily shaped object under translational or rotary motion.

For the unidirectional motion, the viscous and boundary effects must be considered. Experiments for this type of motion have been conducted for a number of bodies, but only that for spheres will be cited. Arbhabhirama[9] found that when the ratio of the diameter of a sphere to the diameter of a fluid filling a concentric spherical shell is 0.259, which is similar to a sphere oscillating in an infinite fluid, the added mass is found to be 1.03 times the added mass obtained from potential flow.

In summary, although some data is available on added mass coefficients in oscillatory flow, most of the experiments have been conducted at small scale and within the low Reynolds number regime. As an example, the following estimate of the added mass of a complicated frame structure such as the STU described below, is cited. Theoretically the oscillatory motion of a load being lowered to the ocean floor and suspended by a cable is a damped simple harmonic motion. If the cable is considered to be elastic, the equation of motion is

$$M_a \ddot{x} + C\dot{x} + kx = 0$$

where M_a is the virtual mass of the load, x is the elongation of the cable, k is the ratio of the restraining force to the elongation of the cable, and C is the coefficient of damping. The solution of this equation is quite complicated, but the period of oscillation is the same as for simple undamped harmonic motion:

$$M_a \ddot{x} + kx = 0$$

Hence, the period $T = 2\pi (M_a/k)$.

On 13 April 1965, a Submersible Test Unit (STU) was lowered by this Laboratory to the ocean floor to a depth of 2,500 feet using a 1.3-inch-diameter polypropylene cable. The cable tensions were recorded as a function of time from the start of lowering operation. The curve of the graph (Figure 35) shows the oscillatory motion of the STU, consequently the average period of 9.8 seconds was obtained while the average tension of the cable in this interval (between 10 and 12 minutes as marked on the figure) was 3,400 pounds. The breaking strength of the cable is 45,000 pounds ("Braided Rope and Cordage Catalog," Samson Cordage Works, Boston, Mass.). From the percent load of breaking strength versus the percent elongation curve of polypropylene cables, the corresponding percent elongation of 4.0 is obtained. Since the

average cable length in this interval is 586 feet, the elongation of the cable is $0.04 \times 586 = 23.4$ feet. The restoring-force constant was determined to be 145 pounds per foot (i.e., 3,400/23.4). The virtual mass of the cable assembly was found to be 11,350 pounds; i.e., $M_a = (T^2/4^2)g = [(9.8)^2 (145)/4^2] 32.2$. Of this 11,350 pounds, 950 pounds is due to the static weight of the suspended cable. The net weight of the STU in water is 5,500 pounds. Thus the added mass coefficient, C_m, is determined to be slightly less than 2.0 (i.e., 10,700/5,500).

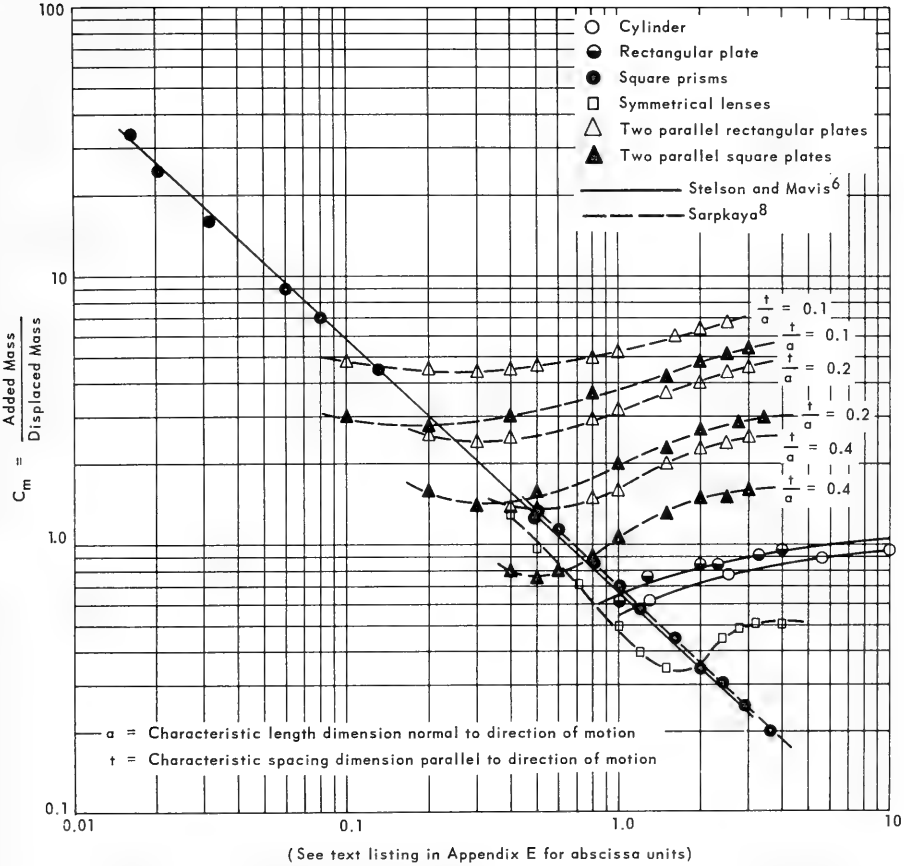

Figure E-1. Added mass coefficient as a function of circular frequency for constant geometric ratios.

REFERENCES

1. Arthur D. Little, Inc. Technical Report no. 1370863 on Project Trident, Bureau of Ships Contract NObsr-81564: Stress analysis of ship-suspended heavily loaded cables for deep underwater emplacements. Cambridge, Mass., Aug. 1963. AD-418028.

2. Marine Advisers, Inc. Report on Contract NBy-32206: The motions of a moored construction-type barge in irregular waves and their influence on construction operation, by P. Kaplan and R. R. Putz. La Jolla, Calif., Aug. 1962.

3. U. S. Naval Civil Engineering Laboratory. Technical Note N-604: The engineering applications of a report entitled "The motions of a moored construction-type barge in irregular waves and their influence on construction operation," by W. J. Pierson and P. Holmes. Port Hueneme, Calif., Aug. 1964.

4. U. S. Navy, David Taylor Model Basin. Report 1221: Theoretical analysis of the effect of ship motion on mooring cables in deep water, by L. F. Whicker. Washington, D. C., Mar. 1958.

5. S. F. Hoerner. Fluid-dynamic drag, 2nd ed. Author, 148 Bustead Drive, Midland Park, N. J., 1965.

6. T. E. Stelson and F. T. Mavis. "Virtual mass and acceleration in fluids," American Society of Civil Engineers, Transactions, vol. 122, 1957, paper no. 2870, pp. 518-525.

7. E. Silberman. Discussion of the paper, "Virtual mass and acceleration in fluids," by T. E. Stelson and F. T. Mavis. American Society of Civil Engineers, Transactions, vol. 122, 1957, pp. 527-529.

8. T. Sarpkaya. "Added mass of lenses and parallel plates," American Society of Civil Engineers, Proceedings, Journal of the Engineering Mechanics Division, vol. 86, EM3, June 1960, pp. 141-152.

9. N. L. Ackermann and A. Arbhabhirama. "Viscous and boundary effects on virtual mass," American Society of Civil Engineers, Proceedings, Journal of the Engineering Mechanics Division, vol. 90, EM4, Aug. 1964, pp. 123-130.

10. O. C. Zienkiewicz and B. Nath. "Analogue procedure for determination of virtual mass," American Society of Civil Engineers, Proceedings, Journal of the Hydraulics Division, vol. 90, HY5, Sept. 1964, pp. 69-81.

11. H. Lamb. Hydrodynamics, 6th ed., 1932. London, Cambridge University Press; New York, Dover Publications.

A Cross-sectional area of the load in the direction of motion

B $\dfrac{C_D \rho A}{2 M_a}$

c Velocity of sound in the cable $= \sqrt{\dfrac{E}{\rho_c}}$

C_D Coefficient of drag applicable to the load

C_m Coefficient of mass applicable to the load

E Modulus of elasticity for the cable

F Safety factor for maximum operating stress in the cable

k A constant $= \dfrac{4 C_D \rho A}{3 \pi C_m M}$

K Constant of friction on the cable due to the surrounding water

L Length of the cable

M Mass of the load

M_a Virtual mass of the load

S Material cross-sectional area of the cable

u $u(x, t)$ = displacement of element from support point

U Displacement amplitude

U' Normalized displacement amplitude $= \dfrac{U}{|U_o|}$

U_1' Normalized displacement amplitude at the array

$|U_o|$ Input displacement amplitude

w Weight per unit length of cable

β Damping parameter $= \dfrac{4 C_D \rho A \, U_o}{3 \pi M_a}$

β_c $\dfrac{K L}{\rho_c c S}$

μ Ratio of cable weight to virtual mass of load $= \dfrac{\rho_c S L}{M_a} \quad \dfrac{w L}{M_a}$

ρ Density of seawater

ρ_c Density of cable material

Σ Amplitude of dynamic stress

Σ' Normalized dynamic stress

Σ_d Allowable dynamic stress in the cable $= \dfrac{\Sigma_{ult}}{F} - \Sigma_{static}$

Σ'_{max} Maximum normalized dynamic stress in the cable $= \dfrac{L \Sigma_d}{|U_o| \Sigma}$

Σ_{static} Static stress in the cable

Σ_{ult} Ultimate tensile strength of the cable

φ Constant defined by Equation 9

Ψ Constant defined by Equation 10

ω Frequency of oscillation $= \dfrac{\omega' c}{L}$

ω' Normalized frequency $= \dfrac{\omega L}{c}$

DISTRIBUTION LIST

CHIEF, BUREAU OF YARDS AND DOCKS (CODE 42)

COMMANDER, NAVAL CONSTRUCTION BATTALIONS, PACIFIC, FPO SAN FRANCISCO 96610

COMMANDING OFFICER, MOBILE CONSTRUCTION BATTALION NO. 7, FPO NEW YORK 09501

COMMANDING OFFICER, MOBILE CONSTRUCTION BATTALION NO. 8, FPO SAN FRANCISCO 96601

COMMANDING OFFICER, AMPHIBIOUS CONSTRUCTION BATTALION 1, SAN DIEGO, CALIF. 92155

COMMANDING OFFICER, AMPHIBIOUS CONSTRUCTION BATTALION 2, FPO NEW YORK 09501

OFFICER IN CHARGE, WESTERN PACIFIC DETACHMENT, AMPHIBIOUS CONSTRUCTION BATTALION 1, FPO SAN FRANCISCO 96662

CHIEF, BUREAU OF MEDICINE AND SURGERY, NAVY DEPARTMENT, WASHINGTON, D. C. 20390

CHIEF, BUREAU OF SHIPS, NAVY DEPARTMENT, WASHINGTON, D. C. 20360

CHIEF, BUREAU OF SUPPLIES AND ACCOUNTS, NAVY DEPARTMENT, WASHINGTON, D. C. 20360

DIRECTOR, NAVAL RESEARCH LABORATORY, WASHINGTON, D. C. 20390

COMMANDING OFFICER, OFFICE OF NAVAL RESEARCH, BRANCH OFFICE, ATTN PATENT DEPARTMENT, 1030 EAST GREEN STREET, PASADENA, CALIF. 91101

COMMANDING OFFICER, ATTN PUBLIC WORKS OFFICER, NAVAL STATION, KEY WEST, FLA. 33040

COMMANDING OFFICER, ATTN PUBLIC WORKS OFFICER, NAVAL STATION, LONG BEACH, CALIF 90802

COMMANDING OFFICER, ATTN PUBLIC WORKS OFFICER, U. S. NAVAL STATION, FPO NEW YORK 09585

COMMANDING OFFICER, ATTN PUBLIC WORKS OFFICER, U. S. NAVAL COMMUNICATION STATION, ROUGH AND READY ISLAND, STOCKTON, CALIF. 95203

COMMANDING OFFICER, NAVAL AMPHIBIOUS BASE, LITTLE CREEK, NORFOLK, VA. 23521

OFFICER IN CHARGE, NAVAL CONSTRUCTION TRAINING UNIT, NAVAL CONSTRUCTION BATTALION CENTER, DAVISVILLE, R. I. 02854

OFFICER IN CHARGE, NAVAL SCHOOL, CIVIL ENGINEER CORPS OFFICERS, NAVAL CONSTRUCTION BATTALION CENTER, PORT HUENEME, CALIF. 93041

SUPERINTENDENT, NAVAL POSTGRADUATE SCHOOL, MONTEREY, CALIF. 93940

PRESIDENT, NAVAL WAR COLLEGE, NEWPORT, R. I. 02844

COMMANDER, ATTN PUBLIC WORKS OFFICER, PUGET SOUND NAVAL SHIPYARD, BREMERTON, WASH. 98314

COMMANDER, ATTN PUBLIC WORKS OFFICER, CHARLESTON NAVAL SHIPYARD, U. S. NAVAL BASE, CHARLESTON, S. C. 29408

COMMANDER, ATTN PUBLIC WORKS OFFICER, PEARL HARBOR NAVAL SHIPYARD, BOX 400,

FPO SAN FRANCISCO 96610

COMMANDING OFFICER AND DIRECTOR, ATTN PUBLIC WORKS OFFICER, NAVY UNDERWATER SOUND LABORATORY, FORT TRUMBULL, NEW LONDON, CONN. 06321

COMMANDING OFFICER AND DIRECTOR, ATTN PUBLIC WORKS OFFICER, U. S. NAVY MINE DEFENSE LABORATORY, PANAMA CITY, FLA. 32402

COMMANDING OFFICER AND DIRECTOR, NAVY MARINE ENGINEERING LABORATORY, ANNAPOLIS, MD. 21402

COMMANDING OFFICER, ATTN PUBLIC WORKS OFFICER, U. S. NAVAL SUPPLY DEPOT, MECHANICSBURG, PA. 17055

COMMANDING OFFICER, ATTN PUBLIC WORKS OFFICER, NAVAL SUPPLY DEPOT, NEWPORT, R. I. 02840

COMMANDING OFFICER, U. S. NAVAL CONSTRUCTION BATTALION CENTER, PORT HUENEME, CALIF. 93041

OFFICER IN CHARGE OF CONSTRUCTION, U. S. NAVY BUREAU OF YARDS AND DOCKS CONTRACTS, FPO SAN FRANCISCO 96680

RESIDENT OFFICER IN CHARGE OF CONSTRUCTION, BUREAU OF YARDS AND DOCKS CONTRACTS, PACIFIC, BOX 418, SAN BRUNO, CALIF. 94067

COMMANDING GENERAL, MARINE CORPS RECRUIT DEPOT, PARRIS ISLAND, S. C. 29905

COMMANDANT, MARINE CORPS SCHOOLS, ATTN PUBLIC WORKS OFFICER, QUANTICO, VA. 22134

COMMANDING GENERAL, ATTN PUBLIC WORKS OFFICER, MARINE CORPS BASE, CAMP LEJEUNE, N. C. 28542

COMMANDING GENERAL, ATTN PUBLIC WORKS OFFICER, MARINE CORPS BASE, CAMP PENDLETON, CALIF. 92055

COMMANDING OFFICER, CAMP SMEDLEY D. BUTLER, U. S. MARINE CORPS, FPO SAN FRANCISCO 96673

COMMANDING OFFICER, ATTN PUBLIC WORKS OFFICER, NAVAL AIR STATION, QUONSET POINT, R. I. 02819

COMMANDING OFFICER, ATTN PUBLIC WORKS OFFICER, U. S. NAVAL AIR STATION, NORTH ISLAND, SAN DIEGO, CALIF. 92135

COMMANDING OFFICER, ATTN PUBLIC WORKS OFFICER, NAVAL AIR STATION, CECIL FIELD, FLA. 32215

COMMANDING OFFICER, ATTN PUBLIC WORKS OFFICER, U. S. NAVAL AIR STATION, GROSSE ILE, MICH. 48138

COMMANDING OFFICER, ATTN PUBLIC WORKS OFFICER, NAVAL AIR STATION, MINNEAPOLIS, MINN. 55450

COMMANDING OFFICER, ATTN PUBLIC WORKS OFFICER, NAVAL AIR STATION, WHIDBEY ISLAND, OAK HARBOR, WASH. 98277

COMMANDING OFFICER, ATTN PUBLIC WORKS OFFICER, U. S. NAVAL AIR STATION, FPO SAN FRANCISCO 96611

COMMANDING OFFICER, ATTN PUBLIC WORKS OFFICER, NAVAL AIR STATION, NEW ORLEANS, LA. 70140

COMMANDING OFFICER, ATTN PUBLIC WORKS OFFICER, U. S. MARINE CORPS AIR STATION, EL TORO, SANTA ANA, CALIF. 92709

COMMANDING OFFICER, ATTN PUBLIC WORKS OFFICER, U. S. NAVAL STATION, FPO SAN FRANCISCO 96640

COMMANDING OFFICER, ATTN PUBLIC WORKS OFFICER, U. S. NAVAL STATION, FPO NEW YORK 09597

COMMANDER, U. S. NAVAL MISSILE CENTER, POINT MUGU, CALIF. 93041

CHIEF OF ENGINEERS, U. S. ARMY, ATTN ENGCW-E, WASHINGTON D. C. 20315

CHIEF OF ENGINEERS, U. S. ARMY, ATTN ENGMC-E, WASHINGTON D. C. 20315

HEADQUARTERS, U. S. AIR FORCE, DIRECTORATE OF CIVIL ENGINEERING, ATTN AFOCE-ES, WASHINGTON D. C. 20330

COMMANDING OFFICER, U. S. NAVAL CONSTRUCTION BATTALION CENTER, ATTN MATERIEL DEPARTMENT, CODE 140, PORT HUENEME, CALIF. 93041

DEFENSE DOCUMENTATION CENTER, BUILDING 5, CAMERON STATION, ALEXANDRIA, VA.

DIRECTOR, COAST AND GEODETIC SURVEY, U. S. DEPARTMENT OF COMMERCE, 6001 EXECUTIVE BOULEVARD, ROCKVILLE, MD. 20852

DIRECTOR OF DEFENSE RESEARCH AND ENGINEERING, ROOM 3C-128, THE PENTAGON, ATTN TECHNICAL LIBRARY, WASHINGTON D. C. 20301

U. S. BUREAU OF RECLAMATION, DEPARTMENT OF INTERIOR, ATTN MR. T. W. MERMEL, WASHINGTON D. C. 20240

FACILITIES OFFICER, ATTN CODE 108, OFFICE OF NAVAL RESEARCH, WASHINGTON D. C.

COMMANDER NAVAL BEACH GROUP TWO, ATTN PROJECT OFFICER, U. S. NAVAL AMPHIBIOUS BASE, LITTLE CREEK, NORFOLK, VA. 23521

U. S. ARMY, ENGINEER RESEARCH AND DEVELOPMENT LABORATORIES, ATTN STINFO BRANCH, FORT BELVOIR, VA. 22060

AIR FORCE WEAPONS LABORATORY, KIRTLAND AIR FORCE BASE, ATTN CODE WLRC, ALBUQUERQUE, N. MEX. 87117

LIBRARY, DEPARTMENT OF METEOROLOGY AND OCEANOGRAPHY, U. S. NAVAL POSTGRADUATE SCHOOL, MONTEREY, CALIF. 93940

LIBRARY OF CONGRESS, WASHINGTON D. C. 20360

LIBRARY, PUBLIC DOCUMENTS DEPARTMENT, DUKE UNIVERSITY, DURHAM, N. C. 27706

LIBRARY, CIVIL ENGINEERING DEPARTMENT, UNIVERSITY OF HAWAII, HONOLULU, HAWAII 96822

DIRECTOR, INSTITUTE OF FISHERIES RESEARCH, UNIVERSITY OF NORTH CAROLINA, MOREHEAD CITY, N. C. 28557

DIRECTOR, U. S. NAVAL RESEARCH LABORATORY, ATTN CODE 2027, WASHINGTON D. C. 20390

CHIEF, MATERIALS BRANCH, OFFICE OF SHIP CONSTRUCTION, MARITIME ADMINISTRATION, WASHINGTON D. C. 20235

OFFICER IN CHARGE, U. S. FLEET WEATHER FACILITY, U. S. NAVAL AIR STATION, NORTH ISLAND, SAN DIEGO, CALIF. 92135

CDR A. R. YINGLING, USN, OCEANOGRAPHIC PROJECTS OFFICER, U. S. NAVAL STATION, LONG BEACH, CALIF. 90802

MR. J. B. ALFERS, ATTN CODE 634C, BUREAU OF SHIPS, NAVY DEPARTMENT, WASHINGTON, D. C. 20360

CDR J. C. FRY, USN, CHIEF OF NAVAL OPERATIONS (OP-09B5), DEPARTMENT OF THE NAVY, BUREAU OF YARDS AND DOCKS, WASHINGTON D. C. 20390

CHIEF, BUREAU OF NAVAL WEAPONS, ATTN MR. T. JOHNSTON, WASHINGTON, D. C. 20360

CHIEF, BUREAU OF SHIPS, ATTN MR. E. A. BUKZIN, WASHINGTON, D. C. 20360

COMMANDING OFFICER, U. S. NAVAL UNDERWATER ORDNANCE STATION, ATTN MR. S. MILLIGAN, NEWPORT, R. I. 02844

COMMANDING OFFICER AND DIRECTOR, U. S. NAVAL APPLIED SCIENCE LABORATORY, ATTN MR. D. H. KALLAS, U. S. NAVAL BASE, BROOKLYN, N. Y. 11251

COMMANDING OFFICER AND DIRECTOR, U. S. NAVY ELECTRONICS LABORATORY, ATTN MR. R. K. LOGAN, SAN DIEGO, CALIF. 92152

COMMANDER, U. S. NAVAL ORDNANCE LABORATORY (WHITE OAK), ATTN MR. R. A. BEUTTENMULLER, SILVER SPRING, MD. 20910

COMMANDER, U. S. NAVAL OCEANOGRAPHIC OFFICE, ATTN MR. J. DEPALMA, WASHINGTON D. C. 20390

HEAD, LIBRARY DIVISION, U. S. NAVAL ORDNANCE TEST STATION, CHINA LAKE, CALIF. 93557

COASTAL ENGINEERING RESEARCH CENTER, CORPS OF ENGINEERS, U. S. ARMY, 5201 LITTLE FALLS ROAD N. W., WASHINGTON D. C. 20016

COMMANDER, U. S. NAVAL OCEANOGRAPHIC OFFICE, ATTN LIBRARY - CODE 1640, WASHINGTON D. C. 20390

OFFICE OF NAVAL RESEARCH, GEOPHYSICS BRANCH, WASHINGTON D. C. 20360

COMMANDER, U. S. NAVAL ORDNANCE TEST STATION, ATTN PASADENA ANNEX LIBRARY, 3202 EAST FOOTHILL BLVD., PASADENA, CALIF. 91107

LT JAMES H. OSBORN, CEC, USN, 415 WEST BROOKSIDE DRIVE, BRYAN, TEX. 77803

MR. D. J. THEODORE, ATTN CODE 14, U. S. COAST AND GEODETIC SURVEY, ROCKVILLE, MD. 20852

LIBRARY, HUDSON LABORATORIES, COLUMBIA UNIVERSITY, 145 PALISADE STREET, DOBBS FERRY, N. Y. 10522

DIRECTOR, LAMONT GEOPHYSICAL FIELD STATION, APO NEW YORK 09856

PLASTICS TECHNICAL EVALUATION CENTER, SMUPA-VP3, PICATINNY ARSENAL, DOVER, N. J. 07801

DIRECTOR, WOODS HOLE OCEANOGRAPHIC INSTITUTION, ATTN REFERENCE ROOM, WOODS HOLE, MASS. 02543

DIRECTOR, MARINE PHYSICAL LABORATORY, SCRIPPS INSTITUTION OF OCEANOGRAPHY, SAN DIEGO, CALIF. 92152

DIRECTOR, APPLIED PHYSICS LABORATORY, UNIVERSITY OF WASHINGTON, 1013 N. E. 40TH STREET, SEATTLE, WASH. 98105

LIBRARY, LAMONT GEOLOGICAL OBSERVATOR, COLUMBIA UNIVERSITY, PALISADES, N. Y. 10964

BINGHAM OCEANOGRAPHIC LABORATORY, YALE UNIVERSITY, P. O. BOX 2025, YALE STATION, NEW HAVEN, CONN. 06520

RESEARCH LIBRARY, CHESAPEAKE BAY INSTITUTE, THE JOHNS HOPKINS UNIVERSITY, OCEANOGRAPHY BUILDING, BALTIMORE, MD. 21218

MIT LIBRARIANS, TECHNICAL REPORTS, ROOM 14 E-210, MASSACHUSETTS INSTITUTE OF TECHNOLOGY, CAMBRIDGE, MASS. 02139

MR. W. M. KECK, LABORATORY OF HYDRAULICS AND WATER RESOURCES, CALIFORNIA INSTITUTE OF TECHNOLOGY, 1201 CALIFORNIA STREET, PASADENA, CALIF. 91109

PROF. G. W. HOUSNER, DEPARTMENT OF CIVIL ENGINEERING, CALIFORNIA INSTITUTE OF TECHNOLOGY, 1201 CALIFORNIA STREET, PASADENA, CALIF. 91109

DR. HERBERT W. GRAHAM, BUREAU OF COMMERCIAL FISHERIES, BIOLOGICAL LABORATORY, WOODS HOLE, MASS. 02543

MR. WILLARD J. PIERSON JR, DEPARTMENT OF METEOROLOGY AND OCEANOGRAPHY, NEW YORK UNIVERSITY, NEW YORK 10453

DIRECTOR, OCEANOGRAPHIC INSTITUTE, FLORIDA STATE UNIVERSITY, TALAHASSEE, FLA. 32306

DIRECTOR, INSTITUTE OF MARINE SCIENCE, THE UNIVERSITY OF TEXAS, PORT ARANSAS, TEX. 78373

FISHERIES-OCEANOGRAPHY LIBRARY, 203 FISHERIES CENTER, UNIVERSITY OF WASHINGTON, SEATTLE, WASH. 98105

CIVIL ENGINEERING DEPARTMENT, TEXAS A AND M UNIVERSITY, COLLEGE STATION, TEX. 77843

MR. LESLIE A. CHAMBERS, ALLAN HANCOCK FOUNDATION, UNIVERSITY OF SOUTHERN CALIFORNIA, LOS ANGELES, CALIF. 90007

MR. R. F. MCALLISTER, PROFESSOR OF OCEANOGRAPHY, FLORIDA ATLANTIC UNIVERSITY, BOCA RATON, FLA. 33432

DR. EVELYN SINHA, EDITOR, OCEANIC COORDINATE INDEX, 7730 HERSCHEL AVENUE, LA JOLLA, CALIF. 92037

DR. KEN PREISS, GEOLOGY AND CIVIL ENGINEERING, DEPARTMENT OF GEOLOGY, UNIVERSITY OF ILLINOIS, URBANA, ILL. 61803

CHIEF, BUREAU OF SHIPS, NAVY DEPARTMENT, WASHINGTON, D.C. 20360
CHIEF, BUREAU OF NAVAL WEAPONS, ATTN MR. T. JOHNSTON, WASHINGTON, D.C. 20360

CHIEF, BUREAU OF SHIPS, ATTN MR. E.A. BUKZIN, WASHINGTON, D.C. 20360

COMMANDING OFFICER, U.S. NAVAL UNDERWATER ORDNANCE STATION, ATTN MR. S. MILLIGAN, NEWPORT, RHODE ISLAND 02844

COMMANDING OFFICER AND DIRECTOR, U.S. NAVAL APPLIED SCIENCE LABORATORY, ATTN MR. D.H. KALLAS, U.S. NAVAL BASE, BROOKLYN, NEW YORK 11251

COMMANDING OFFICER AND DIRECTOR, U.S. NAVY ELECTRONICS LABORATORY, ATTN MR. R. K. LOGAN, SAN DIEGO, CALIF. 92152

COMMANDER, U.S. NAVAL ORDNANCE LABORATORY, WHITE OAK, ATTN MR. R.A. BEUTTENMULLER, SILVER SPRING, MD. 20910

COMMANDER, U.S. NAVAL OCEANOGRAPHIC OFFICE, ATTN MR. J. DE PALMA, WASHINGTON, D.C. 20390

HEAD, LIBRARY DIVISION, U.S. NAVAL ORDNANCE TEST STATION, CHINA LAKE, CALIF. 93557

COASTAL ENGINEERING RESEARCH CENTER, CORPS OF ENGINEERS, U.S. ARMY, 5201 LITTLE FALLS ROAD, N.W., WASHINGTON, D.C. 20016

COMMANDER, U.S. NAVAL OCEANOGRAPHIC OFFICE, ATTN LIBRARY (CODE 1640), WASHINGTON, D.C. 20390

OFFICE OF NAVAL RESEARCH, GEOPHYSICS BRANCH, WASHINGTON, D.C. 20360

DIRECTOR, WOODS HOLE OCEANOGRAPHIC INSTITUTION, ATTN REFERENCE ROOM, WOODS HOLE, MASS. 02543

DIRECTOR, MARINE PHYSICAL LABORATORY, SCRIPPS INSTITUTION OF OCEANOGRAPHY, SAN DIEGO, CALIF. 92152

DIRECTOR, MARINE PHYSICS LABORATORY, UNIVERSITY OF WASHINGTON, 1013 N.E. 40TH STREET, SEATTLE, WASHINGTON 98105

LIBRARY, LAMONT GEOLOGICAL OBSERVATOR, COLUMBIA UNIVERSITY, PALISADES, NEW YORK 10964

BINGHAM OCEANOGRAPHIC LABORATORY, YALE UNIVERSITY, P.O. BOX 2025, YALE STATION NEW HAVEN, CONN. 06520

RESEARCH LIBRARY, CHESAPEAKE BAY INSTITUTE, THE JOHNS HOPKINS UNIVERSITY, ROOM 104-A, OCEANOGRAPHY BUILDING, BALTIMORE, MD. 21218

MIT LIBRARIANS, TECHNICAL REPORTS, ROOM 14E-210, MASSACHUSETTS INSTITUTE OF TECHNOLOGY, CAMBRIDGE, MASS. 02138

MR. W.M. KECK, LABORATORY OF HYDRAULICS AND WATER RESOURCES, CALIFORNIA INSTITUTE OF TECHNOLOGY, 1201 CALIFORNIA STREET, PASADENA, CALIF. 91109

PROF. G.W. HOUSNER, DEPARTMENT OF CIVIL ENGINEERING, ROOM 213, THOMAS LABORATORY, CALIFORNIA INSTITUTE OF TECHNOLOGY, 1201 CALIFORNIA STREET, PASADENA, CALIF. 91109

DR. HERBERT W. GRAHAM, BUREAU OF COMMERCIAL FISHERIES, BIOLOGICAL LABORATORY, WOODS HOLE, MASS. 02543

MR. WILLARD J. PIERSON, JR., DEPARTMENT OF METEROLOGY AND OCEANOGRAPHY, NEW YORK UNIVERSITY, NEW YORK 10453

DIRECTOR, OCEANOGRAPHIC INSTITUTE, FLORIDA STATE UNIVERSITY, TALAHASSEE, FLORIDA 32306

DIRECTOR, INSTITUTE OF MARINE SCIENCE, THE UNIVERSITY OF TEXAS, PORT ARANSAS, TEXAS 78373

FISHERIES-OCEANOGRAPHY LIBRARY, 203 FISHERIES CENTER, UNIVERSITY OF WASHINGTON, SEATTLE, WASHINGTON 98105

CIVIL ENGINEERING DEPARTMENT, TEXAS A AND M UNIVERSITY, COLLEGE STATION, TEXAS 77843

MR. LESLIE A. CHAMBERS, ALLAN HANCOCK FOUNDATION, UNIVERSITY OF SOUTHERN CALIFORNIA, LOS ANGELES, CALIF. 90007

COMM. U.S.N.O.T.S., PASADENA ANNEX, ATTN PASADENA ANNEX LIBRARY, 3202 EAST FOOTHILL BLVD., PASADENA, CALIF. 91107

OFFICER IN CHARGE, U.S. NAVAL BIOLOGICAL LABORATORY, NAVAL SUPPLY CENTER, OAKLAND, CALIF. 94625

COMMANDING OFFICER, NROTC UNIT, RENNSSELAER POLYTECHNIC INSTITUTE, TROY, NEW YORK 12181

CHIEF, BUREAU OF MEDICINE AND SURGERY, ATTN RESEARCH DIVISION, NAVY DEPARTMENT, WASHINGTON, D.C. 20390

OFFICER IN CHARGE, U.S. NAVAL R-D FACILITY, NAVAL SUPPLY CENTER, ATTN LIBRARY, BAYONNE, NEW JERSEY 07002

COMMANDER, AMPHIBIOUS FORCE, U.S. ATLANTIC FLEET, U.S. NAVAL BASE, NORFOLK, VIRGINIA 23511

OFFICER IN CHARGE, U.S. NAVAL SUPPLY R-D FACILITY, NAVAL SUPPLY CENTER, BAYONNE, NEW JERSEY 07002

COMMANDER, NORFOLK NAVAL SHIPYARD, ATTN METALLURGICAL LABORATORY, CODE 3204, PORTSMOUTH, VIRGINIA 23709

CHIEF CHEMIST (CODE 3205), NORFOLK NAVAL SHIPYARD, PORTSMOUTH, VIRGINIA 23709

HEAD OF LABORATORIES, CODE 305, BOSTON NAVAL SHIPYARD, BOSTON, MASS. 02129

U.S. NAVAL APPLIED SCIENCE LABORATORY, TECHNICAL LIBRARY, BUILDING 291, CODE 9832, NAVAL BASE, BROOKLYN, NEW YORK 11251

TECHNICAL LIBRARY, U.S. NAVAL ELECTRONICS LABORATORY, SAN DIEGO, CALIF. 92152

DR. W.A. ZISMAN, CHEMISTRY DIVISION, CODE 6100, U.S. NAVAL RESEARCH LABORATORY, WASHINGTON, D.C. 20390

CHIEF, PAINT AND CORROSION LABORATORY BRANCH, U.S. ARMY ENGINEER DISTRICT, CLOCK TOWER BUILDING, ROCK ISLAND, ILL. 61201

LIBRARY, U.S. ARMY COLD REGIONS RESEARCH AND ENGINEERING LABORATORY, P.O. BOX 282, HANOVER, NEW HAMPSHIRE 03755

CHIEF EDITOR SCIENCES SECTION, AMCRD-RV, U.S. ARMY MATERIAL COMMAND, WASHINGTON, D.C. 20315

AFCRL - RESEARCH LIBRARY, ATTN CRMXLR/STOP 29, L.G. HANSCOM FIELD, BEDFORD, MASS. 01731

MR. P.C. SMITH, PRINCIPAL RESEARCH ENGINEER(SOILS), MATERIALS DIVISION, BUREAU OF PUBLIC ROADS, WASHINGTON, D.C. 20235

HEAD, DOCUMENTS DEPARTMENT, UNIVERSITY OF ALASKA, LIBRARY, COLLEGE, ALASKA 99735

LIBRARY, UNIVERSITY OF NEBRASKA, LINCOLN, NEBRASKA 68508

LIBRARY, UNIVERSITY OF SOUTHERN CALIFORNIA, UNIVERSITY PARK, P.O. BOX 77929,

LOS ANGELES, CALIF. 90007

DR. CHARLES E. LANE, PROFESSOR, INSTITUTE OF MARINE SCIENCE, UNIVERSITY OF MIAMI, CORAL GABLES, FLORIDA 33146

LIBRARY, DOCUMENTS DIVISION, PRINCETON UNIVERSITY, PRINCETON, NEW JERSEY 08540

GENERAL LIBRARY, CALIFORNIA INSTITUTE OF TECHNOLOGY, PASADENA, CALIF. 91109

U. S. Naval Civil Engineering Laboratory
MECHANICS OF RAISING AND LOWERING HEAVY LOADS IN THE DEEP OCEAN: CABLE AND PAYLOAD DYNAMICS, by P. Holmes
TR-433 87 p. illus April 1966 Unclassified

1. Structures in deep ocean 2. Heavy-load dynamics — Deep ocean
I. Y-F015-01-01-001(b)

Based on a theoretical analysis of the cable and payload dynamics during lowering or raising heavy loads in the deep ocean given in Project Trident Technical Report No. 1370863, further calculations of the maximum dynamic stresses expected in the lowering cable are presented covering a wide range of cable and payload parameters. The theoretical analysis is adapted to a proposed design procedure, and two typical design examples are given, the results of which are discussed in terms of the safety of the lowering or raising operations.

In order to make the design procedure applicable with a greater degree of confidence, it is considered necessary to make measurements of cable tensions and load and ship motions during a full-scale operation to fill in deficiencies of data and provide a basis for verification of theory and calculations. In particular, data are needed on the coefficients of drag and mass, which at this stage must of necessity be estimates.

U. S. Naval Civil Engineering Laboratory
MECHANICS OF RAISING AND LOWERING HEAVY LOADS IN THE DEEP OCEAN: CABLE AND PAYLOAD DYNAMICS, by P. Holmes
TR-433 87 p. illus April 1966 Unclassified

1. Structures in deep ocean 2. Heavy-load dynamics — Deep ocean
I. Y-F015-01-01-001(b)

Based on a theoretical analysis of the cable and payload dynamics during lowering or raising heavy loads in the deep ocean given in Project Trident Technical Report No. 1370863, further calculations of the maximum dynamic stresses expected in the lowering cable are presented covering a wide range of cable and payload parameters. The theoretical analysis is adapted to a proposed design procedure, and two typical design examples are given, the results of which are discussed in terms of the safety of the lowering or raising operations.

In order to make the design procedure applicable with a greater degree of confidence, it is considered necessary to make measurements of cable tensions and load and ship motions during a full-scale operation to fill in deficiencies of data and provide a basis for verification of theory and calculations. In particular, data are needed on the coefficients of drag and mass, which at this stage must of necessity be estimates.

U. S. Naval Civil Engineering Laboratory
MECHANICS OF RAISING AND LOWERING HEAVY LOADS IN THE DEEP OCEAN: CABLE AND PAYLOAD DYNAMICS, by P. Holmes
TR-433 87 p. illus April 1966 Unclassified

1. Structures in deep ocean 2. Heavy-load dynamics — Deep ocean
I. Y-F015-01-01-001(b)

Based on a theoretical analysis of the cable and payload dynamics during lowering or raising heavy loads in the deep ocean given in Project Trident Technical Report No. 1370863, further calculations of the maximum dynamic stresses expected in the lowering cable are presented covering a wide range of cable and payload parameters. The theoretical analysis is adapted to a proposed design procedure, and two typical design examples are given, the results of which are discussed in terms of the safety of the lowering or raising operations.

In order to make the design procedure applicable with a greater degree of confidence, it is considered necessary to make measurements of cable tensions and load and ship motions during a full-scale operation to fill in deficiencies of data and provide a basis for verification of theory and calculations. In particular, data are needed on the coefficients of drag and mass, which at this stage must of necessity be estimates.

U. S. Naval Civil Engineering Laboratory
MECHANICS OF RAISING AND LOWERING HEAVY LOADS IN THE DEEP OCEAN: CABLE AND PAYLOAD DYNAMICS, by P. Holmes
TR-433 87 p. illus April 1966 Unclassified

1. Structures in deep ocean 2. Heavy-load dynamics — Deep ocean
I. Y-F015-01-01-001(b)

Based on a theoretical analysis of the cable and payload dynamics during lowering or raising heavy loads in the deep ocean given in Project Trident Technical Report No. 1370863, further calculations of the maximum dynamic stresses expected in the lowering cable are presented covering a wide range of cable and payload parameters. The theoretical analysis is adapted to a proposed design procedure, and two typical design examples are given, the results of which are discussed in terms of the safety of the lowering or raising operations.

In order to make the design procedure applicable with a greater degree of confidence, it is considered necessary to make measurements of cable tensions and load and ship motions during a full-scale operation to fill in deficiencies of data and provide a basis for verification of theory and calculations. In particular, data are needed on the coefficients of drag and mass, which at this stage must of necessity be estimates.

Unclassified
Security Classification

DOCUMENT CONTROL DATA - R&D

(Security classification of title, body of abstract and indexing annotation must be entered when the overall report is classified)

1. ORIGINATING ACTIVITY *(Corporate author)*

U. S. Naval Civil Engineering Laboratory
Port Hueneme, California 93041

2a. REPORT SECURITY CLASSIFICATION
Unclassified

2b. GROUP

3. REPORT TITLE

Mechanics of Raising and Lowering Heavy Loads in the Deep Ocean: Cable and Payload Dynamics

4. DESCRIPTIVE NOTES *(Type of report and inclusive dates)*

Not Final 1 November 1964 - 15 August 1965

5. AUTHOR(S) *(Last name, first name, initial)*

Holmes, P., Ph D

6. REPORT DATE	7a. TOTAL NO. OF PAGES	7b. NO. OF REFS
April 1966	87	11

8a. CONTRACT OR GRANT NO.	9a. ORIGINATOR'S REPORT NUMBER(S)
b. PROJECT NO. Y-F015-01-01-001(b)	TR-433
c.	9b. OTHER REPORT NO(S) *(Any other numbers that may be assigned this report)*
d.	

10. AVAILABILITY/LIMITATION NOTICES

Distribution of this document is unlimited.

11. SUPPLEMENTARY NOTES	12. SPONSORING MILITARY ACTIVITY
	BUDOCKS

13. ABSTRACT

Based on a theoretical analysis of the cable and payload dynamics during lowering or raising heavy loads in the deep ocean given in Project Trident Technical Report No. 1370863, further calculations of the maximum dynamic stresses expected in the lowering cable are presented covering a wide range of cable and payload parameters. The theoretical analysis is adapted to a proposed design procedure, and two typical design examples are given, the results of which are discussed in terms of the safety of the lowering or raising operations.

In order to make the design procedure applicable with a greater degree of confidence, it is considered necessary to make measurements of cable tensions and load and ship motions during a full-scale operation to fill in deficiencies of data and provide a basis for verification of theory and calculations. In particular, data are needed on the coefficients of drag and mass, which at this stage must of necessity be estimates.

DD FORM 1 JAN 64 1473 0101-807-6800

Unclassified
Security Classification

14. KEY WORDS	LINK A		LINK B		LINK C	
	ROLE	WT	ROLE	WT	ROLE	WT
Mechanics						
Emplacement						
Loads						
Deep ocean						
Analysis						
Cable						
Payload						
Dynamics						
Computation						
Stresses						
Drag						
Mass						
Coefficients						

INSTRUCTIONS

1. ORIGINATING ACTIVITY: Enter the name and address of the contractor, subcontractor, grantee, Department of Defense activity or other organization *(corporate author)* issuing the report.

2a. REPORT SECURITY CLASSIFICATION: Enter the overall security classification of the report. Indicate whether "Restricted Data" is included. Marking is to be in accordance with appropriate security regulations.

2b. GROUP: Automatic downgrading is specified in DoD Directive 5200.10 and Armed Forces Industrial Manual. Enter the group number. Also, when applicable, show that optional markings have been used for Group 3 and Group 4 as authorized.

3. REPORT TITLE: Enter the complete report title in all capital letters. Titles in all cases should be unclassified. If a meaningful title cannot be selected without classification, show title classification in all capitals in parenthesis immediately following the title.

4. DESCRIPTIVE NOTES: If appropriate, enter the type of report, e.g., interim, progress, summary, annual, or final. Give the inclusive dates when a specific reporting period is covered.

5. AUTHOR(S): Enter the name(s) of author(s) as shown on or in the report. Enter last name, first name, middle initial. If military, show rank and branch of service. The name of the principal author is an absolute minimum requirement.

6. REPORT DATE: Enter the date of the report as day, month, year, or month, year. If more than one date appears on the report, use date of publication.

7a. TOTAL NUMBER OF PAGES: The total page count should follow normal pagination procedures, i.e., enter the number of pages containing information.

7b. NUMBER OF REFERENCES: Enter the total number of references cited in the report.

8a. CONTRACT OR GRANT NUMBER: If appropriate, enter the applicable number of the contract or grant under which the report was written.

8b, 8c, & 8d. PROJECT NUMBER: Enter the appropriate military department identification, such as project number, subproject number, system numbers, task number, etc.

9a. ORIGINATOR'S REPORT NUMBER(S): Enter the official report number by which the document will be identified and controlled by the originating activity. This number must be unique to this report.

9b. OTHER REPORT NUMBER(S): If the report has been assigned any other report numbers *(either by the originator or by the sponsor)*, also enter this number(s).

10. AVAILABILITY/LIMITATION NOTICES: Enter any limitations on further dissemination of the report, other than those imposed by security classification, using standard statements such as:

(1) "Qualified requesters may obtain copies of this report from DDC."

(2) "Foreign announcement and dissemination of this report by DDC is not authorized."

(3) "U. S. Government agencies may obtain copies of this report directly from DDC. Other qualified DDC users shall request through _____."

(4) "U. S. military agencies may obtain copies of this report directly from DDC. Other qualified users shall request through _____."

(5) "All distribution of this report is controlled. Qualified DDC users shall request through _____."

If the report has been furnished to the Office of Technical Services, Department of Commerce, for sale to the public, indicate this fact and enter the price, if known.

11. SUPPLEMENTARY NOTES: Use for additional explanatory notes.

12. SPONSORING MILITARY ACTIVITY: Enter the name of the departmental project office or laboratory sponsoring *(paying for)* the research and development. Include address.

13. ABSTRACT: Enter an abstract giving a brief and factual summary of the document indicative of the report, even though it may also appear elsewhere in the body of the technical report. If additional space is required, a continuation sheet shall be attached.

It is highly desirable that the abstract of classified reports be unclassified. Each paragraph of the abstract shall end with an indication of the military security classification of the information in the paragraph, represented as *(TS), (S), (C), or (U)*.

There is no limitation on the length of the abstract. However, the suggested length is from 150 to 225 words.

14. KEY WORDS: Key words are technically meaningful terms or short phrases that characterize a report and may be used as index entries for cataloging the report. Key words must be selected so that no security classification is required. Identifiers, such as equipment model designation, trade name, military project code name, geographic location, may be used as key words but will be followed by an indication of technical context. The assignment of links, roles, and weights is optional.